

AN INVESTIGATION OF THE EFFECT OF
SPECIMEN GEOMETRY ON THE OXIDATION
OF NICKEL AT ELEVATED TEMPERATURES

By
JAMES STEPHEN WOLF

A DISSERTATION PRESENTED TO THE GRADUATE COUNCIL OF
THE UNIVERSITY OF FLORIDA
IN PARTIAL FULFILLMENT OF THE REQUIREMENTS FOR THE
DEGREE OF DOCTOR OF PHILOSOPHY

UNIVERSITY OF FLORIDA

April, 1965

IN
DEDICATION
to
my wife
Viola

ACKNOWLEDGMENTS

The author wishes to express his sincere gratitude to Dr. F.N. Rhines for discussing, at length, the subject matter of this research. Without his guidance, interest, and encouragement this dissertation would not have been possible.

The author also wishes to express his appreciation to Dr. J. Kronsbein, Professor of Physics, Dr. C.E. Reid, Professor of Chemistry, Dr. R.E. Reed-Hill, Professor of Metallurgy, and Dr. T.A. Scott, Professor of Physics, for serving on his supervisory committee.

The financial support of a portion of this research by the National Aeronautics and Space Administration is gratefully acknowledged.

Finally, the author wishes to extend his appreciation to the several members of the staff and student body of the Metallurgical and Materials Engineering Department for their encouragement and assistance.

TABLE OF CONTENTS

	Page
DEDICATION	ii
ACKNOWLEDGMENTS.	iii
LIST OF FIGURES.	vii
LIST OF TABLES	xxi
ABSTRACT	xxiv
 CHAPTER	
I. INTRODUCTION.	1
1.1 General Features of the Oxidation Process	1
1.2 Geometric Considerations in the Oxi- dation Process.	3
1.3 Occurrence of Stress Arising from the Oxidation Process	5
1.4 Purpose and Scope of this Research.	10
II. EXPERIMENTAL PROCEDURE.	13
2.1 Materials and General Features of the Specimens	13
2.2 Fabrication of Specimens.	16
2.3 Surface Preparations of Oxidation Specimens	21
2.4 Measurement of Prepared Specimens .	22
2.5 Oxidation of Prepared Specimens . .	25
2.6 Examination of Oxidized Specimens .	39

TABLE OF CONTENTS (Continued)

CHAPTER	Page
III. EXPERIMENTAL RESULTS.	46
3.1 Volmetric Experiments	46
3.2 Preliminary Scale Thickening Experiments	53
3.3 Scale Thickening in a Controlled Environment	66
3.4 Scale Thickening Behavior of Hol- low Cylinders	75
3.5 Dimensional Changes as a Result of Oxidation.	79
3.6 Oxide Microstructure.	90
3.7 Environmental Studies	159
3.8 Oxidation-Creep Experiments . . .	173
3.9 Elevated-temperature Creep Studies	174
IV. DISCUSSION.	183
4.1 Nature of the Scale Formed on Nickel.	183
4.2 Consequence of Unidirectional Transport	187
4.3 Consideration Pertaining to the Existence of Stresses in Scales .	193
4.4 Consideration Pertaining to the Structure of Scales.	204
4.5 A Proposed Mechanism for the Oxidation of Nickel	220
4.6 Interpretation of Results of This Investigation	223

TABLE OF CONTENTS (Continued)

	Page
4.7 Interpretations of Results of Other Investigations.	272
CHAPTER	
V. CONCLUSIONS.	297
APPENDICIES.	299
APPENDIX 1	300
APPENDIX 2	328
APPENDIX 3	347
LIST OF REFERENCES	353
BIOGRAPHICAL SKETCH.	361

LIST OF FIGURES

Figure	Page
1. General features of the oxidation specimens used in this investigation. Magnification approximately 1 1/4 x.	15
2. General features of the specimens used to determine elevated-temperature mechanical properties. Magnification approximately 1 1/4x	17
3. Apparatus employed for oxide sintering and elevated-temperature compressive creep experiments.	20
4. Optical comparator employed in determination of length changes due to oxidation.	24
5. Apparatus employed in volumetric determination of oxidation behavior at 1000°C.	27
6. Schematic diagram of the apparatus employed in performing controlled-environment oxidation experiments at 1000°C.	32
7. Apparatus employed in performing controlled-environment oxidation experiments at 1000°C.	33
8. Schematic drawing of the apparatus employed in performing oxidation-creep experiments at 900°C.	38
9. Oxygen consumption as a function of time for a spheroid of curvature 2.75 cm ⁻¹ oxidized at 1000°C in oxygen at pressure of one-quarter atmosphere.	48
10. Oxygen consumption as a function of time for a spheroid of curvature 3.40 cm ⁻¹ oxidized at 1000°C in oxygen at a pressure of one-quarter atmosphere	49

LIST OF FIGURES (Continued)

Figure		Page
11.	Oxygen consumption as a function of time for a spheroid of curvature 3.99 cm^{-1} oxidized at 1000°C in oxygen at a pressure of one-quarter atmosphere.	50
12.	Oxygen consumption as a function of time for a spheroid of curvature 4.67 cm^{-1} oxidized at 1000°C in oxygen at a pressure of one-quarter atmosphere.. . . .	51
13.	Oxygen consumption as a function of time for a spheroid of curvature 5.23 cm^{-1} oxidized at 1000°C in oxygen at a pressure of one-quarter atmosphere.. . . .	52
14.	Initial parabolic rate constant as a function of specimen curvature for spheroids oxidized at 1000°C in oxygen at a pressure of one-quarter atmosphere.. . . .	54
15.	Final parabolic rate constant as a function of specimen curvature for spheroids oxidized at 1000°C in oxygen at a pressure of one-quarter atmosphere.. . . .	55
16.	Scale thickness as a function of curvature for cylindrical specimens oxidized in air at 1000°C for 16 hours.. . . .	56
17.	Scale thickness as a function of curvature for cylindrical specimens oxidized in air at 900°C for 64 hours.	58
18.	Scale thickness as a function of curvature for cylindrical specimens oxidized in air at 900°C for 16 hours.. . . .	59
19.	Scale thickness as a function of curvature for cylindrical specimens oxidized in air at 1000°C for 64 hours.. . . .	60
20.	Scale thickness as a function of specimen thickness for flat specimens oxidized in air at 1000°C for 16 hours.. . . .	62

LIST OF FIGURES (Continued)

Figure	Page
21. Scale thickness as a function of specimen thickness for flat specimens oxidized in air at 900°C for 64 hours.. . . .	63
22. Scale thickness as a function of specimen size for cylindrical and flat specimens oxidized in air for 16 hours at 1000°C.. . . .	64
23. Scale thickness as a function of specimen size for cylindrical and flat specimens oxidized in air for 64 hours at 900°C.	65
24. Scale thickness as a function of curvature for cylindrical specimens oxidized in dried oxygen at 1000°C for 4 hours.	67
25. Scale thickness as a function of curvature for cylindrical specimens oxidized in dried oxygen at 1000°C for 16 hours.. . . .	68
26. Scale thickness as a function of time for specimens of curvature 0 cm ⁻¹ oxidized at 1000°C. .	70
27. Scale thickness as a function of time for specimens of curvature 4 cm ⁻¹ oxidized at 1000°C. .	71
28. Scale thickness as a function of time for specimens of curvature 8 cm ⁻¹ oxidized at 1000°C. .	72
29. Scale thickness as a function of time for specimens of curvature 12 cm ⁻¹ oxidized at 1000°C .	73
30. Scale thickness as a function of time for specimens of curvature 0, 4, 8 and 12 cm ⁻¹ oxidized at 1000°C.. . . .	74
31. Schematic representation of the surface developed in scale thickness-specimen curvature - oxidation time space by oxidation at 1000°C in dried oxygen.. . . .	76
32. Scale thickness as a function of specimen thickness for specimens oxidized in dried oxygen at 1000°C for 16 hours.. . . .	77

LIST OF FIGURES (Continued)

Figure	Page
33. Axial length change as a function of curvature for cylindrical specimens oxidized in dried oxygen at 1000°C for 5 minutes. . .	80
34. Axial length change as a function of curvature for cylindrical specimens oxidized for various times in dried oxygen at 1000°C, Solid curve represents 5 minute data of Figure 33.	81
35. Axial length change as a function of time for a cylindrical specimen of curvature 6 cm^{-1} subjected to interrupted oxidation at 1000°C.	83
36. Axial length change as a function of time for a cylindrical specimen of curvature 8 cm^{-1} subjected to interrupted oxidation at 1000°C.	84
37. Closure of right-angle bend specimen as a function of oxidation time in air at 1160°C	88
38. Photomicrographs of the external surface of the scale formed on a cylindrical specimen of curvature 2 cm^{-1} oxidized for 16 hours at 900°C. Focal plane at outermost surface (a) and 6.6 microns beneath it (b). Magnification 500x.	91
39. Photomicrographs of the external surface of the scale formed on cylindrical specimens of approximate curvature 9 cm^{-1} (a) and 13 cm^{-1} (b) oxidized for 16 hours at 900°C. Magnification 500x.	93
40. Photomicrograph of the cross section of the scale formed on a cylindrical specimen of curvature 2 cm^{-1} oxidized for 16 hours at 900°C. Electrochemical Etch. Magnification 500x.	94

LIST OF FIGURES (Continued)

Figure		Page
41.	Photomicrographs of the external surface of scales formed on cylindrical specimens oxidized in air for 64 hours at 900°C. Specimen curvatures 1.6 cm ⁻¹ (a) and 3.2 cm ⁻¹ (b). Magnification 500x.	97
42.	Photomicrographs of the external surface of scales formed on cylindrical specimens oxidized in air for 64 hours at 900°C. Specimen curvatures 6.5 cm ⁻¹ (a) and 9.7 cm ⁻¹ (b). Magnification 500x.	98
43.	Photomicrographs of the external surface of scales formed on cylindrical specimens oxidized in air for 64 hours at 900°C. Specimen curvatures 12.9 cm ⁻¹ (a) and 19.8 cm ⁻¹ (b). Magnification 500x.	99
44.	Photomicrograph of the cross section of a scale formed on a cylindrical specimen oxidized in air for 64 hours at 900°C. Specimen Curvature 2.1 cm ⁻¹ . Magnification 500x.	100
45.	Photomicrographs of the external surface of scale formed on cylindrical specimens oxidized in air for 16 hours at 1000°C. Specimen curvature 2.0 cm ⁻¹ (a) and 4.0 cm ⁻¹ (b). Magnification 500x.	102
46.	Photomicrographs of the external surface of scales formed on cylindrical specimens oxidized in air for 16 hours at 1000°C. Specimen curvatures 6.4 cm ⁻¹ (a) and 7.9 cm ⁻¹ (b). Magnification 500x.	103
47.	Photomicrographs of the external surface of scales formed on cylindrical specimens oxidized in air for 16 hours at 1000°C. Specimen curvatures 10.2 cm ⁻¹ (a) and 12.6 cm ⁻¹ (b). Magnification 500x.	104

LIST OF FIGURES (Continued)

Figure		Page
48.	Electron photomicrograph of the external surface of the scale formed on a cylindrical specimen of curvature 6.4 cm^{-1} oxidized in air for 16 hours at 1000°C . Magnification 6000x (a) and 4000x (b). . . .	105
49.	Electron photomicrographs of the external surface of the scale formed on a cylindrical specimen of curvature 8.9 cm^{-1} oxidized in air for 16 hours at 1000°C . Magnification 6000x (a) and 7500x (b). . . .	106
50.	Electron photomicrographs of the external surface of the scale formed on a cylindrical specimen of curvature 15.4 cm^{-1} oxidized in air for 16 hours at 1000°C . Magnification 5000x (a) and 3500x (b). . . .	107
51.	Photomicrographs of the cross section of scales formed on cylindrical specimens of curvature 0 cm^{-1} (a) and 2.0 cm^{-1} (b) oxidized in air for 16 hours at 1000°C . Electrochemical etch. Magnification 500x. .	109
52.	Photomicrographs of the cross section of scales formed on cylindrical specimens of curvature 6.4 cm^{-1} (a) and 9.0 cm^{-1} (b) oxidized in air for 16 hours at 1000°C . Electrochemical etch. Magnification 500x. .	110
53.	Photomicrographs of the cross section of scales formed on cylindrical specimens of curvature 12.6 cm^{-1} (a) and 15.4 cm^{-1} (b) oxidized in air for 16 hours at 1000°C . Electrochemical etch. Magnification 500x. .	111
54.	Photomicrograph of the longitudinal section of the scale formed on a cylindrical specimen of curvature 15.4 cm^{-1} oxidized in air for 16 hours at 1000°C . Electrochemical etch. Magnification 500x.	114

LIST OF FIGURES (Continued)

Figure	Page
55. Electron photomicrograph of the cross section of the scale formed on a cylindrical specimen of curvature 2.0 cm^{-1} oxidized in air for 16 hours at 1000°C . Electrochemical etch. Magnification 5000x.	115
56. Photomicrograph of the cross section of a scale blister formed on a cylindrical specimen of curvature 6.4 cm^{-1} oxidized in air for 16 hours at 1000°C . Electrochemical etch. Magnification 500x.	116
57. Photomicrographs of the cross section of a scale blister formed on a cylindrical specimen of curvature 15.4 cm^{-1} oxidized in air for 16 hours at 1000°C . Electrochemical etch. Magnification 250x (a) and 500x (b).	117
58. X-ray diffraction patterns of scales formed on cylindrical specimens of curvature 2.0 cm^{-1} (a), 6.4 cm^{-1} (b), and 11.1 cm^{-1} (c) oxidized in air for 16 hours at 1000°C . Cylindrical axis parallel to figure titles.	119
59. Photomicrographs of the external surface of scales formed on plane specimens oxidized in air for 16 hours at 1000°C . Reciprocal thickness 1.2 cm^{-1} (a) and 3.2 cm^{-1} (b). Magnification 500x.	120
60. Photomicrographs of the external surface of scales formed on plane specimens oxidized in air for 16 hours at 1000°C . Reciprocal thickness 6.5 cm^{-1} (a) and 10.2 cm^{-1} (b). Magnification 500x.	121
61. Photomicrographs of the scale formed on a plane specimen of reciprocal thickness 16.8 cm^{-1} oxidized in air for 16 hours at 1000°C . External surface (a) and cross section (b). Magnification 500x.	122
62. Photomicrographs of the external surface of scales formed on cylindrical specimens oxidized in air for 64 hours at 1000°C . Specimen curvatures 2.0 cm^{-1} (a) and 6.0 cm^{-1} (b). Magnification 500x.	124

LIST OF FIGURES (Continued)

Figure	Page
63. Photomicrographs of the external surface of scales formed on cylindrical specimens oxidized in air for 64 hours at 1000°C. Specimen curvatures 7.2 cm ⁻¹ and 9.0 cm ⁻¹ (b). Magnification 500x.	125
64. Photomicrographs of the external surface of scales formed on cylindrical specimens oxidized in air for 64 hours at 1000°C. Specimen curvatures 11 cm ⁻¹ (a) and 14.0 cm ⁻¹ (b). Magnification 500x.	126
65. Electron photomicrograph of the external surface of a specimen oxidized in air for 64 hours at 1000°C. Specimen curvature 2.0 cm ⁻¹ . Magnification 4500x.	128
66. Photomicrograph of the cross section of the scale formed on a cylindrical specimen of curvature 6.0 cm ⁻¹ oxidized in air for 64 hours at 1000°C. Magnification 500x. . . .	129
67. X-ray diffraction patterns of scales formed on cylindrical specimens of curvature 2.0 cm ⁻¹ (a), 6.0 cm ⁻¹ (b), 7.2 cm ⁻¹ (c), and 11.0 cm ⁻¹ (d) oxidized in air for 64 hours at 1000°C. Cylinder axes parallel to figure title.	130
68. Photomicrographs of the external surface of scales formed on cylindrical specimens of curvature 2 cm ⁻¹ oxidized in one atmosphere of dried oxygen at 1000°C. Oxidation time 4 hours (a) and 16 hours (b). Magnification 1000x.	132
69. Photomicrographs of the external surface of scales formed on cylindrical specimens of curvature 3 cm ⁻¹ oxidized in one atmosphere of dried oxygen at 1000°C. Oxidation time 4 hours (a) and 16 hours (b). Magnification 1000x.	133

LIST OF FIGURES (Continued)

Figure	Page
70. Photomicrographs of the external surface of scales formed on cylindrical specimens of curvature 4 cm^{-1} oxidized in one atmosphere of dried oxygen at 1000°C . Oxidation time 4 hours (a) and 16 hours (b). Magnification 1000x.	134
71. Photomicrographs of the external surface of scales formed on cylindrical specimens of curvature 5 cm^{-1} oxidized in one atmosphere of dried oxygen at 1000°C . Oxidation time 4 hours (a) and 16 hours (b). Magnification 1000x.	135
72. Photomicrographs of the external surface of scales formed on cylindrical specimens of curvature 6 cm^{-1} oxidized in one atmosphere of dried oxygen at 1000°C . Oxidation time 4 hours (a) and 16 hours (b). Magnification 1000x.	136
73. Photomicrographs of the external surface of scales formed on cylindrical specimens of curvature 7 cm^{-1} oxidized in one atmosphere of dried oxygen at 1000°C . Oxidation time 4 hours (a) and 16 hours (b). Magnification 1000x.	137
74. Photomicrographs of the external surface of scales formed on cylindrical specimens of curvature 8 cm^{-1} oxidized in one atmosphere of dried oxygen at 1000°C . Oxidation time 4 hours (a) and 16 hours (b). Magnification 1000x.	138
75. Photomicrographs of the external surface of scales formed on cylindrical specimens of curvature 9 cm^{-1} oxidized in one atmosphere of dried oxygen at 1000°C . Oxidation time 4 hours (a) and 16 hours (b). Magnification 1000x.	139
76. Photomicrographs of the external surface of scales formed on cylindrical specimens of curvature 10 cm^{-1} oxidized in one atmosphere of dried oxygen at 1000°C . Oxidation time 4 hours (a) and 16 hours (b). Magnification 1000x.	140

LIST OF FIGURES (Continued)

Figure		Page
77.	Photomicrographs of the external surface of scales formed on cylindrical specimens of curvature 11 cm^{-1} oxidized in one atmosphere of dried oxygen at 1000°C . Oxidation time 4 hours (a) and 16 hours (b). Magnification 1000x.	141
78.	Photomicrographs of the external surface of scales formed on cylindrical specimens of curvature 12 cm^{-1} oxidized in one atmosphere of dried oxygen at 1000°C . Oxidation time 4 hours (a) and 16 hours (b). Magnification 1000x.	142
79.	Electron photomicrographs of the external surface of scales formed on cylindrical specimens oxidized in dried oxygen at 1000°C . Curvature 8 cm^{-1} , oxidation time 1 hour (a); and curvature 4 cm^{-1} , oxidation time 16 hours (b). Magnification 500x.	145
80.	Photomicrographs of the cross sections of scales formed on cylindrical specimens of curvature 2 cm^{-1} oxidized in dried oxygen at 1000°C for 16 hours (a) and 64 hours (b). Electrochemical etch. Magnification 500x.	146
81.	Photomicrographs of the external surface of scales formed on plane specimens oxidized in dried oxygen for 16 hours at 1000°C . Reciprocal thickness 6.2 cm^{-1} (a), and 12.2 cm^{-1} (b). Magnification 1000x.	148
82.	Photomicrographs of the external surface of scales formed on plane specimens oxidized in dried oxygen for 16 hours at 1000°C . Reciprocal thickness 25.0 cm^{-1} (a) and 45.2 cm^{-1} (b). Magnification 1000x.	149
83.	Photomicrographs of the external surface of the scale formed on a plane specimen of reciprocal thickness 65.6 cm^{-1} oxidized in dried oxygen for 16 hours at 1000°C . Magnification 1000x (a), and 500x (b).	150

LIST OF FIGURES (Continued)

Figure	Page
84. Photomicrographs of the external surface of the scale formed on a plane specimen of reciprocal thickness 65.6 cm^{-1} oxidized in dried oxygen for 16 hours at 1000°C . Magnification 1000x. Illumination: oblique bright field (a), and polarized light (b). .	151
85. Photomicrographs of the external surface of specimens oxidized in air. Oxidation treatment 1200°C for 16 hours (a) and 1000°C for 124 hours (b). Magnification 500x. . . .	153
86. Adhesion of the scale as a function of specimen size for cylindrical and flat specimens oxidized in air at 900°C . Cylinders, 16 hours (a); cylinders, 64 hours (b); Flat sheet, 64 hours (c).	155
87. Adhesion of the scale as a function of specimen size for cylindrical and flat specimens oxidized in air at 1000°C . Cylinders, 16 hours (a); Flat sheet, 16 hours (b); and cylinders, 64 hours (c).	156
88. Adhesion of the scale as a function of specimen size of cylindrical and flat specimens oxidized in dried oxygen at 1000°C . Cylinders 4 hours (a); 16 hours (b); and flat sheet, 16 hours (c).	157
89. Adhesion of the scale as a function of oxidizing time for specimens of curvature 0, 4, 8, 12 cm^{-1} oxidized in dried oxygen at 1000°C	158
90. Photomicrographs of the external surface of scales formed on cylindrical specimens of curvature 2 cm^{-1} oxidized for 16 hours at 1000°C . Environmental conditions: test 1(a) and test 2(b) of Table 8. Magnification 500x.	163
91. Photomicrograph of the external surface of the scale formed on a cylindrical specimen of curvature 2 cm^{-1} oxidized for 16 hours at 1000°C . Environmental conditions: test 4 of Table 8. Magnification 500x.. . . .	164

LIST OF FIGURES (Continued)

Figure	Page
92. Photomicrograph (a) and X-ray diffraction pattern (b) of the external surface of the scale formed on a cylindrical specimen of curvature 2 cm^{-1} oxidized for 16 hours at 1000°C . Environmental conditions: test 6 of Table 8. Magnification 500x (a). . . .	165
93. Photomicrograph (a) and X-ray diffraction pattern (b) of the external surface of the scale formed on a cylindrical specimen of curvature 2 cm^{-1} oxidized for 16 hours at 1000°C . Environmental conditions: test 7 of Table 8. Magnification 500x (a). . . .	166
94. Photomicrograph (a) and X-ray diffraction pattern (b) of the external surface of the scale formed on a cylindrical specimen of curvature 2 cm^{-1} oxidized for 16 hours at 1000°C . Environmental conditions: test 8 of Table 8. Magnification 500x (a). . . .	168
95. Photomicrograph of the external surface of the scale formed on a cylindrical specimen of curvature 2 cm^{-1} oxidized for 16 hours at 1000°C . Environmental conditions: test 5 of Table 8. Magnification 500x.	169
96. Photomicrographs of the external surface of scales formed on cylindrical specimens of curvature 2 cm^{-1} oxidized for 16 hours at 1000°C . Environmental conditions: test 10 (a) and test 11 (b) of Table 8. Magnification 500x.	171
97. Photomicrograph of the external surface of the scale formed on a cylindrical specimen of curvature 2 cm^{-1} oxidized for 16 hours at 1000°C . Environmental conditions: test 12 of Table 8. Magnification 500x. . . .	172
98. Axial deformation as a function of time for a specimen of Nickel-270 tested in compression at 1000°C . Stress level 754 psi.	175

LIST OF FIGURES (Continued)

Figure		Page
99.	Axial deformation as a function of time for a specimen of Nickel-270 tested in compression at 1000°C. Stress level 1420 psi.	176
100.	Axial deformation as a function of time for a specimen of Nickel-270 tested in compression at 1000°C. Stress level 1975 psi..	177
101.	Axial deformation as a function of time for a specimen of hot-pressed nickel oxide tested in compression at 1000°C. Effective stress level 765 psi.	178
102.	Axial deformation as a function of time for a specimen of hot-pressed nickel oxide tested in compression at 1000°C. Effective stress level 1450 psi.	179
103.	Axial deformation as a function of time for a specimen of hot-pressed nickel oxide tested in compression at 1000°C. Effective stress level 2060 psi.	180
104.	Second stage creep rate as a function of axial compressive stress for nickel and nickel oxide specimens tested at 1000°C. . .	182
105.	Schematic diagram of the proposed diffusion paths of nickel and oxygen prevailing during the formation of nickel oxide.	197
106.	Schematic representation of oxide crystal growth; no favored orientation, (a); some favored orientation, (b); and favored orientation coupled with large grain size (c).	208
107.	Comparison of observed and calculated values of the axial extension of cylindrical specimens oxidized for 16 hours at 1000°C in dried oxygen.	262
108.	Comparison of calculated and observed axial length change as a function of time for a cylindrical specimen of curvature 6 cm ⁻¹ subjected to interrupted oxidation at 1000°C. .	263

LIST OF FIGURES (Continued)

Figure		Page
109.	Comparison of calculated and observed axial length change as a function of time for a cylindrical specimen of curvature 8 cm^{-1} subjected to interrupted oxidation at 1000°C	264
110.	Schematic drawing of scale formation on a cylindrical section.	331
111.	Forces acting on a cylindrical section.. . .	335
112.	Displacements in a cylindrical element. . .	337
113.	Comparison of observed and calculated values of the extension of flat specimens oxidized for 16 hours at 1000°C in dried oxygen. Calculated curve based upon a grain boundary pressure of 1500 psi.	352

LIST OF TABLES

Table	Page
1. Nominal Chemical Analysis of Nickel-270 (<u>37</u>)	13
2. Chemical Analysis of Nickelous Oxide Powder (<u>38</u>)	14
3. Oxidation Schedule Employed With the Vertical Furnace.	30
4. Nominal Chemical Composition of Nickel-200 (<u>33</u>)	31
5. Scale Thicknesses Developed On Hollow Cylinders	78
6. Length Change of Flat Specimens Resulting from Oxidation at 1000°C for 16 Hours	85
7. Dimensions of Helical Specimens Before and After Oxidation.	86
8. Effect of Environmental Conditions on Scale Thickening at 1000°C	161
9. Scale Thicknesses Developed on Oxidation-Creep Specimens.	173
10. Oxygen Consumption as a Function of Time for a Spherical Specimen of Curvature 2.75 cm^{-1} oxidized at 1000°C	301
11. Oxygen Consumption as a Function of Time for a Spherical Specimen of Curvature 3.40 cm^{-1} Oxidized at 1000°C	304
12. Oxygen Consumption as a Function of Time for a Spherical Specimen of Curvature 3.99 cm^{-1} Oxidized at 1000°C	305
13. Oxygen Consumption as a Function of Time for a Spherical Specimen of Curvature 4.67 cm^{-1} Oxidized at 1000°C	306
14. Oxygen Consumption as a Function of Time for a Spherical Specimen of Curvature 5.23 cm^{-1} Oxidized at 1000°C	307

LIST OF TABLES (Continued)

Table	Page
15. Parabolic Rate Constants Derived from Volumetric Data as a Function of Specimen Curvature for Spheroids Oxidized at 1000°C in Oxygen at a Pressure of One-quarter Atmosphere.	308
16. Scale Thickness as a Function of Curvature for Cylindrical Specimens Oxidized in Air at 1000°C for 16 Hours	309
17. Scale Thickness as a Function of Curvature for Cylindrical Specimens Oxidized in Air at 900°C for 64 Hours.	310
18. Scale Thickness as a Function of Curvature for Cylindrical Specimens Oxidized in Air at 900°C for 16 hours.	311
19. Scale Thickness as a Function of Curvature for Cylindrical Specimens Oxidized in Air at 1000°C for 64 Hours	312
20. Scale Thickness as a Function of Specimen Thickness for Flat Specimens Oxidized in Air at 1000°C for 16 Hours	313
21. Scale Thickness as a Function of Specimen Thickness for Flat Specimens Oxidized in Air at 1000°C for 16 Hours	314
22. Scale Thickness as a Function of Curvature for Cylindrical Specimens Oxidized in Dried Oxygen at 1000°C for 4 Hours	315
23. Scale Thickness as a Function of Curvature for Cylindrical Specimens Oxidized in Dried Oxygen at 1000°C for 16 Hours.	316
24. Scale Thickness Resulting from Oxidation in Dried Oxygen at 1000°C for Cylindrical and Flat Specimens	317
25. Axial Length Change as a Function of Curvature for Cylindrical Specimens Oxidized for Five Minutes in Dried Oxygen at 1000°C . . .	318

LIST OF TABLES (Continued)

Table	Page
26. Axial Length Change as a Function of Curvature for Cylindrical Specimens Oxidized for Various Times in Dried Oxygen at 1000°C. . . .	319
27. Axial Length as a Function of Oxidizing Time for Two Cylindrical Specimens Subjected to Interrupted Oxidation at 1000°C in Dried Oxygen	320
28. Axial Deformation as a Function of Time for a Specimen of Nickel-270 Tested in Compression at 1000°C - Stress Level 754 psi	321
29. Axial Deformation as a Function of Time for a Specimen of Nickel-270 Tested in Compression at 1000°C - Stress Level 1430 psi.	322
30. Axial Deformation as a Function of Time for a Specimen of Nickel-270 Tested in Compression at 1000°C - Stress Level 1975 psi	323
31. Axial Deformation as a Function of Time for a Specimen of Hot-pressed Nickel Oxide Tested in Compression at 1000°C - Corrected Stress Level 765 psi.	324
32. Axial Deformation as a Function of Time for a Specimen of Hot-pressed Nickel Oxide Tested in Compression at 1000°C - Corrected Stress Level 1450 psi	325
33. Axial Deformation as a Function of Time for a Specimen of Hot-pressed Nickel Oxide Tested in Compression at 1000°C - Corrected Stress Level 2060 psi	326
34. Degree of Protection Afforded by the Scales Formed on Several Metals as a Function of Oxidizing Temperature (17)	327

Abstract of Dissertation Presented to the Graduate Council
in Partial Fulfillment of the Requirements for the
Degree of Doctor of Philosophy

AN INVESTIGATION OF THE EFFECT OF SPECIMEN GEOMETRY ON
THE OXIDATION OF NICKEL AT ELEVATED TEMPERATURES

By

James Stephen Wolf

April, 1965

Chairman: Dr. F.N. Rhines

Major Department: Department of Metallurgical and Materials
Engineering

The effect of specimen geometry upon the oxidation behavior of unalloyed nickel was investigated at temperatures of 900 and 1000°C for times up to 64 hours. Specimens were fabricated in the form of flat sheet and solid right cylinders. A regular variation in the geometric parameters was produced by systematically varying the sheet thickness and the cylinder diameter. Other specimen geometries were employed in supplementary oxidation experiments.

The short-time scaling behavior was investigated both by volumetric and metallographic means, while metallographic examination alone was employed to measure the extent of oxidation at longer times. Dimensional changes resulting from oxidation were monitored as a function of both the specimen geometry and oxidation

time. In addition, the high-temperature deformation behavior of both nickel and nickel-oxide was explored.

It was found that the scaling process is dependent upon both specimen geometry and oxidation time. Both volumetric and metallographic studies indicated that the scaling process proceeded in the expected parabolic manner relatively early in the oxidation process. At this stage of oxidation, the scale thickening was found to be nearly insensitive to changes in macroscopic specimen dimensions. As the duration of oxidation was increased, the dependence of the scale thickening upon specimen geometry became apparent. Microstructural studies indicated that the onset of the geometric dependence of the scaling behavior could be correlated to the appearance of oxide crystals near the metal-oxide interface.

Measurements of the oxidation-induced deformation of specimens indicated that axial lengthening, in the case of cylinders, and longitudinal growth, in the case of flat specimens, occurred.

A mechanism is proposed for the scaling of nickel which takes into account most of the observed geometry and time dependence of scale thickness, scale microstructure, and deformation behavior. An attempt to extend this model to the oxidation of other metals has indicated that it may have rather general applicability to the field of high-temperature oxidation of metals.

CHAPTER I

INTRODUCTION

Most pure metals when exposed to an oxygen-bearing gas react with it and in due course form one or more layers of reaction product on the metal surface. The presence of metal oxides so formed acts as a barrier between the reactants and in many instances controls their rate of combination. It has become common practice to characterize oxidation processes by rate laws which describe the time dependence of the processes at a fixed temperature. Low oxidizing temperatures usually favor slow reaction rates and formation of thin films whereas high temperatures favor fast reaction rates and formation of thicker films, generally known as scales. It is this latter class of oxidation conditions with which the present research is concerned.

1.1 General Features of the Oxidation Process

The initial stages of oxidation involve a sequence of events whose appearance in time is dependent upon the specific oxidation conditions and material under investigation. These events usually include: adsorption of

oxygen, formation of oxide nuclei, lateral growth of nuclei, and production of a complete oxide film (1, 2, 3, 4). Subsequent to the formation of a coherent layer further growth must take place by transport of material through the layer. While it is agreed that transport processes involve ionic and electronic motion (5, 6, 7, 8), precise mechanisms apparently depend upon the particular metal involved, the oxidizing temperature, and the degree of oxidation attained. Metal oxides do not generally form as stoichiometric compounds, but rather are deficient in either metal or oxygen with one ionic species usually much more mobile than the other. Thus, they may be grouped into one of two major classifications, according to whether the majority of transport takes place via oxygen or metal ions respectively.

The simplest case of oxidation involves the formation of a single oxide on the surface of a pure metal. The rate controlling transport processes in such cases may often be described in terms of the flux of a single ionic species through the bulk of the barrier layer (5). If this flux is inversely proportional to the thickness of the layer, the parabolic scaling law obtains and the oxidation behavior is termed "protective." In cases wherein the rate of scale formation is independent

of the amount of pre-deposited oxide, and therefore oxidation time, the behavior is termed "non-protective" and is described by a linear rate law.

Rather early in the history of quantitative oxidation studies, a parameter known as the Pilling-Bedworth ratio was introduced in an attempt to predict whether or not the scaling of specific metals would be protective (9). At that time, experimental evidence indicated that if the volume of the oxide were greater than the volume of the metal from which it formed, then the oxide would be protective; otherwise it would be non-protective. Later investigations have shown that this principle has little merit except in certain highly restricted cases (10, 11, 12). However, the use of this parameter as an index of relative protection has become almost universally accepted primarily by virtue of circumstances.

1.2 Geometric Considerations in the Oxidation Process

While thermodynamic considerations may be employed to predict whether or not an oxide will form under specific environmental conditions and kinetic considerations may in some cases be used to determine the quantity of oxide which will form in a given time, there is no reliable

method for predicting precisely where in the region of the scale the oxidation reaction will occur. It is generally conceded that in the case of oxygen deficient oxides the oxygen ion diffuses through the scale and unites with the metal in the region of the metal-oxide interface, while for metal deficient oxides the metal ion diffuses outwards through the scale to combine with oxygen near the gas-metal interface (5, 8). The site of oxide formation under conditions of bi-directional diffusion is, as yet, open to question.

In the case of oxides which grow by oxygen transport and have Pilling-Bedworth ratios greater than unity, oxide formation may occur at the metal-oxide interface under conditions of mechanical constraint. For this class of oxidation, the oxide, which is formed between the metal substrate and the pre-existing scale, produces a stress at the interface which may be relieved by plastic deformation or fracture of either the oxide or the metal. Conversely, oxides which grow by metal ion transport, at least when formed on plane surfaces, may be free from constraint provided that the oxide forms only at the gas-oxide interface (11). Constraint-free oxidation also requires a uniform motion of the oxide as it follows the retreating metal-oxide interface.

The formation of this latter class of oxides on surfaces of non-zero curvature may form under conditions

of mechanical constraint even in the case when the volume ratio is balanced by the normal growth rate. This concept is most readily apparent if one considers the oxidation of a spherical specimen. Subsequent to preliminary film formation, the outward diffusion of the metallic ion tends to decrease the volume of metal contained within the spherical shell of oxide on its surface. If this process continues for an appreciable time and the oxide attempts to follow the retreating interface, then each segment of oxide will be laterally constrained by its neighbor as it moves radially inward.

In any situation wherein the oxidation reaction proceeds in the presence of constraints, one would expect stresses to arise which would subsequently be evidenced in the form of deformations.

1.3 Occurrence of Stress Arising from the Oxidation Process

Both direct and indirect evidence exists indicating that stresses do arise as a result of oxidation. The direct evidence is based upon observations of some type of deformation which occurs either in the oxide or the substrate metal, whereas indirect evidence usually involves observations of anomalies in the oxidation rate.

The presence of stresses in very thin films of oxide has been demonstrated by several investigators who

determined that these films are strained with respect to that of the bulk material (8, 13, 15, 16). It has been suggested that this phenomenon, associated with relatively low oxidation temperatures, is transient in the sense that upon continued oxidation the lattice parameter of the product tends to revert to that of the bulk oxide (14, 16). The behavior exhibited in these cases appears to depend on the production of specific crystallographic (epitaxial) relations between the oxide and the underlying metal. It is believed that epitaxial strain does not persist, except in very special instances, during the course of elevated-temperature oxidation.

Oxides of the refractory metals columbium, tantalum, zirconium, and hafnium form by inward diffusions of oxygen and exhibit volumes greater than that of metal consumed in the reaction (17). Phase changes in the scale layers and solution of relatively large amounts of oxygen by these metals, both of which occur during the oxidation process, make the analysis of this oxidation behavior difficult; however, in some instances the evidence for existence of stresses in oxidized specimens is rather strong. Cracks and blisters have been observed in the scales formed on columbium, tantalum and zirconium and, in the case of columbium, blister formation has been correlated with anomalies in rate data determined volume-

trically (18, 19, 20, 21, 22). In addition, flat specimens of both columbium and tantalum which were provided with a protective coating on one side were found to bow as a result of oxidation; their unprotected faces becoming convex (21, 23). Macroscopic deformation exhibited by the product of completely oxidized hafnium also indicates that large stresses are generated during oxidation (24).

Metals which oxidize by outward diffusion of the metallic ion through the scale usually exhibit less complex scaling behaviors and lower oxygen solubilities than do the refractory metals. For this reason, the detection and analysis of phenomena associated with stresses in scales is somewhat simplified. Qualitative experiments, in which wedge-shaped films of nickel oxide produced by oxidation in a thermal gradient were carefully freed from the substrate metal, indicated that both a lateral compressive stress and a stress gradient existed in the oxide (25). The stress in this case was evidenced by wrinkling of the thicker portions and curling of the thinner portions of the scale. In a series of experiments concerning the oxidation behavior of copper at elevated temperatures it was found that the degree of oxide plasticity was an important factor in the overall oxidation behavior (26). Here it was demonstrated that the character of the oxide scale formed on thin-walled cylindrical specimens differed on the inner

and outer surfaces and it was concluded that the diffusion mechanism was dependent upon the state of compressive stress in the oxide. Similarly, different "final forms" of the oxidation product have been attributed to differences in oxide plasticity in the case of iron (27).

It appears that only two research groups have attempted quantitative measurement of the stresses produced in oxide films. The first experiments involved vacuum deposition of various metals on thin mica substrates (28). Subsequent oxidation at room temperature produced curvature of the composite consisting of substrate and metal oxide. When iron and nickel, whose oxides have Pilling-Bedworth ratios greater than unity, were oxidized the oxide was found to be on the convex side of the composite, while the oxidation of magnesium, which has a Pilling-Bedworth ratio less than unity, produced the opposite curvature. By taking into account the geometry and mechanical properties of the components involved, the investigators were able to calculate the stresses in the oxide from the degree of bending of the oxide-substrate composite. Both the calculated stresses, which were of the order of 100,000 psi, and the calculated strains were very much smaller than one would expect to

find on the basis of constrained volume changes resulting from "in situ" conversion of metal to oxide.

The second investigative technique involved monitoring the deformation of copper helices during oxidation at 200° to 500°C (29, 30). It was found that if one side of the helices was provided with a protective coating, then the helix would experience torsion which was, at least initially, indicative of compressive stresses in the oxide. The system comprised of metal helix and its oxide coating were shown to be in elastic equilibrium so that the stresses were calculable from observations of torsion angle. Maximum lateral compressive stresses of approximately 200,000 psi were assigned to the oxide layer.

In these experiments, no deformation was noted in the case of helices which were exposed to oxygen on both their inner and outer surfaces. In contrast, other investigators have found that iron helices oxidized at 700°C tend to "wind-up" as a result of oxidation (31). Comparison of these results indicates that differences in the mechanical properties of the oxides formed in these systems may be a major factor in their contrasting behavior.

1.4 Purpose and Scope of this Research

In spite of the fact that the oxidation of metals has been subjected to quantitative examination for nearly a half century, it is not yet possible to write an "equation of state" which is capable of describing the data of various researchers. This inability to analytically describe the oxidation process applies not only to the relatively complex oxidation of alloys, but also to the relatively simple case of the oxidation of pure metals. For example, a summary of studies of the scaling behavior of nickel indicates that there is a large variation in oxidation rate data, with the process exhibiting activation energies ranging from less than 29 to greater than 54 kilocalories per mole (32). Although such variations may be due to inconsistencies in environmental conditions and purity of metal employed, it is believed that they may also be due in part to the fact that different investigators used specimens of different shape, thereby inducing dissimilar stress states in the scales produced.

It has been indicated that stresses may arise during the oxidation of a pure metal if the scale layer is formed by metal ion transport and is, at the same time, constrained by the contour of its substrate. For this case, it follows that the stress state produced by oxidation should be sensitive to the degree of constraint afforded

by the underlying metal which, in turn, is dictated by the particular specimen geometry employed. If stresses do arise as a result of the oxidation process, then it is conceivable that their presence might alter the scaling behavior with respect to that predicted by classical consideration of diffusion controlled oxidation. To date, neither the role of specimen geometry nor that of stress in the oxidation process has been systematically investigated.

The purpose of this research was therefore to determine the role of specimen geometry on the oxidation process and, from inspection of oxidized specimens, to attempt to deduce the nature and effect of the stresses which arise. It was felt that such a study would aid in the understanding of the overall oxidation process for that technically important class of metals which form oxide by metal ion transport.

High purity nickel was chosen as the metal to be used in this investigation because it is believed that this material represents the simplest one among those possible for study in that the effects of stress may be examined with a minimum amount of ambiguity. This is possible because of the following characteristics of the metal and the oxide:

- 1) Neither the metal nor the oxide undergo change in crystal structure upon cycling from room temperature to the

oxidizing temperature, thus simplifying microscopic interpretations (33, 34).

2) Both the metal and the oxide have approximately the same linear coefficient of thermal expansion thus minimizing "bimetallic" effects (35).

3) The oxide is believed to form by diffusion of the metal ion through the scale, thus the possibility of generating stresses at the metal-oxide interface is minimized (17).

4) The solubility of oxygen in nickel is very low, thus effects arising as a result of oxygen solution in the metal should be relatively small (36).

The type and degree of constraint effective during the oxidation process was studied by oxidizing flat and cylindrical specimens of various size and shape. Cylindrical specimens ranged in diameter from approximately 0.060 to 0.480 inch while the thickness of flat specimens was varied from approximately 0.006 to 0.375 inch. Most of these were oxidized at 900° to 1000°C for various pre-selected times up to 64 hours and subsequently scale thicknesses were determined and oxide microstructures were examined. The deformation resulting from oxidation was measured for several specimens and elevated-temperature mechanical properties of both nickel and nickel-oxide were determined in order to aid in correlating the state of stress with the observed deformations.

CHAPTER II

EXPERIMENTAL PROCEDURE

2.1 Materials and General Features of the Specimens

Two commercially available grades of high-purity nickel have been employed in this investigation. Mond-process carbonyl nickel shot, in the form of slightly flattened spheroids, was used in preliminary volumetric studies of oxidation rate. It nominally contains 99.7 to 99.9 weight per cent nickel with carbon and oxygen being the major impurities(32). All other metallic specimens were fabricated from a single lot of Nickel-270 bar stock. This material, supplied through the courtesy of the International Nickel Company in the form of one-half inch rounds, is characterized by the chemical analysis given in Table 1.

TABLE 1

NOMINAL CHEMICAL ANALYSIS OF NICKEL-270 (37)

<u>Element</u>	<u>Weight per cent</u>
Ni	99.95
C	0.005
Fe	0.005
Others (including cobalt)	0.003 each

Oxidation specimens were fabricated in several different forms including solid and hollow right cylinders, flat and bent sheet, and helices. The diameter of solid cylinders and the thickness of sheet material were employed as testing parameters and were varied roughly one order of magnitude. A photograph illustrating the general features of some of these specimens is shown in Figure 1.

Metallic specimens were also fabricated in forms suitable for mechanical testing. These were used to determine high-temperature creep and oxidation creep behavior of Nickel-270. These were necessarily of non-standard form in order to take advantage of pre-existing special purpose testing equipment.

In addition to metallic specimens, a test bar of nickel oxide was fabricated by hot pressing nickelous oxide powder. The manufacturer's analysis of the oxide powder used is given in Table 2.

TABLE 2

CHEMICAL ANALYSIS OF NICKELOUS OXIDE POWDER (38)

<u>Element or Compound</u>	<u>Weight Per Cent</u>
NiO	99.5
Co	0.10
Zn	0.01
Cu	0.005
Fe	0.002
Others	Balance



Figure 1: General features of the oxidation specimens used in this investigation. Magnification approximately $1\frac{1}{4} \times$.

The overall features of specimens used to determine elevated temperature mechanical properties are illustrated in the photograph of Figure 2.

2.2 Fabrication of Specimens

All metallic specimens, with the exception of flat sheet, were machined from bar stock such that their final cylindrical surfaces were approximately coaxial with the original bar. Hollow cylinders were fabricated by counter-drilling and rearing solid cylinders. An 8-inch metalworking lathe was used for all operations. In the machining of external surfaces, the depth of cut was consistently reduced from a maximum of 0.015 inch throughout the cutting process. As the final diameters were approached, lubricant-free cuts of a depth less than 0.001 inch were made. This procedure was adopted in order to minimize distortion and contamination of the finished surface. Specimens thus fabricated were mechanically polished successively with 240, 320, 400, and 600-grit silicon carbide papers. The total amount of metal removed from the surface was approximately 0.001 inch. Finished specimen diameters ranged from 0.060 to 0.480 inches.

Cylindrical specimens used in length-change studies were provided with a pair of circumferential grooves approximately 0.010 deep spaced about one-half inch apart. This operation, executed prior to mechanical polishing, was



Figure 2: General features of the specimens used to determine elevated-temperature mechanical properties. Magnification approximately $1\frac{1}{4}x$.

accomplished by the use of a special grooving tool ground to an angle of 25 degrees. The tool was fed with the bisector of its angle normal to the specimen axis providing the set of well-defined reference marks used in subsequent length measurements.

Flat specimens were fabricated from bar stock by first milling a pair of flat surfaces parallel to the rod axis and the cold-rolling to pre-selected gages. Final specimen thicknesses produced ranged from approximately 0.005 to 0.375 inches. Mechanical polishing was performed as outlined above for cylindrical specimens. Those flat sections which were to be examined for dimensional changes were provided with two drilled reference holes one-sixteenth inch in diameter spaced about one-half inch apart. The effects of cold work in these specimens due to the rolling and drilling operations were reduced by vacuum annealing at 1000°C for 5 minutes prior to final mechanical polishing.

Helical and right-angle bend specimens were fabricated from thin cold-rolled, annealed nickel strip which was provided with a 600-grit metallographic finish. Both types of specimen were fabricated simply by bending the sheet around cylindrical mandrils. Typical helices were approximately 2 inches in length and contained five or six tightly spaced turns. Each plane leg of the bend specimens was approximately one-half inch square. Both types of

specimen were provided with small punched holes which accepted support wires used in subsequent annealing and oxidizing operations.

Metallic creep specimens were produced in two forms: one for tensile oxidation creep studies at 900°C , the other for compressive creep studies at 1000°C . The forms had an overall length of approximately 3 inches with a centrally located gage section approximately $1 \frac{9}{16}$ inches long and 0.0185 inch in diameter. The latter had an overall length of approximately 1 inch with a centrally located gage section approximately one-half inch long and 0.250 inch in diameter. The ends of this specimen were carefully squared to reduce the possibility of buckling.

A combination of hot pressing and sintering operations were utilized to produce the single nickel oxide creep specimen investigated. The apparatus, especially constructed to produce and test this specimen, is shown in Figure 3. The following schedule was used to produce this specimen:

- 1) Press at 1200°C and 800 psi for 1 hour
- 2) Press at 1300°C and 40 psi for 8 hours
- 3) Sinter with temperature slowly rising from 1200°C to 1490°C for $5 \frac{1}{2}$ hours.

The resulting specimen was in the form of a right cylinder approximately $\frac{3}{8}$ inch in diameter and one-half inch long.

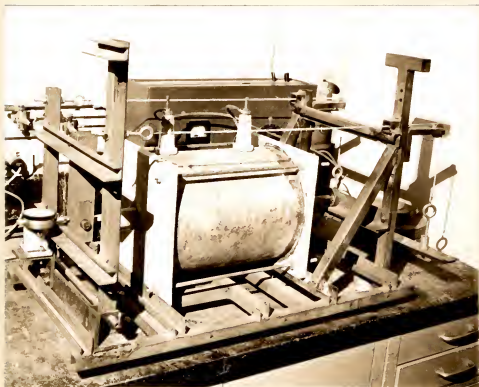


Figure 3: Apparatus employed for oxide sintering and elevated-temperature compressive creep experiments.

The central region of the specimen was reduced to a 0.3 inch diameter over a length of 0.2 inch which served as the gage length for subsequent mechanical testing.

2.3 Surface Preparation of Oxidation Specimens

The surface of the Mond process carbonyl nickel spheroids, used in preliminary volumetric studies, was prepared for oxidation by immersion of the as-received material in a 50 per cent solution of nitric acid at room temperature. After 2 minutes of etching, the specimens were removed, washed thoroughly with distilled water and stored in clean glass vessels. Measurements of specimen dimensions were made at this point in the processing. Just prior to oxidation the specimens were immersed in acetone to remove traces of grease due to chance improper handling. Tweezers, cleaned in acetone, were employed to place the specimen in the cold zone of the oxidation apparatus.

The oxidation and oxidation creep specimens fabricated from Nickel-270 were cleaned in acetone after mechanical polishing and then electropolished. In this operation the specimen was the anode and a helix of cold-rolled and annealed Nickel-270 served as the cathode. The electropolishing solution was composed of:

817 cc	H_3PO_4	
134 cc	H_2SO_4	
40 cc	H_2O	(distilled)
156 gms	CrO_3	(taken into solution)

A satisfactory polish was obtained after 10 minutes of polishing at a current density of 0.4 amperes per square centimeter with the solution temperature adjusted between 35° and 45° C. This operation removed between 0.0005 and 0.001 inch of material and produced the standard highly reflective specimen surface provided most of the oxidation specimens investigated.

It was found that agitation of the solution was necessary to prevent striations from appearing on flat specimens. No such tendency for the formation of striations was noted in the case of cylindrical specimens.

Following the electropolishing operation, specimens were handled in a manner identical to that of the spheroidal specimens described above with the exclusion of the etching process.

2.4 Measurement of Prepared Specimens

Two different techniques were employed to determine the dimensions of specimens both prior to and following oxidation. Those specimens which were provided with special reference markings were monitored for length change using a Jones and Lamson optical comparator having a magnification of 31 1/4 diameters. A small spring-loaded vise, with a machined base, was used to position the specimen on the comparator. Fiducial marks on the vise and

the specimen helped to insure that the same cross section of the specimen was being monitored. The photograph of Figure 4 shows the comparator with the vise and a cylindrical specimen in position for measurement.

In the case of cylindrical specimens the projected length of each side, between reference grooves, was measured. The diameter was determined twice at a distance midway between reference marks. It was assumed that the groove wall would oxidize uniformly so that apparent changes in specimen length could be attributed to actual plastic deformation of the specimen. Observations made on sections through such grooves indicate that this assumption is at least approximately valid.

In the measurement of length changes of flat specimens due to oxidation, the specimen vise was modified to position the plane of the specimen nearly perpendicular to the optical axis of the comparator. The separation for drilled holes was determined from measurements of the position of their edges and subsequent calculation of the position of their centers. Changes in separation are again attributed to plastic deformation of the specimen, the major assumption involved being that the edges of the reference holes oxidize similarly.

Multiple independent determinations indicated that the probable error associated with these measurements of the dimensions of cylindrical specimens was about ± 0.00005



Figure 4: Optical comparator employed in determination of length changes due to oxidation.

inch, while that for flat specimens was approximately ± 0.00007 inch.

All specimens other than those provided with reference markings were measured using machinists micro-meters. Significant dimensions were measured three times at various points on the specimens. Deviations from the mean values seldom exceeded 0.0002 inch. Internal diameters of hollow cylinders and helices were measured to within ± 0.001 inch using a set of cylindrical machinists gages.

Relatively coarse determinations of angular changes developed in right-angle specimens were made using a small protractor. The error associated with these measurements was approximately $\pm 2\ 1/2$ degrees.

2.5 Oxidation of Prepared Specimens

Throughout the course of this research several different techniques have been employed to acquire information concerning the oxidation process. In addition to the variations in geometric form and size of specimens, their high temperature environment has been systematically altered. Effects of the following environmental variables upon the scaling behavior have been explored: atmosphere surrounding the specimen, time-temperature profile, and application of mechanical stress. The following sections describe the oxidation processes and equipment utilized.

In each case, verification of the oxidation temperature was made prior to and subsequent to the experiment by using a Model 2745 Leeds and Northrup potentiometer in conjunction with a chromel-alumel thermocouple.

2.51 Volumetric Studies

An investigation of the oxidation kinetics of spheroidal specimens was carried out at constant pressure using the volumetric apparatus shown in Figure 5. Specimens were oxidized individually in order to determine the effect of size alone on their oxidation behavior at 1000°C. The technique employed afforded a record of oxygen consumption as a function of time for each of the specimens studied.

Prior to oxidation, the specimens were secured at the cool upper end of the quartz reaction tube by means of an externally fixed magnet. A thin pad of non-reactive aluminum silicate wool was placed within the reaction chamber at its closed end. This was done to prevent the falling specimen from breaking the reaction tube. The apparatus was designed so that the closed end of the reaction tube was in the center of the heated zone of the furnace at the same time that the standard taper fitting at its upper end was properly mated with the remainder of the system.

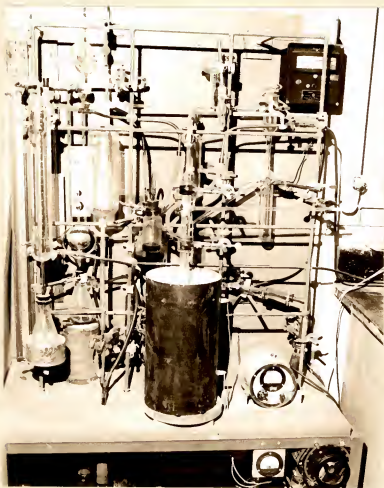


Figure 5: Apparatus employed in volumetric determination of oxidation behavior at 1000°C.

The system was prepared for the oxidation experiment by alternately evacuating it with a small mechanical pump and backfilling it with oxygen. The final system pressure was adjusted to approximately one-quarter atmosphere with the main gate valve and the upper stopcock of the gas reservoir in the "closed" position. This minimized the volume of the system thereby increasing its sensitivity. System pressure was determined by readings of the mercury manometer which was connected between the system and room atmosphere.

After allowing approximately 30 minutes for the system to reach equilibrium, the stopcock in the reference leg of the differential manometer was closed and the specimen was dropped into the reaction zone by withdrawing the magnet. As the oxidation reaction progressed, the differential manometer became unbalanced due to consumption of the gas. By carefully changing the mercury level in the calibrated gas burette, balance of the differential manometer could be maintained. The oxidation process was monitored by noting the displacement of this mercury column necessary to keep the differential manometer balanced.

2.52 Preliminary Scale Thickening Experiments

Preliminary experiments were conducted to secure information about the structure of the oxide and rate of its

formation. Cylindrical and flat specimens of Nickel-270 were oxidized for preselected times at 900°C and 1000°C in stagnant air using small resistance furnaces. The thickness of scale formed and its structure were determined metallographically.

The vertical furnace shown in Figure 5 was utilized for batch-type oxidation studies wherein a series of specimens of given geometric form but differing in size, were oxidized simultaneously. This technique was selected in order to minimize the possibility of introducing extraneous specimen-to-specimen variation.

A disk-shaped ceramic boat, supported from nichrome hanger wires, was loaded with six to eight specimens and lowered into the heated control zone of the furnace. The control thermocouple was then positioned at the center of the boat and a thin ceramic cover was placed over the open upper end of the furnace core in order to reduce convective heat loss.

The oxidation schedule employed in the use of this furnace is given in Table 3.

Other preliminary studies were carried out by oxidizing a series of cylindrical specimens of various diameter in stagnant air for 64 hours at $1000^{\circ} \pm 1/6^{\circ}\text{C}$. A horizontal furnace, utilizing a 1 1/8 inch bore combustion tube as its core, was employed in this series of experiments.

Due to the small core diameter specimens were oxidized individually.

TABLE 3

OXIDATION SCHEDULE EMPLOYED WITH THE VERTICAL FURNACE

Specimen Shape	Oxidation Temperature	Oxidation Time
Cylinder	$900^{\circ}\text{C} \pm 3^{\circ}\text{C}$	16 hours
Cylinder	$900^{\circ}\text{C} \pm 3^{\circ}\text{C}$	64 hours
Cylinder	$1000^{\circ}\text{C} \pm 3 \frac{1}{2}^{\circ}\text{C}$	16 hours
Sheet	$900^{\circ}\text{C} \pm 3^{\circ}\text{C}$	64 hours
Sheet	$1000^{\circ}\text{C} \pm 3 \frac{1}{2}^{\circ}\text{C}$	16 hours

2.53 Controlled Environment Experiments

Preliminary experiments indicated that factors other than specimen geometry or oxidizing time and temperature may affect the scaling behavior. In order to insure that the oxidation of specimens might proceed unperturbed by secondary effects, apparatus was constructed which provided very close control of specimen surroundings, oxidizing atmosphere, and temperature level. The main portion of the equipment consisted of a gas-tight reaction tube made of Nickel-200 whose composition is given in Table 4.

TABLE 4

NOMINAL CHEMICAL COMPOSITION OF NICKEL-200 (33)

Element	Weight Per Cent
Ni+Co	99.4
Mn	0.2
Fe	0.15
Cu,C	0.1
S	0.005

The main portion of the tube was fabricated from a 36 inch length of thick-walled pipe. Two areas of the wall, one on either side of the intended hot zone, were machined away to reduce the axial heat flow. The tube was fitted with a water-cooled brass plug at one end and an external copper cooling coil and brass flange at the other. A mating flange was prepared with provisions for a sighting hole, an alumina push rod, and gas inlet and exhaust. A second gas exhaust was placed near the plugged end of the tube and was used during purging operations. The schematic drawing of Figure 6 and the photograph of Figure 7 show the relative placement of the reaction tube, the furnace, and associated equipment. This system was capable of maintaining a temperature of 1000°C with a short term temperature

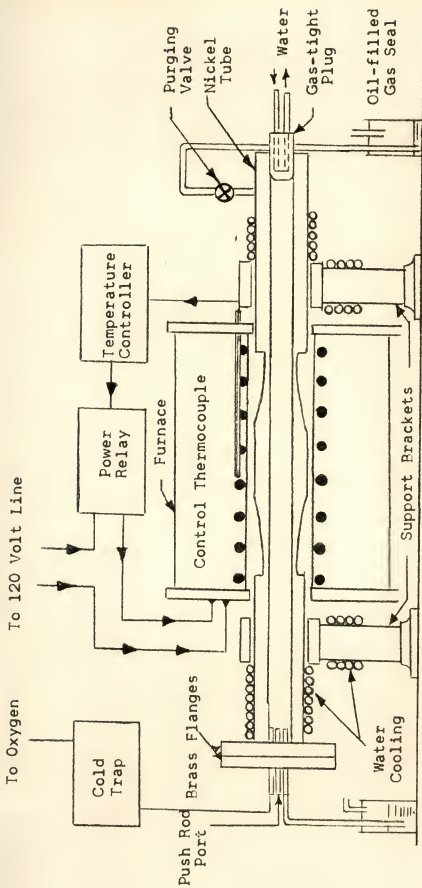


Figure 6: Schematic diagram of the apparatus employed in performing controlled-environmental oxidation experiments at 1000°C.

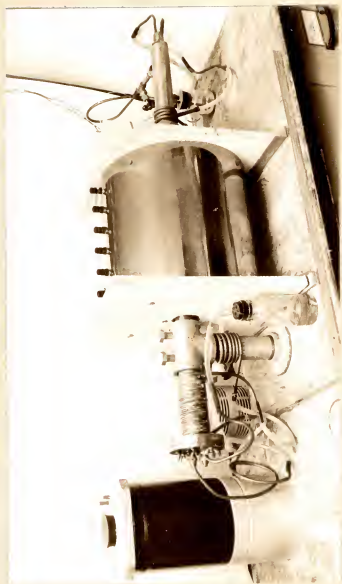


Figure 7: Apparatus employed in performing controlled-environment oxidation experiments at 1000°C.

variation of $\pm 1/10^{\circ}\text{C}$. Long term temperature variations, i.e., over a period of 16 hours, were seldom found to exceed one degree centigrade.

The oxidizing atmosphere was diminished in water vapor content by passing commercial tank oxygen through a copper coil which was immersed in a mixture of dry ice and acetone. Thus, to a first approximation, a specimen within the reaction tube was surrounded by an environment which contained only oxygen gas and nickel oxide.

Prepared specimens were placed in the flanged end of the reaction tube which was sealed by means of a gasket and the mating flange. Cold-trapped oxygen was passed through the system for 45 to 60 minutes prior to the beginning of oxidation. After this purging operation, the capped push rod port was opened and a close fitting alumina rod was inserted. The specimen was then moved into the heated zone of the furnace and the push rod was withdrawn. The port was then quickly recapped and the oxygen flow adjusted to give a nearly static pressure slightly in excess of one atmosphere. Upon completion of oxidation, the specimen was slowly cooled in oxygen by pushing it from the heated zone.

Most of the specimens oxidized in this apparatus were utilized for studies of scale thickness and structure as well as dimensional change. These studies were conducted

at a single temperature - 1000°C . Oxidation times of 4 and 16 hours were employed in studying the behavior of cylinders. In addition, a series of 5 minute oxidation studies were made to determine the effect of residual fabrication stresses on the length change. Supplementary oxidation experiments, ranging in duration from 1 to 64 hours, were also performed; however, the full range of specimen diameters was not employed in these cases.

2.54 Special Experiments

A series of experiments, each involving a small group of specimens, were performed in order to gather additional information concerning the oxidation process. Each of these experiments contained at least one special feature which placed it outside of the scope of oxidation procedures previously discussed.

Special studies of dimensional changes were made in the case of two cylindrical and six flat specimens of differing sizes. In order to minimize possible effects which might arise from residual fabrication stresses or major grain rearrangement, each specimen was annealed in vacuum for 5 minutes at 1000°C prior to oxidation. A portion of the volumetric apparatus, Figure 5, was utilized in this operation. Although the pressure was rather high

during the annealing period (approximately 20 microns) the specimens showed no visual evidence of tarnishing. Each specimen was then electropolished and measured three times.

Five of the above flat specimens were oxidized for 16 hours at 1000°C in the nickel reaction tube furnace. Dimensional changes were then determined. The remaining flat specimen and the two cylindrical specimens were subjected to oxidation under the same conditions; however, their oxidation was interrupted several times in order to determine the dependence of dimensional change upon oxidation time. This technique of interrupted oxidation was employed in order to minimize possible effects of specimen-to-specimen variation.

The ability of the oxidation process to induce dimensional changes was investigated in another manner through the use of helical and right-angle-bend specimens. After initial fabrication, but prior to oxidation, each specimen was annealed in air for 5 minutes in order to relieve forming stresses. Straightening and measuring operations were then performed. Helical specimens were oxidized at 1000°C while bend specimens were oxidized at temperatures ranging from 970°C to 1160°C . Air was used as the oxidant in each case.

The effect of steady loading on scaling behavior was studied at 900°C in a series of oxidation-creep

experiments. Loads, corresponding to axial tensile stresses up to 1000 psi, were applied while the specimen was maintained at the oxidizing temperature. The apparatus used in these experiments is shown schematically in Figure 8. The upper pull rod was secured to the support arm through a universal joint which prevented excessive anaxial loading. After the furnace had reached the oxidizing temperature, the specimen and pull rod assembly were introduced through the top of the quartz furnace tube and centered within it. The loading weights and load pan were then quickly brought into position, coaxial about the lower pull rod, by means of a jackscrew-driven platform and a retaining nut was screwed to the rod end. The load was applied when the test specimen reached proper temperature by slowly lowering the weight-supporting platform. The loading sequence was reversed after 64 hours had elapsed.

The effect of thermal cycling about a mean temperature of 1000°C was also explored. The amplitude and period of the temperature cycle was usually altered by either adjusting the furnace supply voltage or displacing the control thermocouple from its normal position at the center of the heated zone. In one case, a small clock motor was employed to drive the specimen into and out of the hottest portion of the furnace. All specimens used in this study were cylinders of nearly identical diameter.

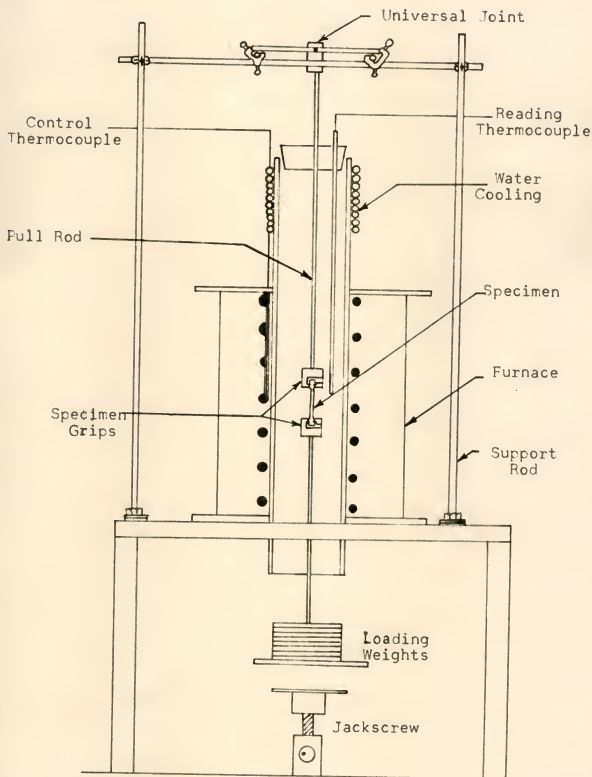


Figure 8: Schematic drawing of the apparatus employed in performing oxidation-creep experiments at 900°C.

Finally, a small number of isolated oxidation experiments were performed under various experimental conditions in order to gain supplementary general information about the scaling process.

2.6 Examination of Oxidized Specimens

Immediately following oxidation, specimens were examined for dimensional changes. Subsequent to this operation the character of the oxide scale was investigated metallographically. In some instances X-ray diffraction and electron microscopy were employed to provide additional information.

2.6.1 Scale Thickness Determinations

In order to determine the thickness of the scale formed during oxidation by metallographic methods, the oxidized specimens were sectioned through a centrally located zone. Cylindrical specimens were sectioned normal to their axes and flat specimens were sectioned normal to their largest surfaces. Spalling of the oxide from the metal during this operation was suppressed by applying a heavy coating of lacquer to the surface prior to cutting. A jewelers handsaw was used to minimize the size of the disturbed area near the cut surface and to reduce the

possibility of accidentally bending the specimens. Subsequent to the sectioning operation, the cut surface of each specimen was adjusted by sanding with metallographic papers. The lacquer coating was then removed with acetone.

Specimens were mounted in red bakelite and were positioned so that their cut surfaces were exposed for examination. A hand-operated hydraulic mounting press made by Buehler Ltd. was used in this operation. A surface suitable for microscopic examination was provided by polishing first with 240, 320, 400, and 600-grit silicon carbide papers, then with 6 and 1 micron diamond, and finally chemically etching the polished surface. The etching process was performed by immersing the polished specimen in a solution containing one volume each of nitric and acetic acids diluted with two volumes of distilled water. A satisfactory immersion time was found to be 3 to 6 minutes with the etching solution at a temperature of 25°C to 30°C. This etchant attacked both the metal and the bakelite, leaving the relatively unaltered oxide clearly delineated. It also provided the metallic nickel with a surface responsive to polarized light.

The scale thickness of each specimen, prepared in the manner described above, was determined by measurements made using a Bausch and Lomb research metallograph. Polarized light was used in this operation primarily because it

afforded a sharp contrast in color which facilitated and improved the accuracy of measurements. The oxide layer which was to be measured appeared as a green band surrounded on one side by red bakelite and bounded on the other by the dark-grey metal.

All measurements were made using the same objective lens and filar eyepiece. The magnification provided was approximately 1000 diameters. A Bausch and Lomb metric stage micrometer was adopted as the length standard for this procedure and the filar eyepiece was calibrated with it. Several independent determinations of scale thickness, usually 18, were made for each specimen. The average value of scale thickness and its associated probable error (50 per cent expectation) were calculated in each case. Since instrument-associated errors are much smaller than the observed probable errors, the latter may be interpreted as an index of the scale roughening.

2.62 Examination of Oxide Grain Structure

Except in the case of either very short-time or low-temperature oxidizing conditions, the oxide grain structure was within the range of resolution of the light microscope. The surface structure of the oxide could be observed in the as-formed (and cooled) condition without resorting to special preparation. This type of examination

was used extensively in the present work as a tool for studying the effects of geometric parameters.

Cross sections of the oxide grain structure were studied using the specimen preparation technique previously described for scale thickness determinations. A single step was added to the process in order to delineate the grain structure of the oxide. This consisted of etching the specimens electrochemically subsequent to the immersion etching process.

The etching process which was developed removed a suitable thickness of oxide but did not cause undue erosion of the metallic portion of the specimens. The electrolyte consisted of one volume each of acetic and hydrofluoric acids in solution with four volumes of distilled water. The specimen served as the cathode and the anode was fabricated from a sheet of type 430 stainless steel. Electrical contact to the specimen was facilitated by carefully drilling a small hole through the side of the bakelite mount to a depth which allowed the bit to penetrate the surface layer of oxide. A wire was passed through this hole to contact the specimen which was positioned beneath the level of the electrolyte. A potential of 10 to 15 volts, applied for a period of 4 minutes with the electrolyte temperature adjusted to approximately 25°C , produced a satisfactory degree of etching.

2.63 Electron Microscope Studies

The microstructure of oxide scales was investigated by applying standard procedures of electron microscopy. Chromium-shadowed collodion replicas of both external surfaces and prepared cross sections of oxidized specimens were examined using a Phillips Model-100 electron microscope. Magnifications of 5,000 to 30,000 diameters were employed to observe the structural features.

2.64 X-ray Diffraction Studies

Several oxidized cylindrical specimens were examined in order to determine whether or not the oxide crystals were preferentially aligned. A technique, developed for this purpose, utilized the Laue camera and accessories of a standard Norelco X-ray diffraction unit.

A nickel-filtered collimated beam of copper radiation, approximately 1 millimeter in diameter was allowed to strike an oxidized specimen perpendicular to an element of its cylinder. The specimen was adjusted so that approximately one-half to two-thirds of the beam was intercepted. Since the oxide grain size was relatively small, the cones of diffracted radiation were moderately well defined. The unintercepted portion of the X-ray beam and 2 or 3 of these resultant cones were recorded with

a flat-plate camera set 20 to 30 millimeters beyond the point of interception of the beam with the specimen.

2.7 Elevated-Temperature Creep Studies

The plastic deformation of both nickel and nickel oxide was investigated at 1000°C using the apparatus shown in Figure 3. The cylindrical specimens used in these experiments were axially compressed at stress levels ranging from approximately 500 to 2000 psi.

Loads were applied through a single lever with a mechanical advantage of approximately $2 \frac{2}{3}$ and were transmitted to the specimens by means of alumina push rods 0.375 inch in diameter. A close-fitting ceramic sleeve enclosing the specimen and push rod ends prevented the assembly from buckling. Length changes, indicated on a sensitive micrometer rigidly attached to the frame of the testing machine, were recorded as a function of time.

A series of calibration experiments, performed with pre-selected loads, were employed to determine the deformation of the testing machine components. The information derived from these tests was used to correct the time-deformation data subsequently obtained in testing nickel and nickel oxide specimens. Values of the second stage creep rate were determined graphically from plots of

corrected deformation versus elapsed time. In all cases, it was assumed that all of the deformation observed took place within the gage section of the specimen.

CHAPTER III

EXPERIMENTAL RESULTS

3.1 Volumetric Experiments

The volume of oxygen consumed by nickel spheres was measured as a function of the length of time that they were exposed to oxygen at 1000°C. This was then normalized to a unit area basis for each of the specimens studied. The normalized quantity, expressed as cubic centimeters of oxygen at a pressure of one quarter atmosphere and a temperature of 21°C per square centimeter of specimen surface was plotted against the square root of the reaction time. Choice of this particular function is based on the normally observed high-temperature parabolic scaling behavior of nickel (33) which, for this type of an experiment, may be expressed in the form:

$$V = K_V t^{1/2} + C. \quad (1)$$

Here, V is the volume of oxygen consumed, K_V is the volume-based parabolic rate constant, t is the duration of oxidation at 1000°C, and C is a constant which accounts for the fact that a certain amount of gas is consumed prior to the time at which the oxidation process follows the parabolic law.

The volumetric data for five spherical specimens of different diameters are presented in Tables 10 through 14 of Appendix 1 and in graphical form as shown in Figures 9 through 13. Two major features of these data are immediately apparent.

1) Each set of data points may be described by two straight line segments, the first of which has a greater slope than the second. If parabolic scaling behavior is assumed, this then indicates that the rate constant changes to some smaller value after the reaction has proceeded to the point indicated by the slope change.

2) There appears to be a specimen-to-specimen variation in both the initial and final rates of reaction in spite of the fact that the oxygen consumption has been normalized to unit surface area. This behavior indicates that the rate of reaction is not dependent on surface area alone.

The rate constants associated with the initial portion of the reaction, denoted as K_{V1} , and those associated with the final portion of the reaction, denoted as K_{V2} , were evaluated for each specimen by determining the slopes of the straight line segments shown in Figures 9 through 13. It was attempted to separate the oxidation behavior of these specimens on the basis of a geometric parameter. The parameter chosen was total curvature, which in the case of

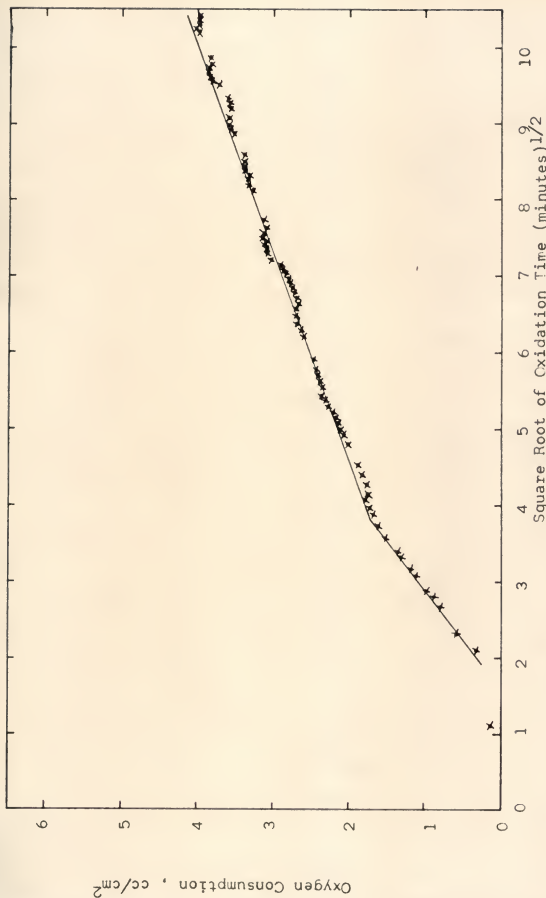


Figure 9: Oxygen consumption as a function of time for a spheroid of curvature 2.75 cm^{-1} oxidized at 1000°C in oxygen at pressure of one-quarter atmosphere.

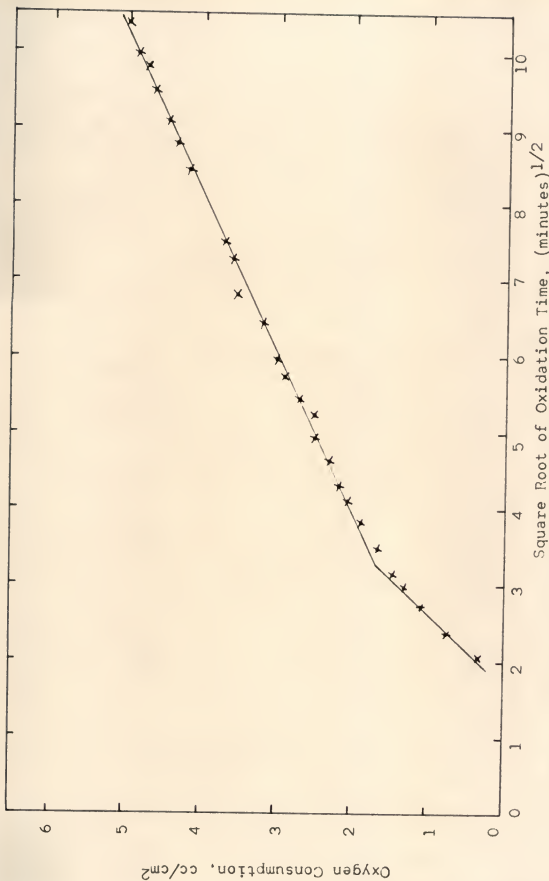


Figure 10: Oxygen consumption as a function of time for a spheroid of curvature 3.40 cm^{-1} oxidized at 1000°C in oxygen at a pressure of one-quarter atmosphere.

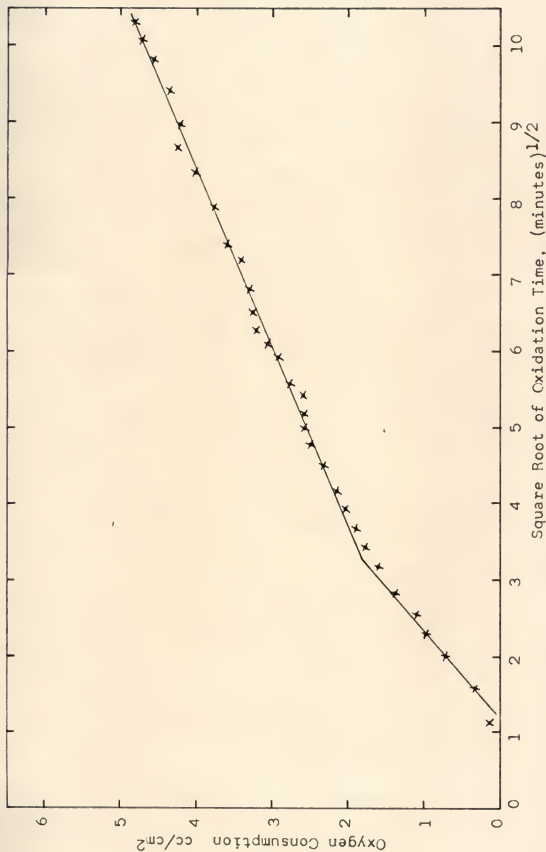


Figure 11: Oxygen consumption as a function of time for a spheroid of curvature 3.99 cm⁻¹ oxidized at 1000°C in oxygen at a pressure of one-quarter atmosphere

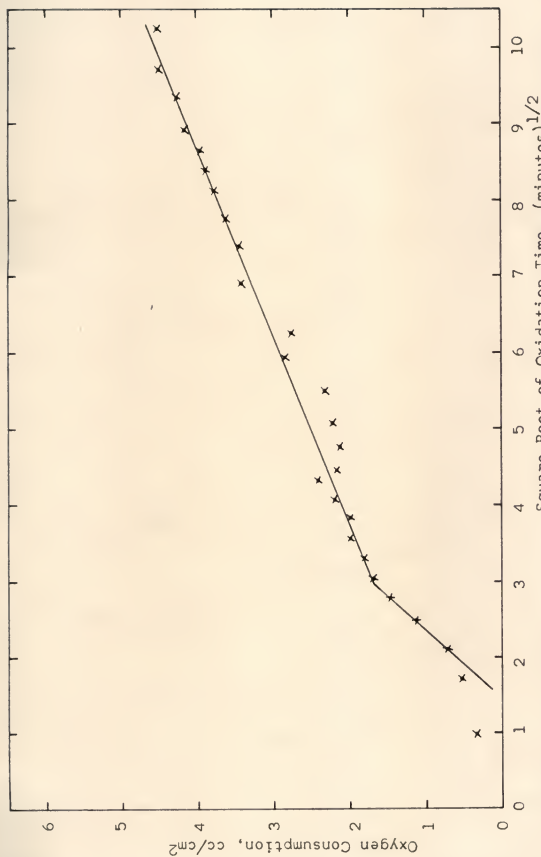


Figure 12: Oxygen consumption as a function of time for a sphere of curvature 4.67 cm⁻¹ oxidized at 1000°C in oxygen at a pressure of one-quarter atmosphere

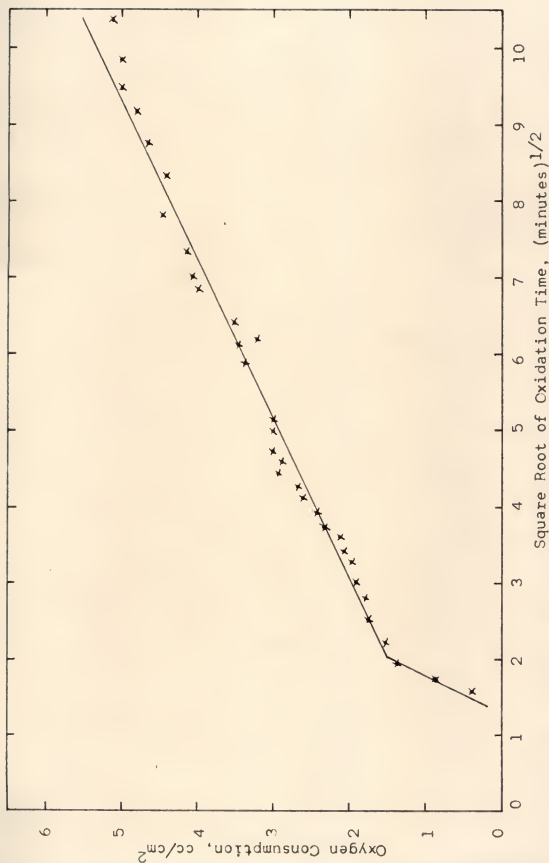


Figure 13: Oxygen consumption as a function of time for a spheroid of curvature 5.23 cm^{-1} oxidized at 1000°C in oxygen at a pressure of one-quarter atmosphere.

a sphere may be defined as two times the reciprocal of the radius.* Plots of the initial and final rate constants as a function of curvature are shown in Figures 14 and 15, respectively. These figures indicate that there is a trend for increasing rate of reaction with increasing curvature. Numerical values of the rate constants are presented in Table 15.

3.2 Preliminary Scale Thickening Experiments

The results of scale thickness determinations for cylindrical specimens oxidized in air at 900°C and 1000°C indicate that, for each series investigated, there is a trend for increasing scale thickness with increasing curvature. It should be noted that in no case does the scale thickness exceed 1/30 of the specimens radius. The curvature in the case of cylinders is defined herein as the reciprocal of their radii.

This dependence of scale thickening on specimen curvature is shown, perhaps most strikingly, by the graph of Figure 16 which was drawn from data for specimens oxidized in the vertical furnace for 16 hours at 1000°C. The decreased value of scale thickness, in this instance

*Throughout this work, total curvature will be defined as follows: curvature = $(\frac{1}{r_1} + \frac{1}{r_2})$, where r_1 and r_2 are principle radii. Convex surfaces will be assigned a positive curvature.



Figure 14: Initial parabolic rate constant as a function of specimen curvature for spheroids oxidized at 1000°C in oxygen at a pressure of one-quarter atmosphere.



Figure 15: Final parabolic rate constant as a function of specimen curvature for spheroids oxidized at 1000°C in oxygen at a pressure of one-quarter atmosphere.

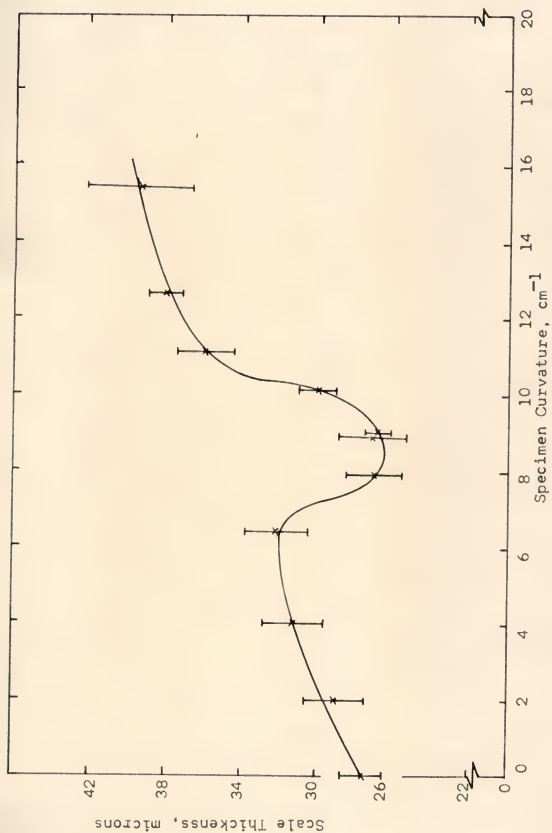


Figure 16: Scale thickness as a function of curvature for cylindrical specimens oxidized in air at 1000°C for 16 hours.

near the midrange of curvatures investigated, was observed to some extent in each of the series of specimens investigated. Its character was, however, found to be dependent on the particular conditions of oxidation. For example, specimens oxidized in the same furnace at 900°C for 64 hours exhibit a decrease in scale thickening which appears to persist to the highest values of curvature investigated, as shown in Figure 17. The presence of the thickness minimum is less well defined for shorter oxidation times as may be seen by comparing the curve of Figure 17 with that of Figure 18, the latter representing specimens oxidized for 16 hours under otherwise identical conditions. It should be noted that simple parabolic growth of the scale is not being evidenced; for if it were, there would be a two-to-one relationship in the thicknesses of scales formed for the case of Figures 17 and 18 - an effect which is not observed.

Further evidence for seemingly anomalous behavior is seen in the comparison of the thickness-curvature graphs of Figures 16 and 19 representing the results of 1000°C oxidation in air for 16 and 64 hours respectively. In spite of the difference in environmental conditions under which each series of specimens was oxidized, one would expect that there should have been approximately twice as much scale formed during 64 hours as there was during 16 hours.

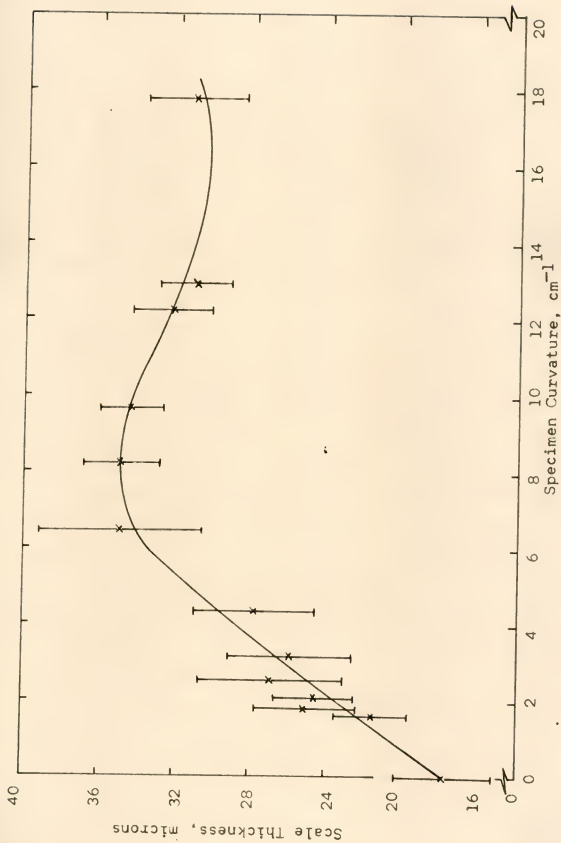


Figure 17: Scale thickness as a function of curvature for cylindrical specimens oxidized in air at 900°C for 64 hours

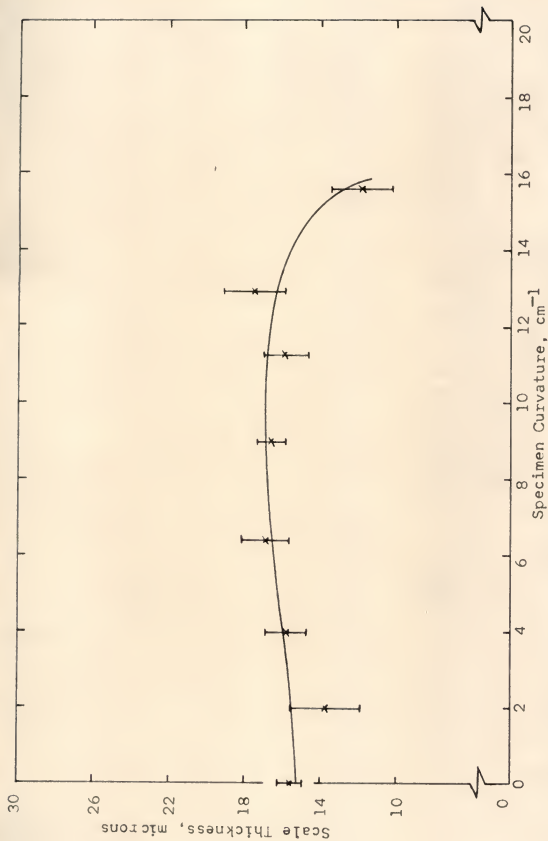


Figure 18: Scale thickness as a function of curvature for cylindrical specimens oxidized in air at 900°C for 16 hours.

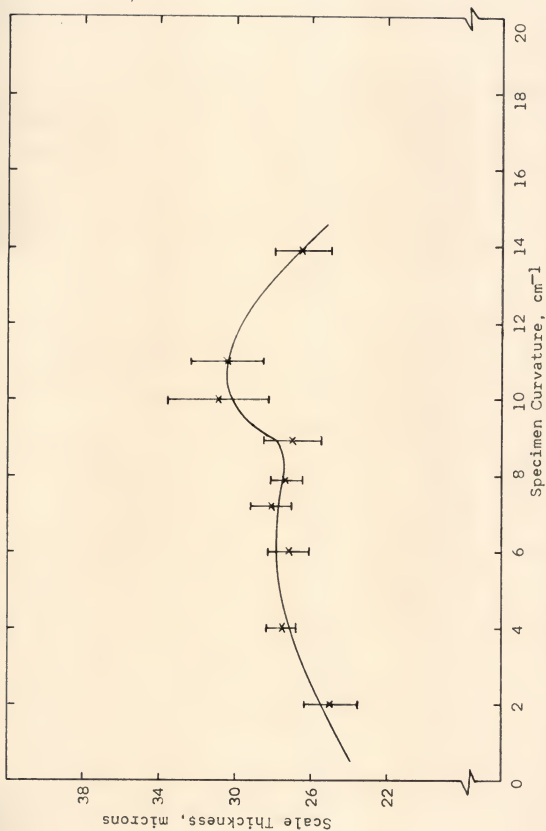


Figure 19: Scale thickness as a function of curvature for cylindrical specimens oxidized in air at 1000°C for 64 hours.

It is readily seen that this is not the case and it appears that either oxidation is not proceeding by a parabolic growth mechanism or seemingly minor changes in environment are drastically modifying the oxidation process.

All flat specimens, of course, have zero curvature. The sensitivity of the scale thickening process to curvature, found in the case of cylindrical specimens, suggested that some parameter be devised to test the effect of the size of flat specimens on their scaling behavior. It was arbitrarily decided that the ratio of scale thickness to original cross-sectional area provide the desired analog. Thus, reciprocal sheet thickness was chosen to replace curvature in the case of flat specimens. Plots based on this parameter are shown in Figures 20 and 21 for 16-hour air oxidation at 1000°C and 64-hour air oxidation at 900°C respectively. These graphs indicate that as the sheet thickness is diminished the scale thickness also decreases, at least initially. This is in contrast to the trend for increased scale thickness with decreasing specimen size observed in the case of cylindrical specimens. The curves of Figures 16 and 20 are superimposed and presented in Figure 22 by employing a common size parameter. In the case of cylindrical specimens this parameter is the curvature while for flat specimens it is the reciprocal thickness. The curves of Figures 17 and 21 are similarly superimposed

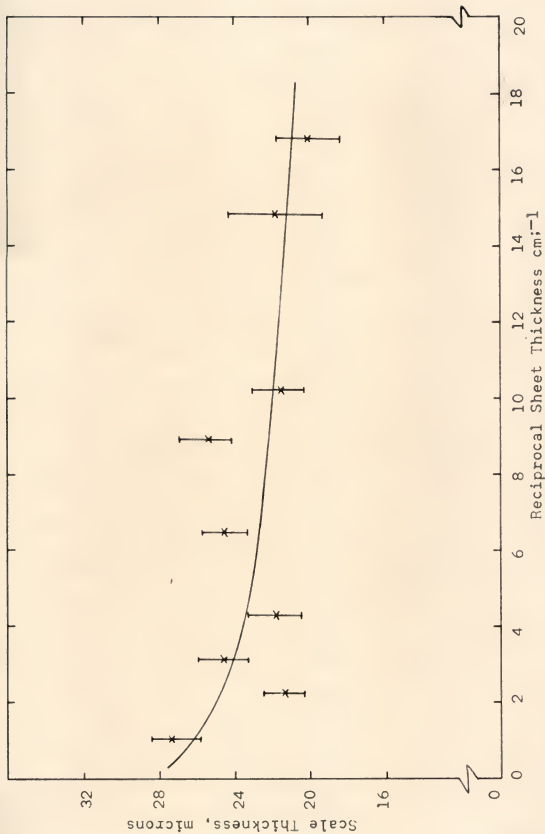


Figure 20: Scale thickness as a function of specimen thickness for flat specimens oxidized in air at 1000°C for 16 hours

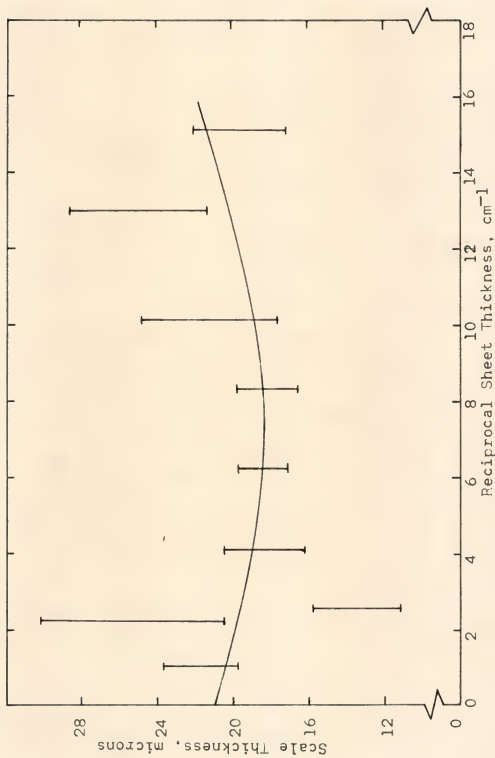


Figure 21: Scale thickness as a function of specimen thickness for flat specimens oxidized in air at 900°C for 64 hours.

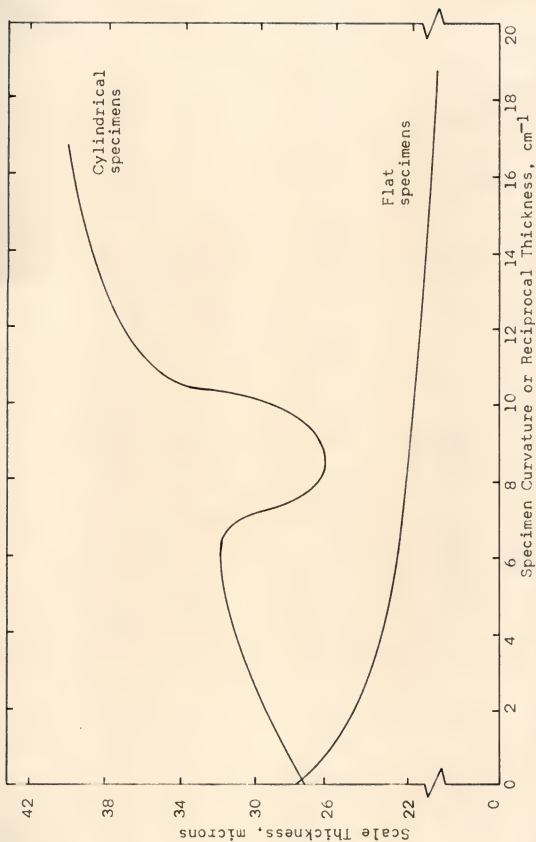


Figure 22: Scale thickness as a function of specimen size for cylindrical and flat specimens oxidized in air for 16 hours at 1000°C.

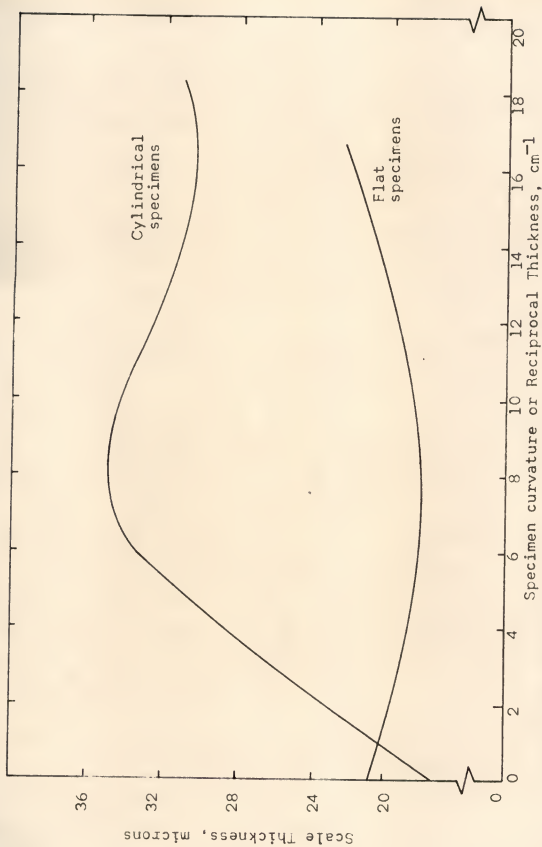


Figure 23: Scale thickness as a function of specimen size for cylindrical and flat specimens oxidized in air for 64 hours at 900°C.

and the result is shown in Figure 23. Both superpositions clearly demonstrate that, when identical oxidizing environments are employed, cylindrical specimens form thicker scales than do flat specimens. The scale thickness data of Figures 16 through 21 are presented in Tables 16 through 21, respectively.

3.3 Scale Thickening in a Controlled Environment

Two series of cylindrical specimens having various curvatures were oxidized in dried oxygen at 1000°C using the nickel reaction tube furnace. The results of scale thickness determination for oxidation times of 4 and 16 hours are presented graphically in Figures 24 and 25 respectively. The general features of these curves indicate the same trends cited earlier for air oxidation studies. The scaling behavior again appears to deviate from that which would be predicted by the parabolic law and there is a trend for increasing scale thickness with increasing curvature.

The 16-hour data, Figure 25, exhibit a region of decreased scale thickening near the midpoint of the range of curvatures investigated as did the specimens oxidized for 16 hours in air, Figure 16. Comparison of these figures indicates that the amount of scale formed in oxygen was, however, only approximately one-half that which was formed in air. This fact is in direct opposition to the known pressure dependence of the scaling rate of

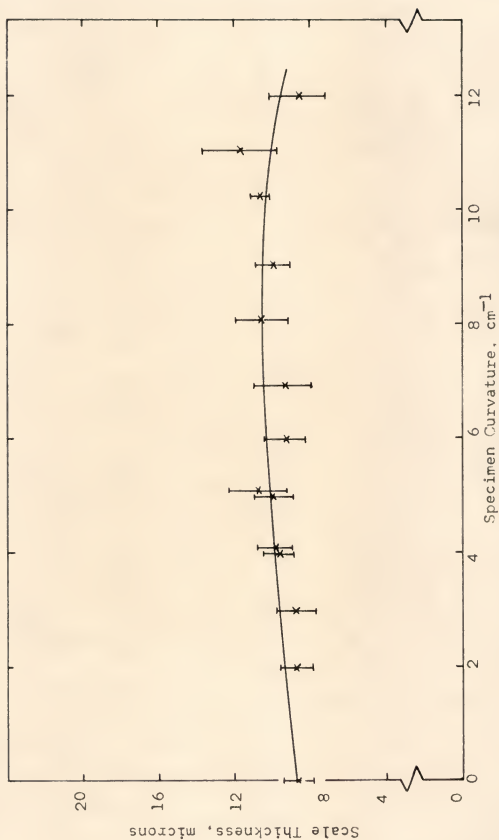


Figure 24: Scale thickness as a function of curvature for cylindrical specimens oxidized in dried oxygen at 1000°C for 4 hours

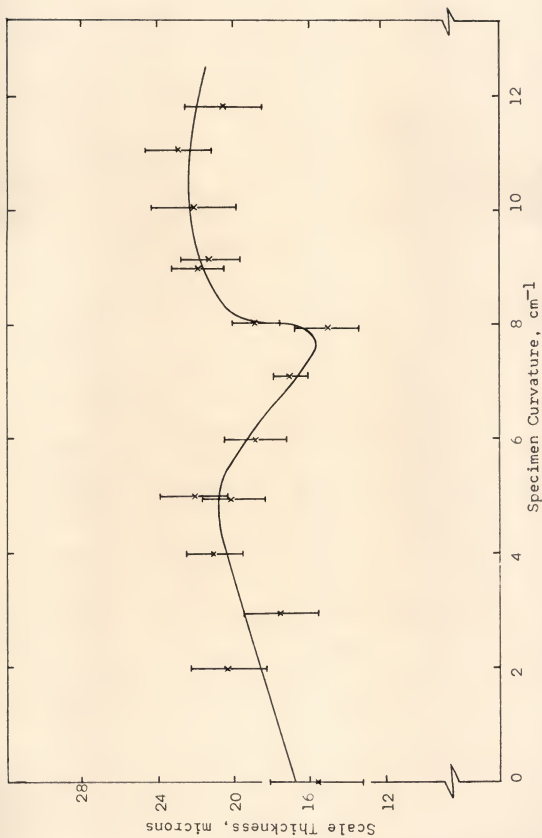


Figure 25: Scale thickness as a function of curvature for cylindrical specimens oxidized in dried oxygen at 1000°C for 16 hours

nickel which on both theoretical and experimental grounds should increase with increasing oxygen pressure (39).

Thus while the qualitative behavior is similar, there is evidently some environmental parameter, other than oxygen pressure and temperature, which plays a major role in the scaling behavior.

Cylinders having curvatures of approximately 0, 4, 8, and 12 cm⁻¹ were oxidized in the nickel tube furnace at 1000°C for various times up to 64 hours. The scale thicknesses were determined and plotted against the square root of oxidation time. The results of these determinations are shown graphically in Figures 26 through 29, and are summarized in Figure 30. It is seen that as the curvature is increased, the specimens initially oxidize at a higher rate and deviate from the initial behavior earlier. The specimens apparently cannot recover from these initial deviations to assume their original rate; however, specimens of the highest curvature tested could apparently recover enough to thicken at an average rate greater than that of specimens of lower curvature.

The unusual type of non-parabolic scale thickening just cited aids in understanding the character of the data shown in Figures 24 and 25. If we consider a three-dimensional model of the data shown in Figures 24 through 30, then each of the graphs may be thought of as a specific

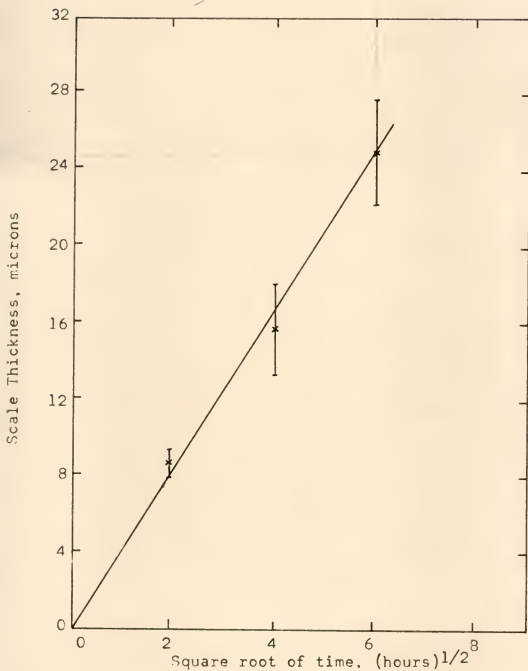


Figure 26: Scale thickness as a function of time for specimens of curvature 0 cm^{-1} oxidized at 1000°C

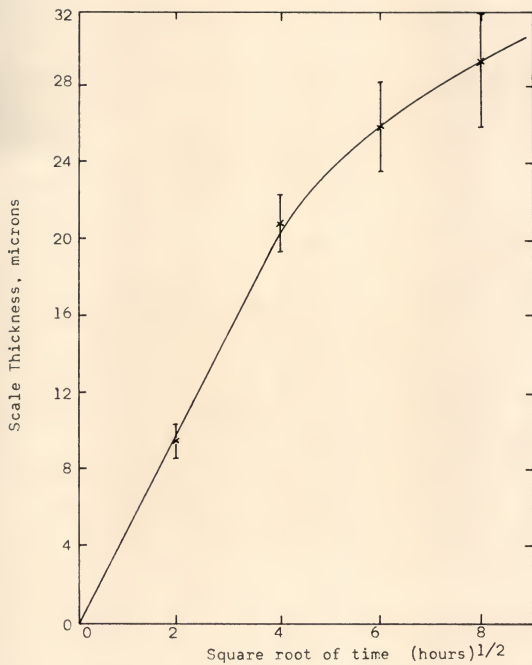


Figure 27: Scale thickness as a function of time for specimens of curvature 4cm^{-1} oxidized at 1000°C .

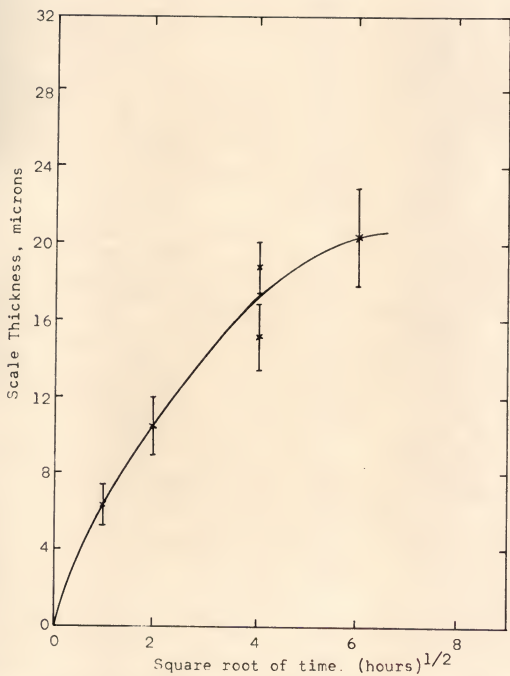


Figure 28: Scale thickness as a function of time for specimens of curvature 8 cm^{-1} oxidized at 1000°C .

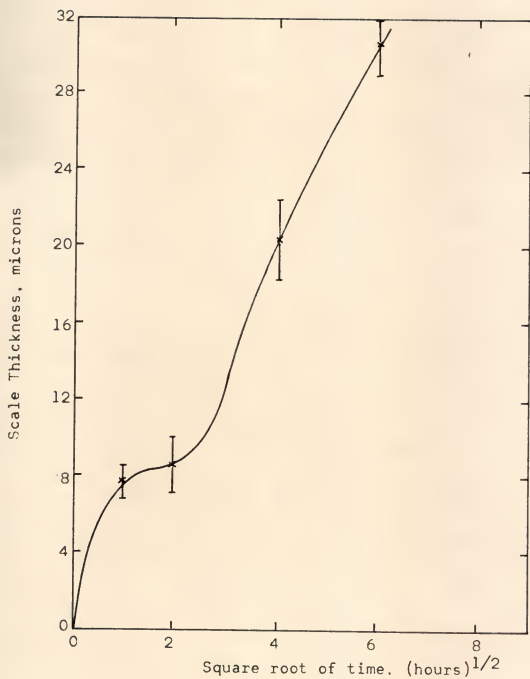


Figure 29: Scale thickness as a function of time for specimens of curvature 12 cm^{-1} oxidized at 1000°C .

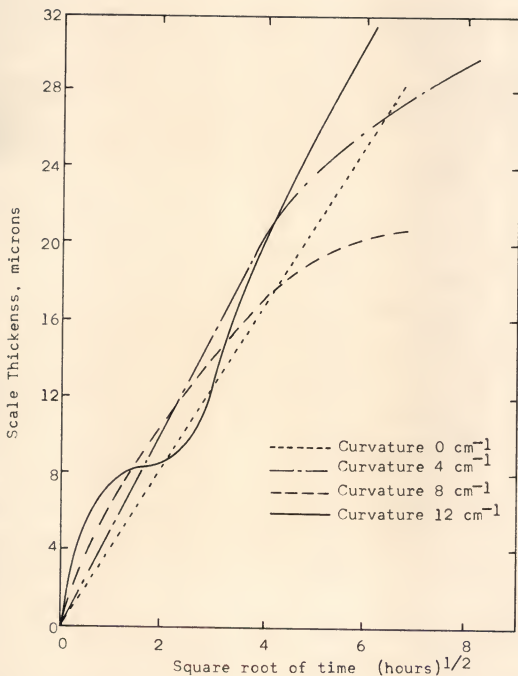


Figure 30: Scale thickness as a function of time for specimens of curvature 0, 4, 8, and 12 cm⁻¹ oxidized at 1000°C.

plane cut through a special surface. This surface is contained in the space whose coordinates are: scale thickness, specimen curvature, and square root of the oxidation time. Figure 31 shows a schematic representation of the surface and its associated sections. From this model it is seen that the curvature-thickness behavior and the time-thickness behavior are interdependent. Thus, the former behavior may be readily explained if reasons for the latter behavior are understood.

A single group of five specimens in the form of flat plates was oxidized for 16 hours at 1000°C in the nickel tube furnace. Measurements of scales indicated a trend for decreasing specimen thickness as shown in Figure 32. This is the same as the trend found earlier for specimens oxidized in air. It was noted that the thickness of scale formed on flat specimens was generally less than that produced on cylindrical specimens oxidized under the same conditions, while the irregularity of the metal-oxide interface was more pronounced in the case of flat specimens.

The values of scale thickness produced during oxidation in the controlled environment apparatus are presented in Tables 22 through 24.

3.4 Scale Thickening Behavior of Hollow Cylinders

Two oxidation experiments were performed using specimens in the form of hollow cylinders. One group of specimens was oxidized in stagnant air at 900°C for 64

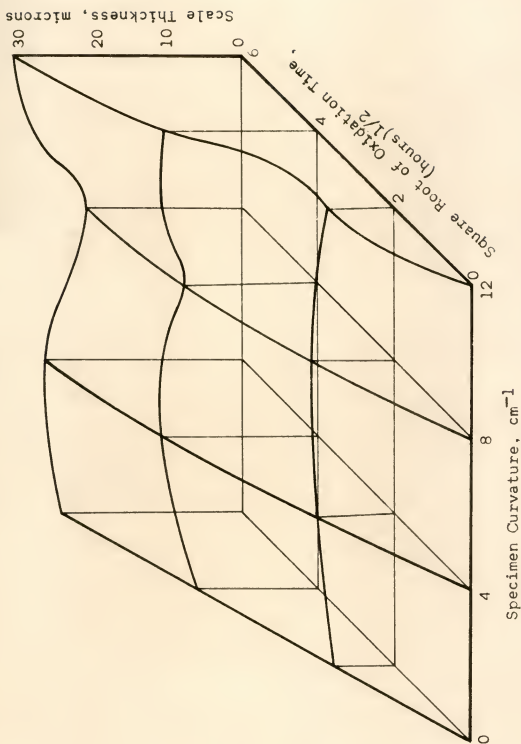


Figure 31: Schematic representation of the surface developed in scale thickness-specimen curvature - oxidation time space by oxidation at 1000°C in dried oxygen.

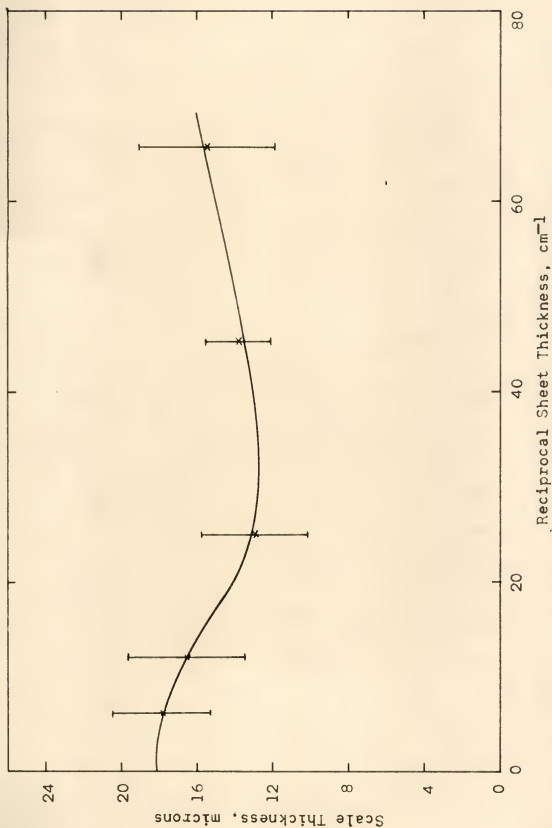


Figure 32: Scale thickness as a function of specimen thickness for specimens oxidized in dried oxygen at 1000°C for 16 hours.

hours, the other in dried oxygen at 1000°C for 36 hours. Measurements of the thicknesses of the resulting scales are presented in Table 5.

TABLE 5
SCALE THICKNESSES DEVELOPED ON HOLLOW CYLINDERS

Curvature*, cm^{-1}	Scale Thickness, microns	
	900°C	1000°C
2.14	20.9 ± 1.6	17.6 ± 1.0
1.81	26.6 ± 1.6	15.4 ± 0.8
1.64	24.6 ± 2.8	18.2 ± 1.6
-2.07	21.3 ± 0.7	22.4 ± 1.8
-2.98	18.8 ± 1.9	29.0 ± 2.6
-6.10	18.0 ± 0.9	24.9 ± 3.7

The data of Table 5 indicate that while the thickness of scale formed on convex surfaces is greater than that formed on concave surfaces at 900°C, the relationship is reversed for those specimens oxidized at 1000°C.

*Negative values of curvature indicate (concave) internal surfaces.

3.5 Dimensional Changes as a Result of Oxidation

Several specimens, in the form of solid right-cylinders, were oxidized at 1000°C in one atmosphere of oxygen using the nickel reaction-tube furnace. Subsequently they were inspected for dimensional changes. A series of specimens was oxidized for 5 minutes in order to determine the magnitude of the effect that residual stresses or other peculiarities of the material might have on the dimensional stability of the specimens. The results of these measurements are shown graphically in Figure 33. They suggest that this material possesses a rather complex system of residual stresses. Some uncertainty in the data is to be expected due to both specimen-to-specimen variation and, especially for specimens of smaller diameter, the difficulty associated with producing specimens which are truly coaxial with the as-received stock.

Lengths were also measured for specimens prepared and oxidized in the same manner with the exception that oxidation times were in excess of 5 minutes. These data are shown in Figure 34 with the curve for the 5-minute oxidation data superimposed. The major conclusion to be drawn from this figure is that specimens oxidized in excess of 5 minutes tend to increase in length due to oxidation if their diameter is smaller than that associated with a

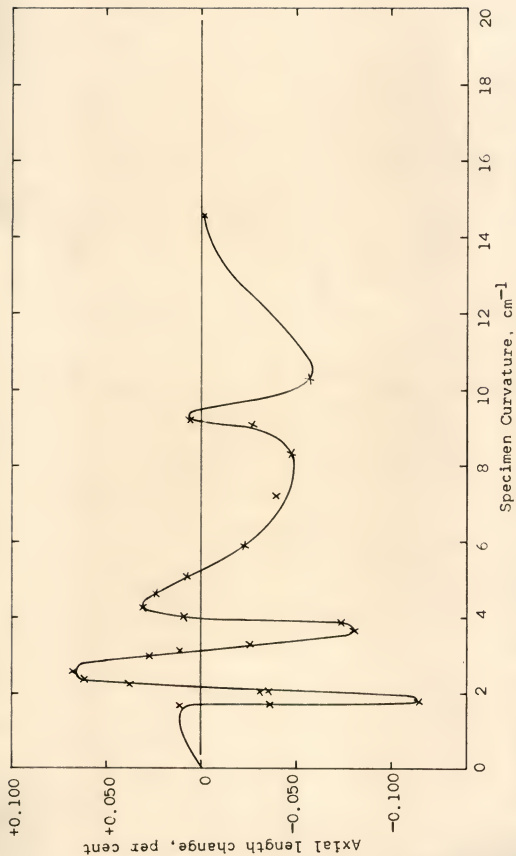


Figure 33: Axial length change as a function of curvature for cylindrical specimens oxidized in dried oxygen at 1000°C for 5 minutes.

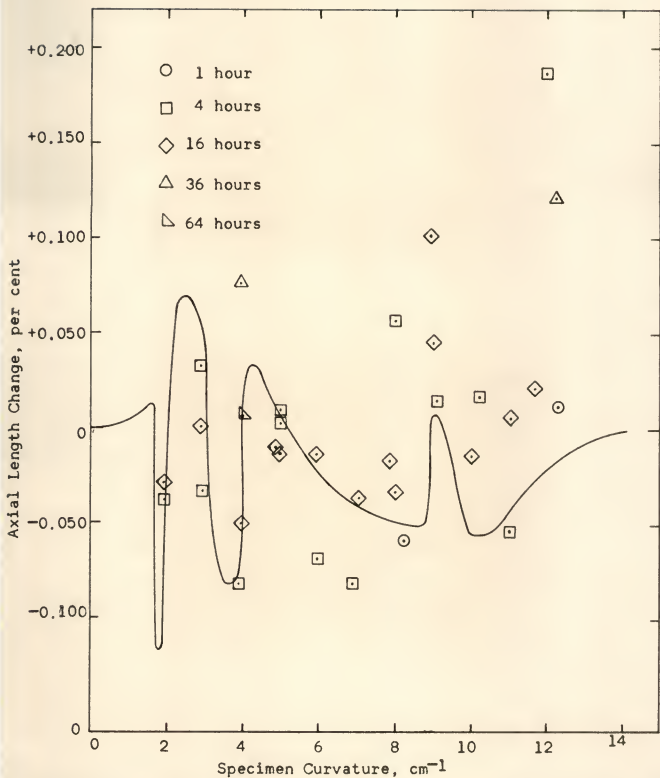


Figure 34: Axial length change as a function of curvature for cylindrical specimens oxidized for various times in dried oxygen at 1000°C. Solid curve represents 5 minute data of Figure 33.

curvature of approximately 7 cm^{-1} , while specimens of larger diameter do not exhibit such behavior. The lack of uniformity in the data for specimens of smaller diameter suggests that some differences in specimen fabrication or preparation may be providing a major influence.

In order to avoid this source of error, two cylindrical specimens were annealed in vacuum and then subjected to interrupted oxidation at 1000°C . Length measurements were carefully performed before and after each oxidation period. The results of these measurements are shown in Figures 35 and 36 for cylindrical specimens of curvature 6 and 8 cm^{-1} respectively. Subsequent to initial fluctuations in length, the specimens exhibited a roughly parallel behavior, first elongating as oxidation progressed and later decreasing in length. The onset of the length decrease apparently occurs earlier in time for the specimen of lower curvature. Elongation data for both continuous and interrupted oxidation studies are presented in Tables 25 through 27 of Appendix 1.

A series of vacuum annealed flat specimens was also monitored for dimensional change as a result of oxidation at 1000°C for 16 hours. The results of this experiment are given in Table 6.

The data indicate that the elongation of these specimens tends to increase as their thickness is decreased. It should be pointed out that there is an uncertainty in length change associated with the tendency for the specimens to buckle during the oxidation process. This effect would

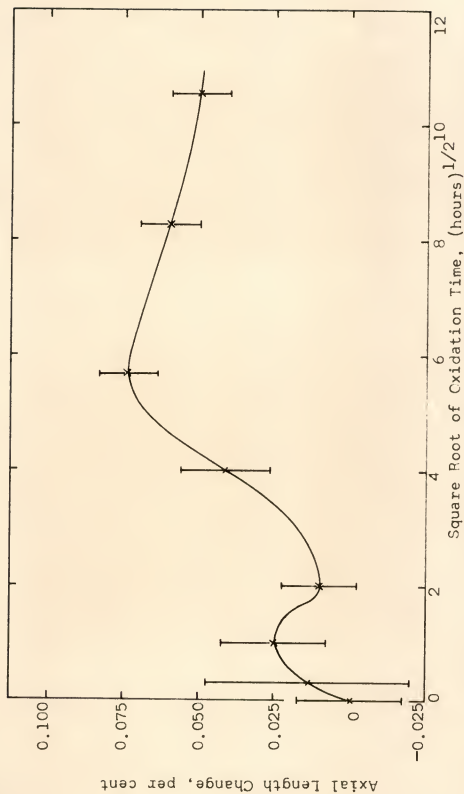


Figure 35: Axial Length change as a function of time for a cylindrical specimen of curvature 6 cm^{-1} subjected to interrupted oxidation at 1000°C .

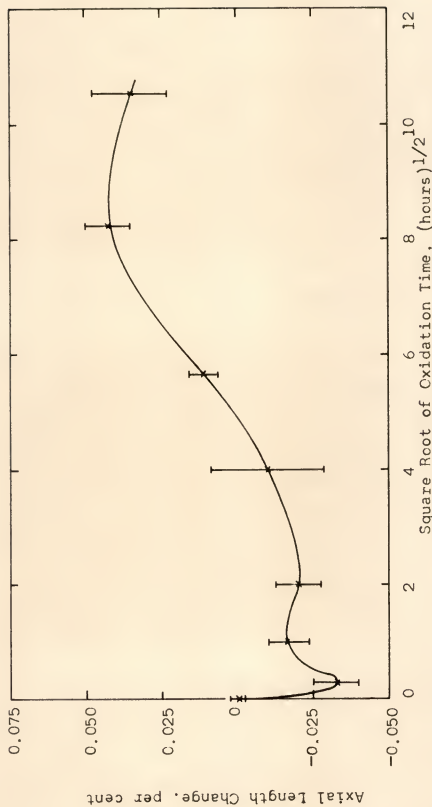


Figure 36: Axial length change as a function of time for a cylindrical specimen of curvature 8 cm^{-1} subjected to interrupted oxidation at 1000°C .

tend to reduce the measured gage length of oxidized specimens, especially in the case of thin sheets. The trend for increasing length change with decreasing specimen thickness, appears to persist in spite of this fact. However, some of the irregularity in the data should probably be associated with the buckling phenomenon.

TABLE 6

LENGTH CHANGE OF FLAT SPECIMENS RESULTING FROM OXIDATION
AT 1000°C FOR 16 HOURS

Specimen Thickness (inch)	Length Change (Per cent)
0.0322	+ 0.119 \pm 0.020
0.0157	+ 0.084 \pm 0.020
0.0087	+ 0.177 \pm 0.020
0.0060	+ 0.137 \pm 0.020

Since small dimensional changes were observed to result from oxidation of relatively massive specimens, it was felt that larger effects could be observed if the specimen size was reduced so that the thickness of the metal and the oxide were more nearly equal. Specimens used to test this concept were fabricated from thin sheet by forming it into the shape of helices and right-angle bends.

Helical specimens, fabricated from 0.0065 inch nickel sheet and then annealed, were oxidized at 1000°C in air. The deformations resulting from this treatment are given in Table 7.

TABLE 7

DIMENSIONS OF HELICAL SPECIMENS BEFORE AND AFTER OXIDATION

Specimen	External Diameter (inch)	Length (inch)	Number of Turns
#1 - Before oxidation	0.2054	1.7461	2
#1 - After 115 minutes	0.2045	1.7461	2
#2 - Before oxidation	0.0910	3.4305	6.5
#2 - After 1255 minutes	0.0880	3.4361	6.9

The data of Table 7 indicate that the helical specimens appear to "wind-up" during oxidation. In both cases the external diameter was decreased and, for the specimen oxidized the longer time, the number of turns and the length were observed to increase.

A second experiment was conducted using a right-angle bend specimen fabricated from 0.0065 inch flat stock formed on a mandril 0.099 inch in diameter. This

specimen was oxidized in air by hanging it in a vertical furnace which was controlled at 1160°C . In this position, the angle of the bend should have increased if the specimen experienced only the effect of gravity. Inspection of the specimen at selected intervals of time over a period of 30 hours, however, indicated that the angle continuously closed. Measurements of the specimen showed that the degree of closure was approximately proportioned to the square root of oxidation time, as is illustrated in the graph of Figure 37.

The results of this experiment and the preceding one, though qualitative in nature, indicate that sizeable stresses are acting in the region of the scale layer. In both cases, though the specimens were thin, the thicknesses of scale developed were less than one-tenth that of the metal.

Two groups of right-angle bend specimens, fabricated from 0.0065 and 0.0035 inch sheet stock, were formed on mandrills of pre-selected diameter. After annealing these specimens were oxidized for approximately 2 hours at 1100°C in stagnant air. The results of this test indicated that thinner specimens and smaller bend radii favor closure of the angle. Some specimens, having bend radii larger than approximately 0.125 inch, exhibited

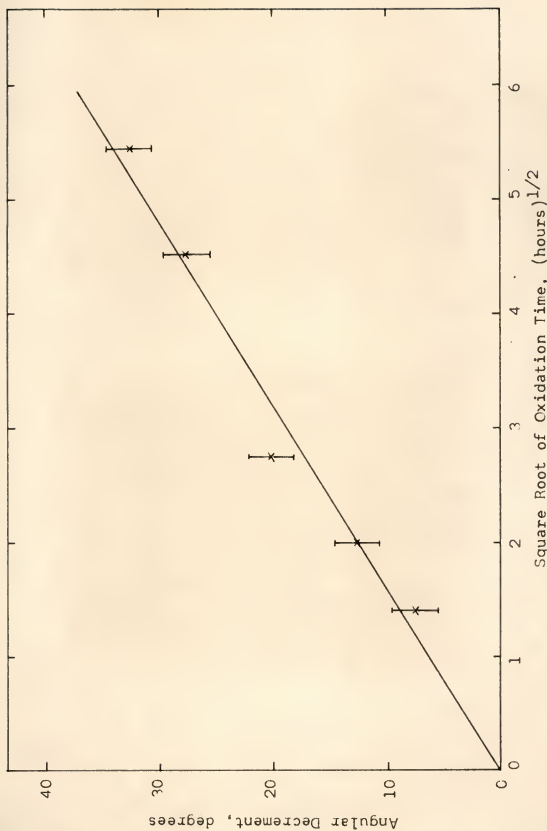


Figure 37: Closure of right-angle bend specimen as a function of oxidation time in air at 1160°C

a widening of the angle upon oxidation. This effect is thought to be due to creep at the oxidation temperature induced by gravity. Flat control specimens which were hung vertically and oxidized with those mentioned above did not show any evidence of bending.

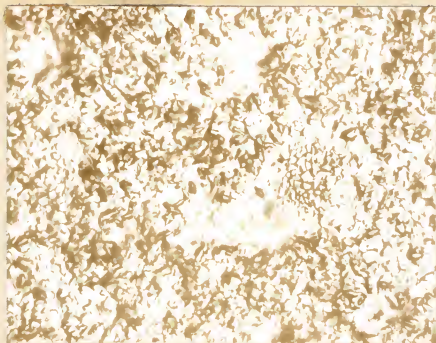
3.6 Oxide Microstructure

Metallographic examination of oxidized specimens indicated that the microstructures of the scales formed were strongly dependent upon the nature of the oxidizing environment. For the sake of clarity, the results of these examinations are grouped into divisions within which the environment is approximately constant and the specimen geometry is used as a testing parameter.

Throughout this presentation, photomicrographs of external oxide surfaces developed on cylindrical specimens are oriented such that the cylindrical axis is parallel to the figure title. Photomicrographs of oxidized surfaces of flat specimen and electron photomicrographs are presented without specific correlation between principle directions of the specimen and the text.

3.6.1 Preliminary Experiments-Vertical Furnace

Photomicrographs of cylindrical specimens oxidized in air for 16 hours at 900°C are shown in Figures 38 through 40. The surface structure of the oxide formed on a specimen of approximate curvature 2 cm^{-1} is shown at two elevations in Figure 38. The upper photograph illustrates the grain structure of the outermost portion of the oxide scale while the lower one, taken with the focal plane positioned approximately 6.6 microns beneath the outermost



(a)

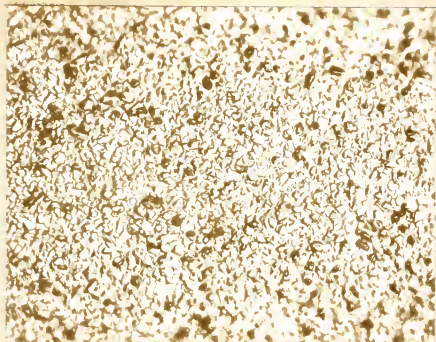


(b)

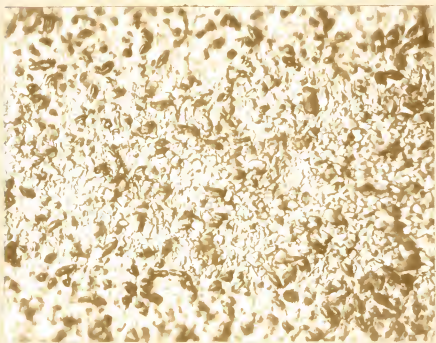
Figure 38: Photomicrographs of the external surface of the scale formed on a cylindrical specimen of curvature 2 cm^{-1} oxidized for 16 hours at 900°C . Focal plane at outermost surface (a) and 6.6 microns beneath it (b). Magnification 500x.

surface, shows a much finer grain size. It is not believed that this structural difference is due to local exfoliation of the scale; but rather, that both of these surfaces, separated by about one-half of the average thickness of the scale, coexisted at the oxidizing temperature. The upper photograph shows, in addition to the angular grains, several dark regions having light, acicular centers. These are apparently grain segments, roughly in the form of prisms or pyramids, which protrude above the general level of the microstructure. Microscopic examination shows that these features are bounded by curved surfaces and do not have the angular character of the remainder of the grain structure.

Figure 39 illustrates the grain structure developed on specimens of approximate curvatures 9 and 13 cm⁻¹. Comparison with Figure 38 shows that specimens with higher curvatures tend to develop grain facets more nearly tangent to the cylindrical surface giving the impression that the metal surface is more completely covered by oxide. The density and size of protrusions is seen to first decrease and then increase as the curvature is increased. The photomicrograph of Figure 40 shows a cross section of the same specimen illustrated in Figure 38. It illustrates



(a)



(b)

Figure 39: Photomicrographs of the external surface of the scale formed on cylindrical specimens of approximate curvature 9 cm^{-1} (a) and 13 cm^{-1} (b) oxidized for 16 hours at 900°C . Magnification 500x.



Figure 40: Photomicrograph of the cross section of the scale formed on a cylindrical specimen of curvature 2 cm^{-1} oxidized for 16 hours at 900°C . Electrochemical Etch. Magnification 500x.

that the grain structure is essentially columnar with some columns extending away from the metal beyond their neighbors. The oxide structure appears relatively dense and free from gross mechanical defects such as cracks or fissures. Some of the dark areas within the oxide are undoubtedly due to "pull-outs" resulting from mechanical polishing.

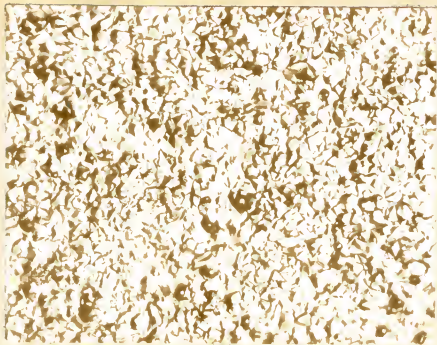
Figures 41 through 44 illustrate the grain structure of the oxide formed on cylindrical specimens having various radii of curvature during oxidation in air for 64 hours at 900°C. The oxide microstructures are in many respects similar to those developed during the 900°C, 16-hour oxidation treatment, especially for those specimens possessing smaller curvatures. There is, however, a general coarsening of the grain size with time as may be seen by comparing the photomicrographs of Figures 38 through 40 with those of Figures 41 through 44. The 64-hour specimens exhibit microstructural features which appear to be more highly dependent upon specimen curvature than was the case for the 16-hour oxidation treatment.

The oxide grain size as well as the size of protrusions from the surface increases sharply with an increase of curvature from approximately 1.6 to 3.2 cm⁻¹. Accompanying this change, there also appears to be an overall increase in the amount of distortion in the structure. In addition, in Figure 41b it may be seen that, at least in some cases,

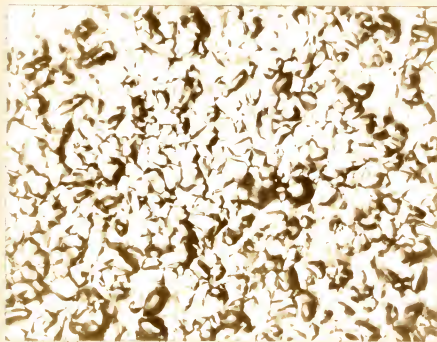
the protrusions are associated with either the boundaries or edges of grains rather than their centers. Upon increasing the specimen curvature in excess of 10cm^{-1} , the grain shape becomes more acicular and the distortion of the structure becomes decentralized with the oxide grains apparently acting in unison as shown in the photomicrograph of Figure 43a. The protrusions, noted for specimens with smaller values of curvature, are now nearly absent. At the highest value of curvature investigated (approximately 19.8 cm^{-1}) the grains take on an even more acicular nature and the protrusions and surface distortion are apparently absent.

The photomicrograph of Figure 44 shows a cross section of the grain structure for a specimen with curvature approximately equal to 2.1 cm^{-1} . Voids have apparently formed within the oxide and seem to be associated primarily with a zone near the metal-oxide interface. The grain structure is again seen to be generally crack-free and columnar in nature with voids in most cases associated with the boundary network. Some oxide appears to have formed beneath the general level of the scale to produce locally thicker regions of scale.

The photomicrographs of Figures 45 through 50 show the grain structure of the scale developed on cylindrical

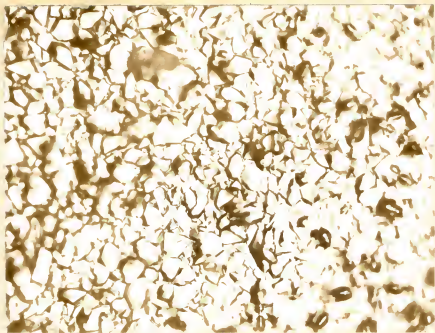


(a)

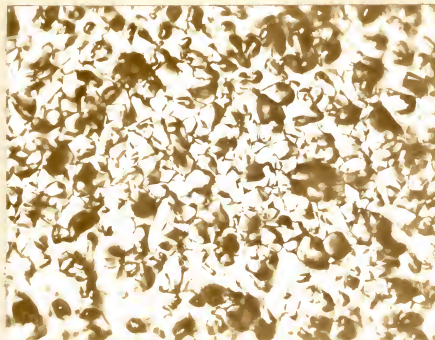


(b)

Figure 41: Photomicrographs of the external surface of scales formed on cylindrical specimens oxidized in air for 64 hours at 900°C. Specimen curvatures 1.6 cm^{-1} (a) and 3.2 cm^{-1} (b). Magnification 500x.



(a)

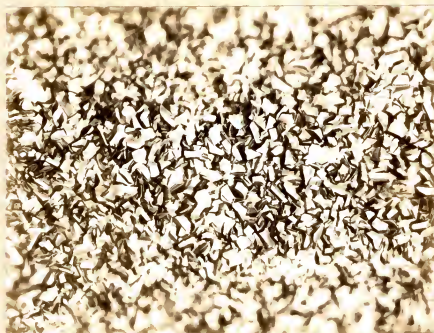


(b)

Figure 42: Photomicrographs of the external surface of scales formed on cylindrical specimens oxidized in air for 64 hours at 900°C. Specimen curvatures 6.5 cm^{-1} (a) and 9.7 cm^{-1} (b). Magnification 500x.



(a)



(b)

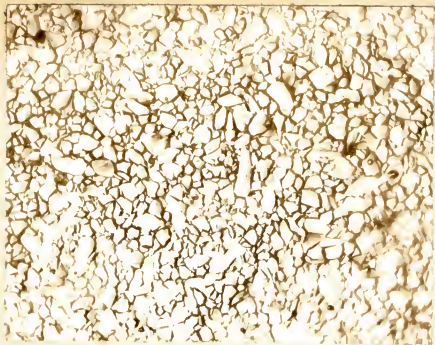
Figure 43: Photomicrographs of the external surface of scales formed on cylindrical specimens oxidized in air for 64 hours at 900°C. Specimen curvatures 12.9 cm^{-1} (a) and 19.8 cm^{-1} (b). Magnification 500x.



Figure 44: Photomicrograph of the cross section of a scale formed on a cylindrical specimen oxidized in air for 64 hours at 900°C. Specimen Curvature 2.1 cm^{-1} . Magnification 500x.

specimens oxidized for 16 hours in air at 1000°C . As in the case of those specimens oxidized for 64 hours in air at 900°C , these exhibit a sharp increase in oxide grain size as the specimen curvature is initially increased followed by the appearance of acicular crystals at higher values of curvature. The initial change in oxide grain size is accompanied by the appearance of high concentration of large oxide protrusions, as shown in Figure 45 for specimens of curvature 2.0 and 4.0 cm^{-1} . A further increase in curvature to a value of 6.4 cm^{-1} , Figure 46a, apparently produces a general distortion of the scale as evidenced by the small region of sharp focus in this photomicrograph. Figures 45b and 46a both illustrate that the favored positions for formation of protrusions are at grain corners and edges, and especially at those regions which seem to involve intimate contact between oxide grains. These figures also show some grain facets which are convex in form.

The slightly rounded angular grains as well as the oxide protrusions disappear as the specimen curvature is increased to 7.9 cm^{-1} . They are replaced by a structure consisting of acicular grains with a large fraction of these facets tangent to the specimen surface, as shown in



(a)



(b)

Figure 45: Photomicrographs of the external surface of scale formed on cylindrical specimens oxidized in air for 16 hours at 1000°C. Specimen curvature 2.0 cm^{-1} (a) and 4.0 cm^{-1} (b). Magnification 500x.

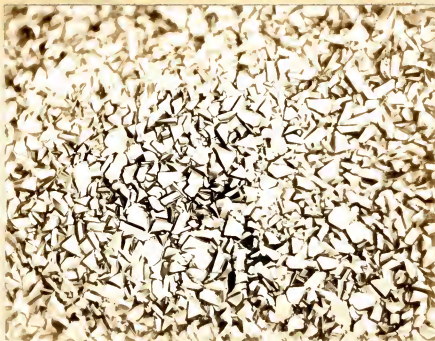


(a)

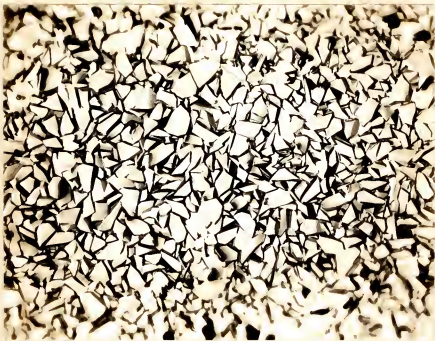


(b)

Figure 46: Photomicrographs of the external surface of scales formed on cylindrical specimens oxidized in air for 16 hours at 1000°C. Specimen curvatures 6.4 cm^{-1} (a) and 7.9 cm^{-1} (b). Magnification 500x.



(a)



(b)

Figure 47: Photomicrographs of the external surface of scales formed on cylindrical specimens oxidized in air for 16 hours at 1000°C. Specimen curvatures 10.2 cm^{-1} (a) and 12.6 cm^{-1} (b). Magnification 500x.



(a)



(b)

Figure 48: Electron photomicrographs of the external surface of the scale formed on a cylindrical specimen of curvature 6.4 cm^{-1} oxidized in air for 16 hours at 1000°C . Magnification 6000x (a) and 4000x (b).



(a)



(b)

Figure 49: Electron photomicrographs of the external surface of the scale formed on a cylindrical specimen of curvature 8.9 cm^{-1} oxidized in air for 16 hours at 1000°C . Magnification 6000x (a) and 7500x (b).



(a)



(b)

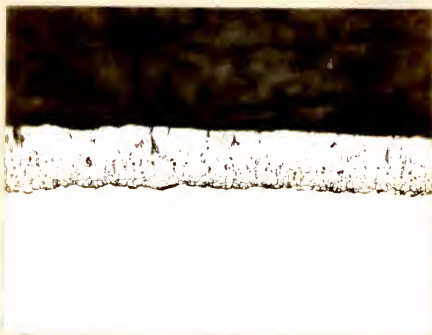
Figure 50: Electron photomicrographs of the external surface of the scale formed on a cylindrical specimen of curvature 15.4 cm^{-1} oxidized in air for 16 hours at 1000°C . Magnification 5000x (a) and 3500x (b).

Figure 46b. This type of structure persists, and further increases in specimen curvature serve only to provide a larger fraction of grain facets tangent to the specimen surface giving the microstructure a "filled-in" appearance. Small protrusions again appear when the external surface is sufficiently "filled-in." This is illustrated in the photomicrograph of Figure 47b which shows the oxide developed on a specimen having curvature 12.6 cm^{-1} .

The surface structure of the scales formed on cylindrical specimens of curvature 6.4, 8.9, and 15.4 cm^{-1} are shown in detail in the electron photomicrographs of Figures 48 through 50 respectively. It is seen that in many cases the crystal facets possess some curvature as may be inferred from the differences in shading on a given facet. These differences are most readily apparent in the electron photomicrographs of Figure 48; a specimen previously cited for possessing a scale with a distorted microstructure. Careful inspection of Figure 48a reveals localized areas of deformation apparently associated with grain-to-grain contact while Figure 48b shows a field of small angular oxide grains partially surrounding a large-grained structure containing a protrusion. This area of mixed grain sizes is not representative of the specimen surface. A comparison of Figures 49 and 50 illustrate the "filling-in" process associated with increasing specimen curvature noted earlier.



(a)



(b)

Figure 51: Photomicrographs of the cross sections of scales formed on cylindrical specimens of curvature 0 cm^{-1} (a) and 2.0 cm^{-1} (b) oxidized in air for 16 hours at 1000°C . Electrochemical etch. Magnification 500x.

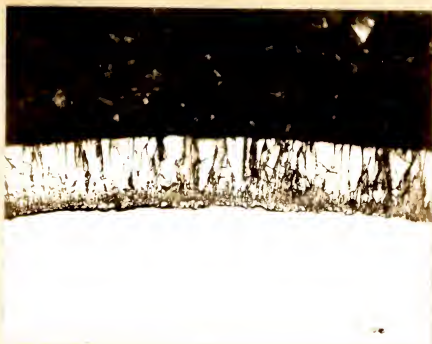


(a)

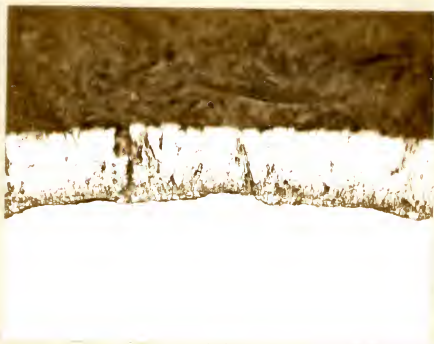


(b)

Figure 52: Photomicrographs of the cross sections of scales formed on cylindrical specimens of curvature 6.4 cm^{-1} (a) and 9.0 cm^{-1} (b) oxidized in air for 16 hours at 1000°C . Electrochemical etch. Magnification 500x.



(a)



(b)

Figure 53: Photomicrographs of the cross sections of scales formed on cylindrical specimens of curvature 12.6 cm^{-1} (a) and 15.4 cm^{-1} (b) oxidized in air for 16 hours at 1000°C . Electrochemical etch. Magnification 500x.

An example of a protrusion arising between two oxide grains is shown in the upper-right portion of Figure 50b.

The cross-sectional structure of the oxide for specimens of various curvature, is illustrated in the photomicrographs of Figures 51 through 53. The grain shape is basically columnar except near the metal-oxide interface where it exhibits a nearly equiaxial structure. As the curvature is increased, the width of the columns becomes greater and the structure becomes less regular due primarily to damage incurred by the polishing operation. Near the midrange of curvatures investigated, circumferential cracking of the oxide is evident while it appears to be absent at either extreme of the series. The onset of severe circumferential cracking was found to coincide with the onset of acicular external oxide grain structure. A longitudinal section of the scale, for the specimen of curvature 15.4 cm^{-1} is shown in Figure 54. Some evidence for crack formation, paralleled to the metal-oxide interface may be seen in the columnar grain structure. Figure 55 is an electron photomicrograph of an electrochemically polished cross section showing details of the columnar oxide grain structure for a specimen having curvature 2.0 cm^{-1} . The fine lines generally appearing nearly parallel to the column axes are residual scratches from the mechanical

polishing operation. The oxide grain boundaries appear as deep grooves, indicating that the electrical properties of the grain boundary regions are much different than those of the surrounding grains.

Figures 56 and 57 provide evidence supporting the contention that blisters form in the scale during the oxidation process rather than as a result of cooling. Both figures indicate that porous blisters formed when the scale was approximately one-third of its final thickness. The shearing surfaces and the intimate contact of the oxide crystals bounding it are evident from inspection of the photomicrographs. There is a tendency for such blister formation to increase with increasing specimen curvature.

It was found that the external surface of the oxide developed a preferred orientation which was determined by X-ray techniques. Figure 58 shows a series of three diffraction patterns. These indicate that a wire texture is present for specimens of curvature 2.0 and 11.1 cm^{-1} while nearly random orientation of the oxide grains prevails for the specimen having curvature 6.4 cm^{-1} . Analysis of these patterns, which result from the $\{111\}$ and $\{200\}$ diffraction cones, indicates that many of the grains have their $\langle 100 \rangle$ directions aligned parallel to the cylinder axis of the specimen.



Figure 54: Photomicrograph of the longitudinal section of the scale formed on a cylindrical specimen of curvature 15.4 cm^{-1} oxidized in air for 16 hours at 1000°C . Electrochemical etch. Magnification 500x.



Figure 55: Electron photomicrograph of the cross section of the scale formed on a cylindrical specimen of curvature 2.0 cm^{-1} oxidized in air for 16 hours at 1000°C . Electrochemical etch. Magnification $5000\times$.

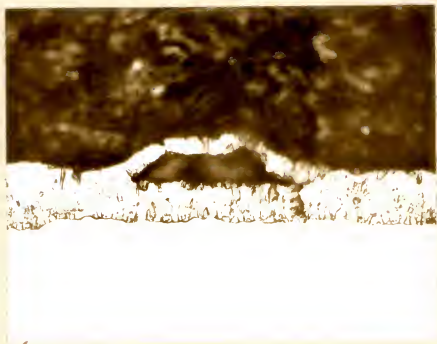
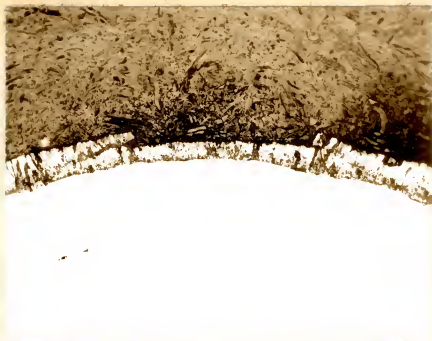


Figure 56: Photomicrograph of the cross section of a scale blister formed on a cylindrical specimen of curvature 6.4 cm^{-1} oxidized in air for 16 hours at 1000°C . Electrochemical etch. Magnification 500x.



(a)

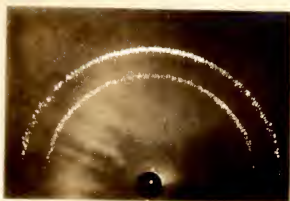


(b)

Figure 57: Photomicrographs of the cross section of a scale blister formed on a cylindrical specimen of curvature 15.4 cm^{-1} oxidized in air for 16 hours at 1000°C . Electrochemical etch. Magnification 250x (a) and 500x (b).

The final series of experiments performed with the vertical furnace employed flat specimens of various thickness. Oxide microstructures, developed as a result of oxidation in air for 16 hours at 1000°C, are shown in Figures 59 through 61. As the thickness of the specimen is decreased, the oxide grain size first decreases and then increases again. The oxide protrusions present on the thickest specimen, Figure 59a, disappear as the thickness of the sheet is diminished and do not reappear except on the thinnest specimens investigated as seen in Figure 61a. This observation infers that the protrusions are formed at the oxidizing temperature. Their favored positions of formation are again seen to be at points of grain-to-grain contact.

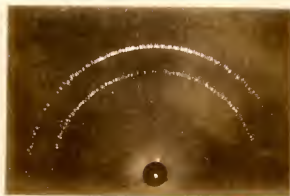
Figure 61b shows a cross-sectional view of the oxide grain structure formed on the thinnest specimen investigated. The grain structure essentially consists of thin columns as opposed to the more fan-like crystals formed on the smallest cylindrical specimen oxidized under identical conditions, Figure 53. In addition, there is no indication of a region of equiaxial crystals near the metal-oxide interface as there was in the case of cylindrical specimens.



(a)

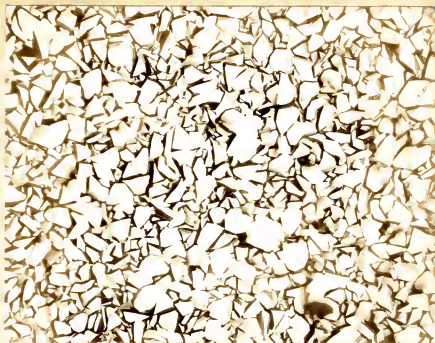


(b)



(c)

Figure 58: X-ray diffraction patterns of scales formed on cylindrical specimens of curvature 2.0 cm^{-1} (a), 6.4 cm^{-1} (b), and 11.1 cm^{-1} (c) oxidized in air for 16 hours at 1000°C . Cylindrical axis parallel to figure titles.



(a)



(b)

Figure 59: Photomicrographs of the external surface of scales formed on plane specimens oxidized in air for 16 hours at 1000°C. Reciprocal thickness 1.2 cm⁻¹ (a) and 3.2 cm⁻¹ (b). Magnification 500x.

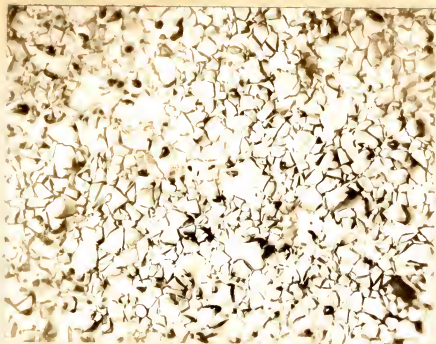


(a)

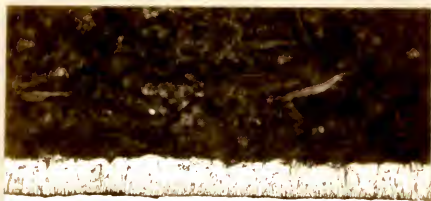


(b)

Figure 60: Photomicrographs of the external surface of scales formed on plane specimens oxidized in air for 16 hours at 1000°C. Reciprocal thickness 6.5 cm^{-1} (a) and 10.2 cm^{-1} (b). Magnification 500x.



(a)



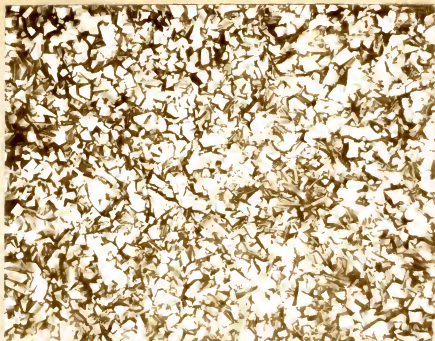
(b)

Figure 61: Photomicrographs of the scale formed on a plane specimen of reciprocal thickness 16.8 cm^{-1} oxidized in air for 16 hours at 1000°C . External surface (a) and cross section (b). Magnification 500x.

3.62 Preliminary Experiments - Horizontal Furnace

The external surfaces of the oxide grain structure formed on cylindrical specimens of various curvature during oxidation in air at 1000°C are shown in Figures 62 through 64. The microstructure is seen to differ radically from that produced by oxidation in the vertical furnace, Figures 45 through 47. In many instances, the grain shape is seen to be highly angular or nearly idiomorphic and there appears to be no evidence of oxide protrusions. As the specimen curvature is increased from 1.0 to 7.2 cm⁻¹ the fraction of grain facets tangent to the surface diminishes giving rise to the effect that the surface of the specimen is less completely covered by oxide. Further increases in curvature produce grains with stepped facets as shown in Figure 63b. For the specimens of highest curvature investigated, the fraction of grains with stepped surfaces diminished, Figure 64, and the microstructure again becomes similar to that produced at lower values of curvature (compare, for example, Figures 64b and 62b). The grain size of the oxide per se appears to be nearly independent of the specimen diameter over the range of curvature investigated.

The electron photomicrograph of Figure 65 shows details of the surface structure, including some grains having stepped facets, for a specimen of curvature 2.0 cm⁻¹.

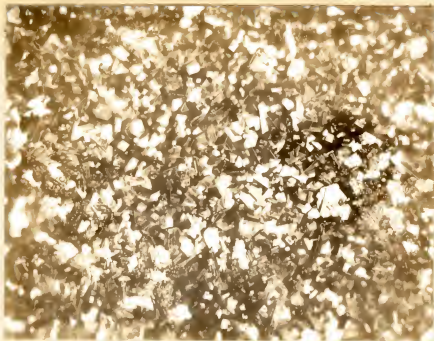


(a)

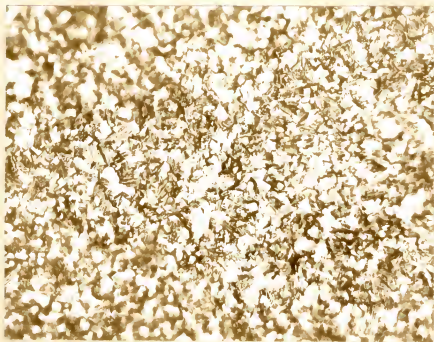


(b)

Figure 62: Photomicrographs of the external surface of scales formed on cylindrical specimens oxidized in air for 64 hours at 1000°C. Specimen curvatures 2.0 cm^{-1} (a) and 6.0 cm^{-1} (b). Magnification 500x.



(a)

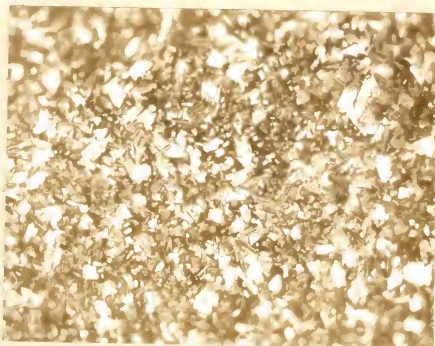


(b)

Figure 63: Photomicrographs of the external surface of scales formed on cylindrical specimens oxidized in air for 64 hours at 1000°C. Specimen curvatures 7.2 cm⁻¹ and 9.0 cm⁻¹ (b). Magnification 500x.



(a)



(b)

Figure 64: Photomicrographs of the external surface of scales formed on cylindrical specimens oxidized in air for 64 hours at 1000°C. Specimen curvatures 11 cm^{-1} (a) and 14.0 cm^{-1} (b). Magnification 500x.

The columnar nature of the grain structure is illustrated in the photomicrograph of the scale cross section shown in Figure 66.

X-ray diffraction patterns of the external surface of the oxide revealed that a wire texture was again present in some of the scales. These patterns, shown in Figure 67, indicate that the $\langle 111 \rangle$ directions of the oxide crystals tend to be aligned parallel to the cylinder axes. This is in contrast to the $\langle 100 \rangle$ wire texture developed on those specimens oxidized in the vertical furnace. It is seen that as the curvature of the specimens is increased, the tendency for alignment alternately increases and decreases.

3.63 Controlled Environment Experiments

The microstructures of the scales formed in the nickel tube furnace on specimens under an atmosphere of dried oxygen at 1000°C differ significantly from those discussed earlier. Surface distortion is almost always present and the oxide grain size is considerably smaller than that of air-formed scales. The specimens used in this portion of the investigation were varied in curvature by steps of 1 cm^{-1} over the range from 2 to 12 cm^{-1} . Curvatures were usually maintained to within ± 2 per cent of the integral value given.



Figure 65: Electron photomicrograph of the external surface of a specimen oxidized in air for 64 hours at 1000°C. Specimen curvature 2.0 cm^{-1} . Magnification 4500x.

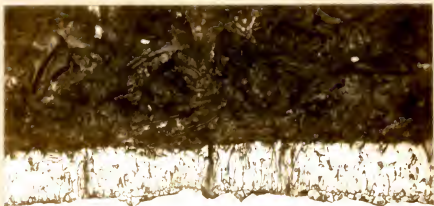
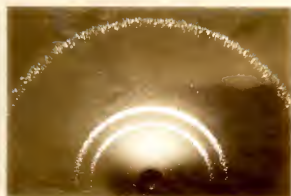
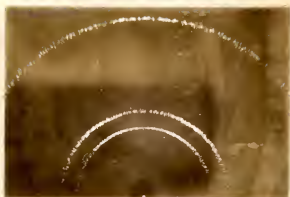


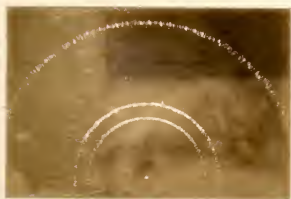
Figure 66: Photomicrograph of the cross section of the scale formed on a cylindrical specimen of curvature 6.0 cm^{-1} oxidized in air for 64 hours at 1000°C . Magnification 500x.



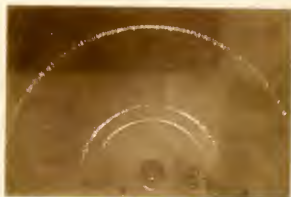
(a)



(b)



(c)

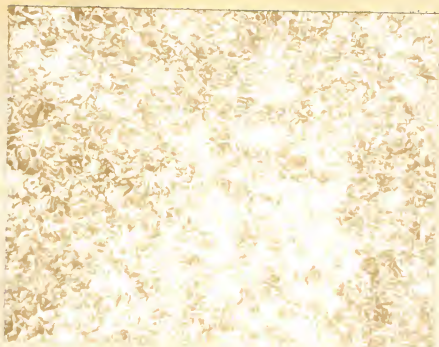


(d)

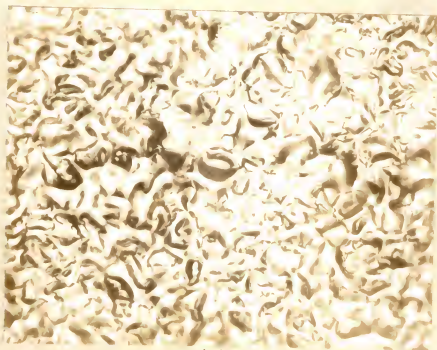
Figure 67: X-ray diffraction patterns of scales formed on cylindrical specimens of curvature 2.0 cm^{-1} (a), 6.0 cm^{-1} (b), 7.2 cm^{-1} (c), and 11.0 cm^{-1} (d) oxidized in air for 64 hours at 1000°C . Cylinder axes parallel to figure title.

The photomicrographs of Figures 68 through 78 are arranged in order of increasing curvature with the 4-hour microstructure positioned at the top and the 16-hour microstructure positioned at the bottom of each figure. Among the noteworthy features illustrated by these figures are the following:

- 1) There is usually a correlation both in the structure and in the shading of the microstructures developed during the 4- and 16-hour oxidation treatments. This indicates that the final microstructure is dependent upon the pre-existing scale layer.
- 2) The amount of distortion exhibited by the scale appears to follow an alternating pattern as the curvature is continuously increased over the range investigated; distortion maximum being evident at approximate specimen curvatures of 2, 6, and 11 cm^{-1} . A darker shading in the photomicrographs is seen to correspond with these maxima.
- 3) There is, in the microstructures of those specimens oxidized for 4 hours, an inhomogeneity in the microstructure evidenced as light-colored "islands" which are positioned closer to the metal than the surrounding oxide crystals. This feature is most prominent for specimens of curvature 5 cm^{-1} , Figure 71a. Its apparent

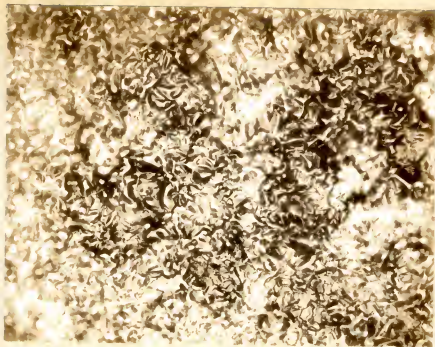


(a)

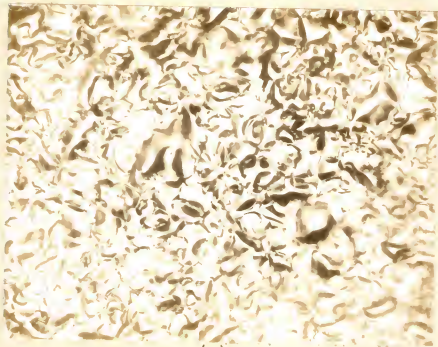


(b)

Figure 68: Photomicrographs of the external surface of scales formed on cylindrical specimens of curvature 2 cm^{-1} oxidized in one atmosphere of dried oxygen at 1000°C . Oxidation time 4 hours (a) and 16 hours (b). Magnification $1000\times$.

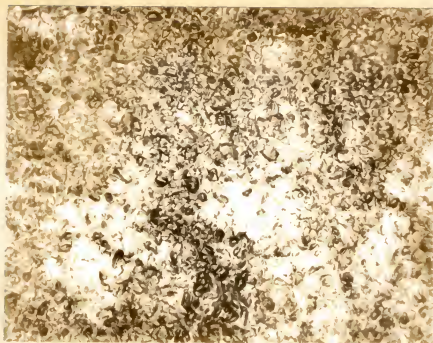


(a)

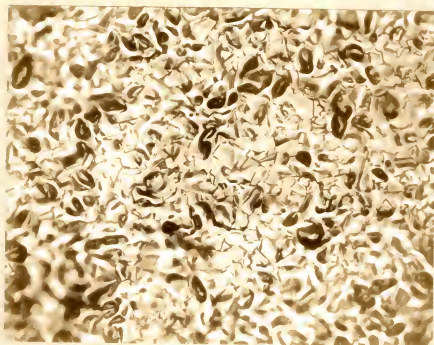


(b)

Figure 69: Photomicrographs of the external surface of scales formed on cylindrical specimens of curvature 3 cm^{-1} oxidized in one atmosphere of dried oxygen at 1000°C . Oxidation time 4 hours (a) and 16 hours (b). Magnification 1000x.

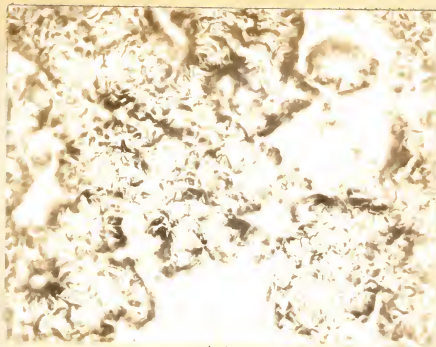


(a)

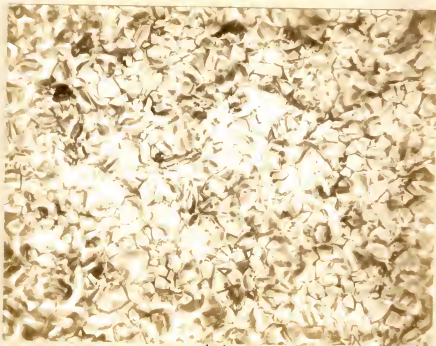


(b)

Figure 70: Photomicrographs of the external surface of scales formed on cylindrical specimens of curvature 4 cm^{-1} oxidized in one atmosphere of dried oxygen at 1000°C . Oxidation time 4 hours (a) and 16 hours (b). Magnification 1000x.

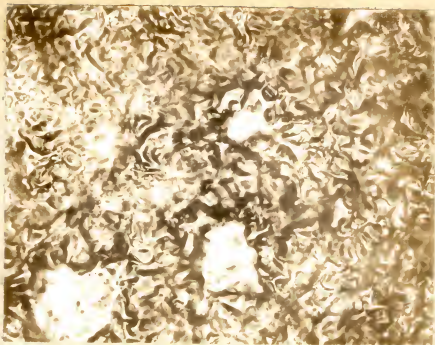


(a)



(b)

Figure 71: Photomicrographs of the external surface of scales formed on cylindrical specimens of curvature 5 cm-1 oxidized in one atmosphere of dried oxygen at 1000°C. Oxidation time 4 hours (a) and 16 hours (b). Magnification 100Cx.

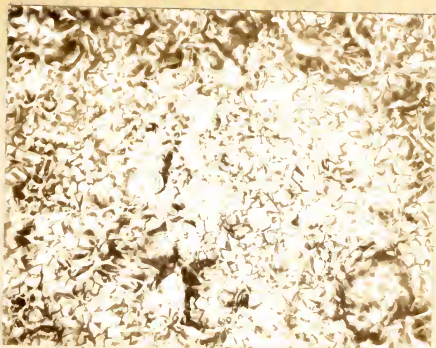


(a)

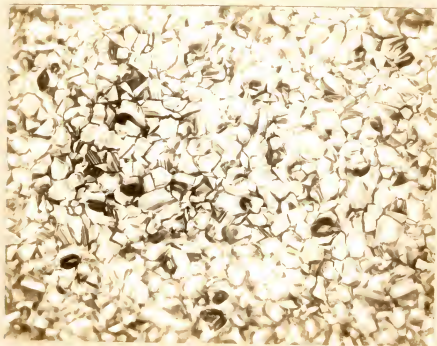


(b)

Figure 72: Photomicrographs of the external surface of scales formed on cylindrical specimens of curvature 6 cm^{-1} oxidized in one atmosphere of dried oxygen at 1000°C . Oxidation time 4 hours (a) and 16 hours (b). Magnification $1000\times$.



(a)

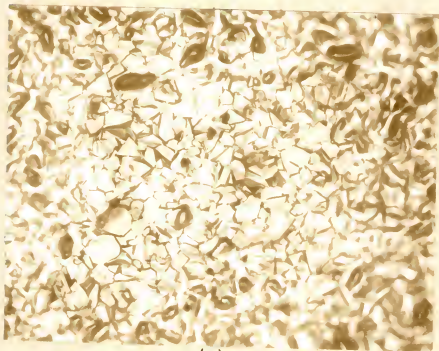


(b)

Figure 73: Photomicrographs of the external surface of scales formed on cylindrical specimens of curvature 7 cm^{-1} oxidized in one atmosphere of dried oxygen at 1000°C . Oxidation time 4 hours (a) and 16 hours (b). Magnification 1000x.

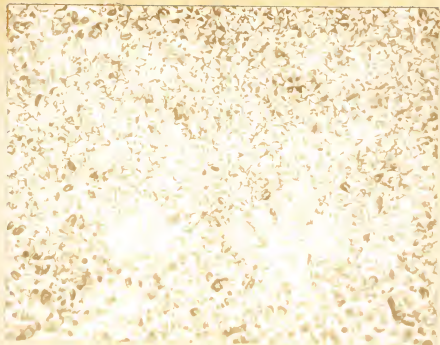


(a)



(b)

Figure 74: Photomicrographs of the external surface of scales formed on cylindrical specimens of curvature 8 cm^{-1} oxidized in one atmosphere of dried oxygen at 1000°C . Oxidation time 4 hours (a) and 16 hours (b). Magnification $1000\times$.



(a)



(b)

Figure 75: Photomicrographs of the external surface of scales formed on cylindrical specimens of curvature 9 cm^{-1} oxidized in one atmosphere of dried oxygen at 1000°C . Oxidation time 4 hours (a) and 16 hours (b). Magnification 1000x.



(a)



(b)

Figure 76: Photomicrographs of the external surface of scales formed on cylindrical specimens of curvature 10 cm^{-1} oxidized in one atmosphere of dried oxygen at 1000°C . Oxidation time 4 hours (a) and 16 hours (b). Magnification 1000x.



(a)



(b)

Figure 77: Photomicrographs of the external surface of scales formed on cylindrical specimens of curvature 11 cm^{-1} oxidized in one atmosphere of dried oxygen at 1000°C . Oxidation time 4 hours (a) and 16 hours (b). Magnification $1000\times$.



(a)



(b)

Figure 78: Photomicrographs of the external surface of scales formed on cylindrical specimens of curvature 12 cm^{-1} oxidized in one atmosphere of dried oxygen at 1000°C . Oxidation time 4 hours (a) and 16 hours (b). Magnification $1000\times$.

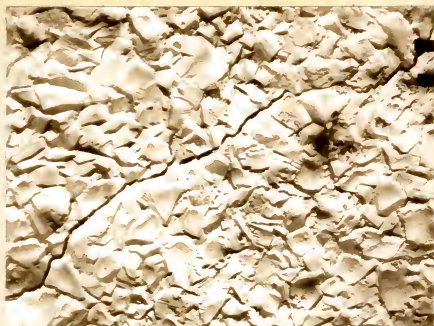
effect on the microstructure of specimens oxidized for 16 hours is shown in the photomicrograph of Figure 71b.

4) The favored sites for oxide protrusions, as determined from inspection of the less-distorted microstructures of the 16-hour specimens, again appears to be at points of grain-to-grain contact. Although it is not easily discernible from the photomicrographs, certain of the grains were found to have apparently convex facets,

Details of the oxide surface structure are shown in the electron photomicrographs of Figure 79 for specimens oxidized 1 and 16 hours at 1000°C. Figure 79a illustrates that early in the oxidation process, grains have a distorted appearance exhibiting both convex and concave surfaces, while relatively few flat surfaces are in evidence. A crack in the scale, running diagonally across the photomicrograph, is seen to be basically intergranular in nature. Comparison of the photomicrographs of Figure 79 shows that there is an appreciable increase in grain size between the first and sixteenth hours of oxidation. The lower photomicrograph indicates that the surface distortion of the scale tends to localize at longer oxidation times, favoring areas of grain-to-grain contact. Many of the grain surfaces, while nearly flat, still exhibit slight convex and concave character and several areas of upheaval near the oxide grain boundaries are visible.

The cross-sectional character of the oxide crystals is shown in the photomicrographs of Figure 80 for specimens of curvature 4 cm^{-1} oxidized for 16 and 64 hours. The grain structure is once again seen to be columnar. For the shorter oxidation time, the oxide is apparently dense and free of mechanical faults, while at longer times severe circumferential cracking is noted and the scale is apparently more susceptible to mechanical failure resulting from the polishing operation. A comparison of the photomicrographs of this figure and those of the preceding one indicates that the oxide grains grow in size at a rate much slower than that which would be predicted from a parabolic growth law.

Oxide microstructures, developed on flat specimens oxidized for 16 hours at 1000°C in dried oxygen, are shown in the photomicrographs of Figures 81 through 84. These show that as the thickness of the original sheet specimen is reduced, the regularity of the oxide structure is diminished. Although protrusions are evident at points of grain contact, especially for the thicker specimens, the major distortion of the surface appears to take the form of cooperative displacement of the oxide crystals. This is evidenced by the fact that some areas containing several grains are displaced in elevation with respect to others.

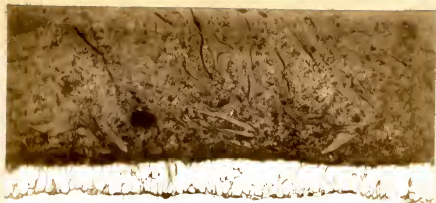


(a)



(b)

Figure 79: Electron photomicrographs of the external surface of scales formed on cylindrical specimens oxidized in dried oxygen at 1000°C. Curvature 8 cm^{-1} , oxidation time 1 hour (a); and curvature 4 cm^{-1} , oxidation time 16 hours (b). Magnification 5000x.



(a)



(b)

Figure 80: Photomicrographs of the cross sections of scales formed on cylindrical specimens of curvature 2 cm^{-1} oxidized in dried oxygen at 1000°C for 16 hours (a), and 64 hours (b). Electrochemical etch. Magnification 500x.

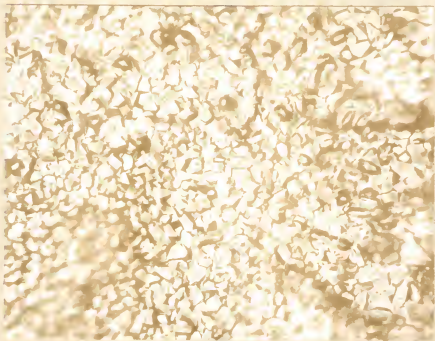
As the sheet thickness is reduced to less than approximately 0.016 inch, light-colored "islands" begin to appear similar to those encountered in the 4-hour oxidation of cylinders. As in the previous case, these "islands" were found to lie a few microns beneath the outermost surface of the oxide. In the photomicrographs of Figure 83, the focal plane is adjusted to the level of the external surface, while in Figure 84 it is adjusted to the level of an "island." The photomicrograph of Figure 84a, taken using oblique bright field illumination, shows markings in the surface suggestive of the flow lines, but there is no evidence of an oxide grain structure. Inspection of the same area with polarized light revealed the crystallographic deformation markings shown in Figure 84b. These markings were found to be associated with the majority of the light-colored areas on the thinnest specimen studied (approximately 0.006 inch). The similarly-shaped and colored areas of thicker specimens did not exhibit these markings when examined with polarized light, but rather had a color similar to that of the surrounding oxide.

3.64 Near-Equilibrium Microstructure

Two specimens were oxidized in stagnant air under time-temperature conditions which allowed a considerable amount of atomic rearrangement at the external surface of

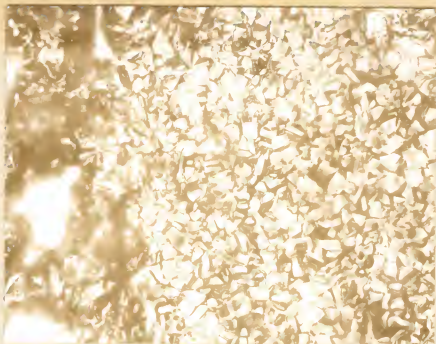


(a)



(b)

Figure 81: Photomicrographs of the external surface of scales formed on plane specimens oxidized in dried oxygen for 16 hours at 1000°C. Reciprocal thickness 6.2 cm^{-1} (a), and 12.2 cm^{-1} (b). Magnification 1000x.

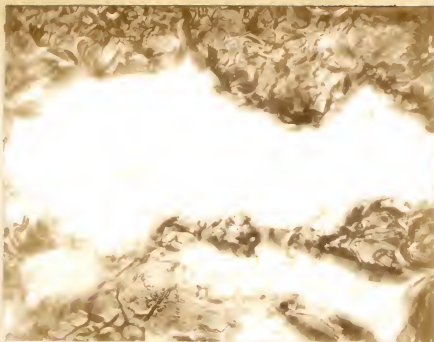


(a)

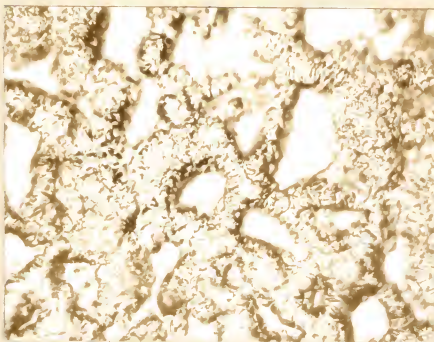


(b)

Figure 82: Photomicrographs of the external surface of scales formed on plane specimens oxidized in dried oxygen for 16 hours at 1000°C. Reciprocal thickness 25.0 cm^{-1} (a), and 45.2 cm^{-1} (b). Magnification 1000x.

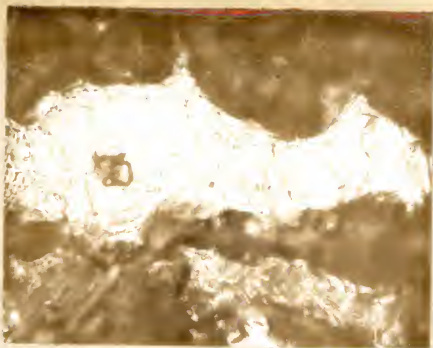


(a)

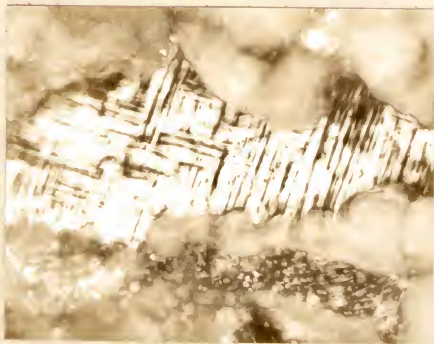


(b)

Figure 83: Photomicrographs of the external surface of the scale formed on a plane specimen of reciprocal thickness 65.6 cm^{-1} oxidized in dried oxygen for 16 hours at 1000°C . Magnification 1000x (a), and 500x (b).



(a)



(b)

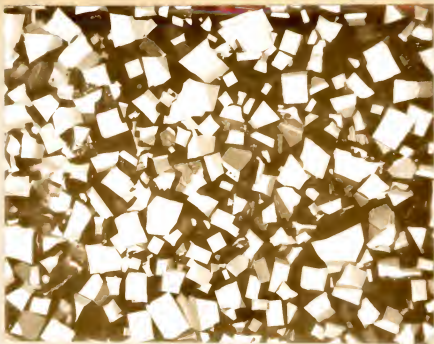
Figure 84: Photomicrographs of the external surface of the scale formed on a plane specimen of reciprocal thickness 65.6 cm^{-1} oxidized in dried oxygen for 16 hours at 1000°C . Magnification 1000x. Illumination: oblique bright field (a), and polarized light (b).

the oxide. It was felt that under these conditions the surface structure would approach its equilibrium configuration more closely than any of the other specimen surfaces studied. The microstructures resulting from oxidation at 1200°C for 16 hours and 1000°C for 124 hours are shown in the photomicrographs of Figure 85. Aside from the pitting exhibited by the specimen oxidized at 1000°C, the microstructures are remarkably similar. The crystals tend to be highly idiomorphic, possess flat facets, and be relatively well isolated from neighboring crystals. Thus, oxide protrusions arising from grain-to-grain contact are absent.

3.65 Oxide Adherence

Exfoliation of scales from specimens as a result of cooling from the oxidizing temperature was not observed. This behavior has been attributed to the remarkably similar coefficients of thermal expansion of the metal and the oxide (35). Metallographic inspection of the oxide has, however, indicated that the oxide is not always totally adherent to the metal.

Portions of almost all the specimens oxidized in this investigation were examined in cross section after being mounted in bakelite. The mounting process involves a single thermal cycle in which the specimen, surrounded



(a)



(b)

Figure 85: Photomicrographs of the external surface of specimens oxidized in air. Oxidation treatment 1200°C for 16 hours (a) and 1000°C for 124 hours (b). Magnification 500x.

by a plastic powder, is heated under pressure from room temperature to approximately 150°C and then is again cooled to room temperature. During the high-temperature portion of this cycle, the external surface of the oxide is brought into intimate contact with and is bonded to the plastic mounting material. Subsequent cooling of the specimen generates tensile stresses in the scale which are in some cases large enough to cause localized failure. Thus, the mounting process per se may be considered as a qualitative mechanical test of the soundness of the scale. In all cases fracture was found to occur within the oxide layer. Favored regions of fracture were found to be either near the center of the scale or near the metal-oxide interface. Figures 86 through 89 show the degree of adhesion of the scale in terms of the per cent contact with the metal as a function of specimen size for several of the oxidation conditions investigated. These results indicate that adhesion is favored if either the specimen size is large or the oxidation time is long. Figure 89 shows a reversal in the time dependence from the generalization as the specimen size is extended to the minimum investigated. This behavior implies that some faults in the scales which were incurred in the initial portions of the oxidation process may be repaired upon continued oxidation.

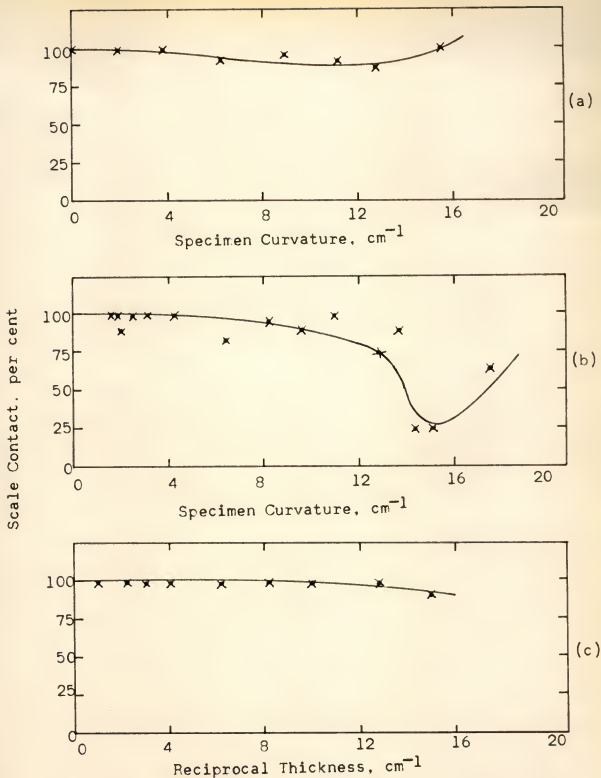


Figure 86: Adhesion of the scale as a function of specimen size for cylindrical and flat specimens oxidized in air at 900°C . Cylinders, 16 hours (a); cylinders, 64 hours (b); Flat sheet, 64 hours (c).

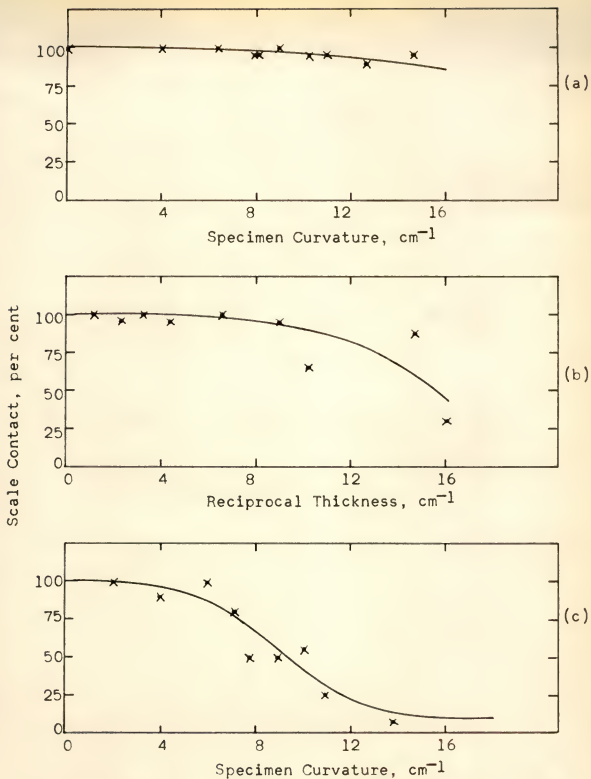


Figure 87: Adhesion of the scale as a function of specimen size for cylindrical and flat specimens oxidized in air at 1000°C. Cylinders, 16 hours (a); Flat sheet, 16 hours (b); and cylinders, 64 hours (c).

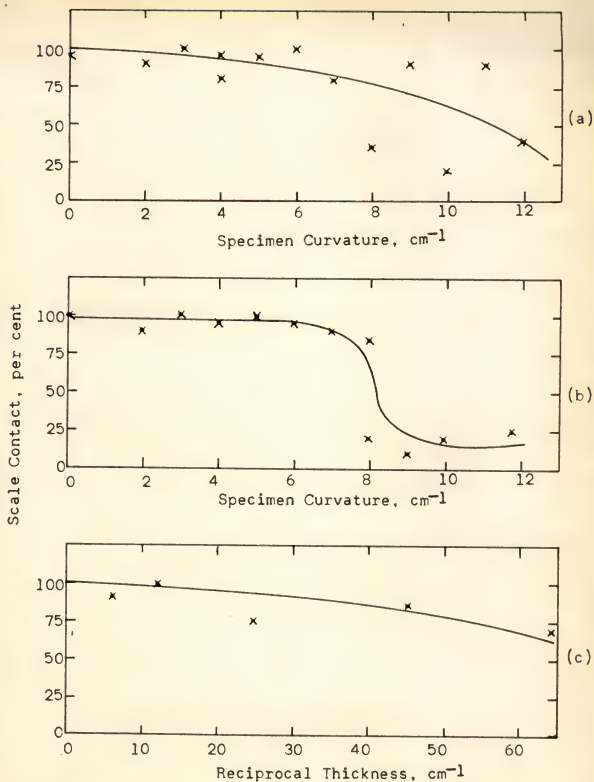


Figure 88: Adhesion of the scale as a function of specimen size of cylindrical and flat specimens oxidized in dried oxygen at 1000°C . Cylinders, 4 hours (a); 16 hours (b); and flat sheet, 16 hours (c).

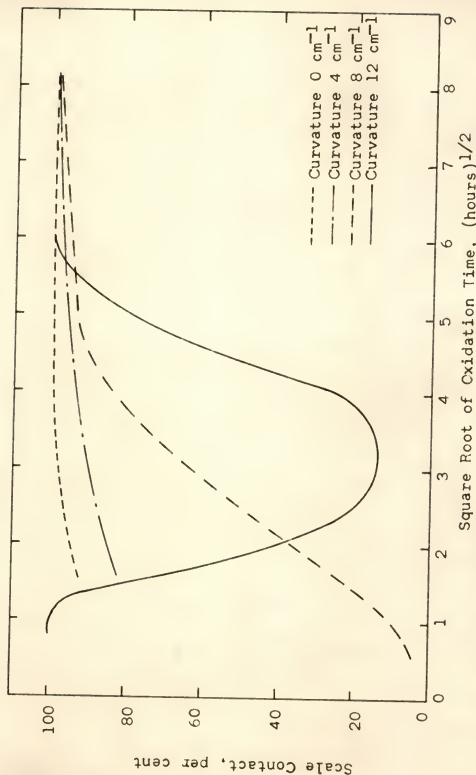


Figure 89: Adhesion of the scale as a function of oxidizing time for specimens of curvature 0, 4, 8, 12 cm⁻¹ oxidized in dried oxygen at 1000°C.

3.7 Environmental Studies

Both the scale thickening behavior and the oxide microstructure were found to be highly dependent upon the particular furnace and associated environmental conditions which existed at the time of oxidation. The specimens within each of the series of oxidation experiments discussed previously were oxidized under conditions which were as nearly constant as possible so that the geometric parameters were the variables of primary importance. In the case of the preliminary oxidation studies in air, the effect of possible instabilities in the local laboratory atmosphere were questioned. The systematic behavior of the data indicated that the magnitude of effects arising from this source of error were usually ignorable; however, at least in one instance, when ammonia vapor from a cleaning solution was present in the atmosphere, anomalous results were obtained. Considerations of this nature lead to the subsequent employment of controlled atmosphere oxidation studies.

At least three major differences in environmental conditions existed in the horizontal and vertical furnaces used for preliminary oxidation studies; these were: degree of stagnation of the air, type of furnace ceramic, and time-temperature profile. In spite of these differences, the same general trend was found for the dependence of scale

thickening on specimen curvature, while absolute values of scale thickness and microstructural studies indicated that their effect was not negligible.

A series of cylindrical specimens of curvature 2 cm^{-1} were oxidized for 16 hours at 1000°C under several different conditions in an attempt to determine the relationship of the environmental parameters to the oxidation process and to provide some degree of correlation between preliminary oxidation specimens treated in different furnaces. The conditions of each test performed and the results, in terms of scale thickness, are given in Table 8. Values of scale thickness shown in parentheses are reduced from observed values by a factor 1.3 in order to account for the known pressure dependence of the oxidation rate constant (39). The trade names "Volcanus" and "JM-20" noted in the table are aluminum silicate-based ceramics manufactured by the Coors Porcelain Company and the Johns-Manville Corporation respectively. "Volcanus" is a relatively inert, vitrified, gas-tight ceramic with a maximum service temperature of approximately 1600°C , while "JM-20" is a porous firebrick used primarily for its insulating qualities at service temperatures below 1100°C .

The information presented in Table 8, in conjunction with metallographic evidence, indicates the following results:

- 1) Tests 1 and 2: The addition of small amounts of water vapor, present in commercially available oxygen gas,

TABLE 8

EFFECT OF ENVIRONMENTAL CONDITIONS ON SCALE THICKENING AT 1000°C

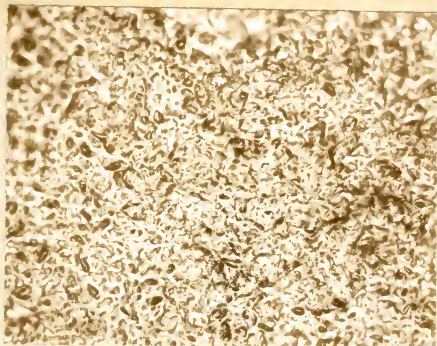
Test	Furnace Ceramic	Oxidizing Gas	Amplitude of Temperature Variations (°C)	Character of temperature variation	Scale Thickness (microns)
1	Nio	Dry Oxygen - 1 ATM	1/10	Sinusoidal	(15.0-17.3)
2	Nio	Oxygen - 1 ATM	1/6	Sinusoidal	(12.5-14.2)
3	Nio	Oxygen - 1 ATM	1 1/4	Sinusoidal	(11.4-13.2)
4	Quartz	Oxygen - 0.22 ATM	1 1/2	Sinusoidal	10.8-13.4
5	Nio	Air	6	Sinusoidal	21.2-24.5
6	"Volcanus" Air		1/6	Sinusoidal	15.7-17.1
7	"Volcanus" Stagnant air		1/6	Sinusoidal	12.9-15.1
8	"Volcanus" Stagnant air		3 1/4	Sinusoidal	15.9-18.7
9	"Volcanus" Stagnant air with "JM-20"		1/4	Sinusoidal	18.8-20.8
10	"JM-20" Stagnant air		1 1/2	Sinusoidal	19.1-22.7
11	"JM-20" Stagnant air		3 1/4	Sawtooth Type 1	25.1-28.5
12	"JM-20" Stagnant air		1 1/2	Sawtooth Type 2	26.5-30.1
13	"JM-20" Air		3 1/4	Sawtooth Type 1	29.7-32.9

decrease both the scale thickness and surface roughness of the oxide. The latter effect is illustrated by the photomicrographs of Figure 90. The conditions of test 1 are identical to those used with the controlled environment oxidation studies.

2) Test 4: Reduction of oxygen pressure does not affect the value of scale thickness in excess of that which is expected on the basis of the known pressure dependence of the scaling rate. There is however, a marked reduction in distortion of the oxide surface as shown in the photomicrograph of Figure 91.

3) Tests 2 and 6: The use of air instead of oxygen as the oxidant increases the scaling rate slightly and provides the oxide grains with both stepped surfaces and a $\langle 111 \rangle$ wire texture as illustrated in Figure 92.

4) Tests 6 and 7: Oxidation in stagnant air reduces the scale thickness with respect to that found on specimens oxidized in moving air. The stepped surfaces diminish in favor of formation of angular oxide grains and the wire texture weakens. These effects are shown in Figure 93. The conditions of test 7 are identical to those used with the horizontal furnace during preliminary oxidation studies.



(a)



(b)

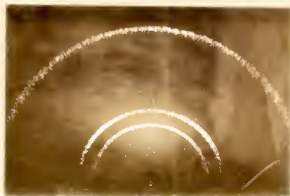
Figure 90: Photomicrographs of the external surface of scales formed on cylindrical specimens of curvature 2 cm^{-1} oxidized for 16 hours at 1000°C . Environmental conditions: test 1(a) and test 2(b) of Table 8. Magnification 500x.



Figure 91: Photomicrograph of the external surface of the scale formed on a cylindrical specimen of curvature 2 cm^{-1} oxidized for 16 hours at 1000°C . Environmental conditions: test 4 of Table 8. Magnification 500x.



(a)



(b)

Figure 92: Photomicrograph (a) and X-ray diffraction pattern (b) of the external surface of the scale formed on a cylindrical specimen of curvature 2 cm^{-1} oxidized for 16 hours at 1000°C . Environmental conditions: test 6 of Table 8. Magnification 500x (a).



(a)



(b)

Figure 93: Photomicrograph (a) and X-ray diffraction pattern (b) of the external surface of the scale formed on a cylindrical specimen of curvature 2 cm^{-1} oxidized for 16 hours at 1000°C . Environmental conditions: test 7 of Table 8. Magnification 500x (a).

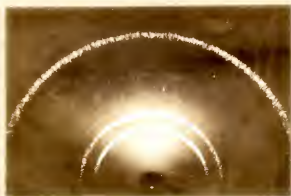
5) Tests 7 and 8: A thermal fluctuation of $\pm 3 \frac{1}{4}^{\circ}\text{C}$ about the mean temperature of 1000°C produces an increase in scale thickening, acicular grains at the oxide surface, and a $\langle 100 \rangle$ wire texture. The oxide microstructure and diffraction pattern are both shown in Figure 94. The results of tests 2 and 3 indicate that a thermal fluctuation of $\pm 1 \frac{1}{4}^{\circ}\text{C}$ has little effect on the oxide microstructure or thickness. The results of tests 5 and 6 indicate that a thermal fluctuation of $\pm 6^{\circ}\text{C}$ (about a mean temperature of 996°C) produces a major increase in scale thickening. This high-amplitude thermal cycle also produces the distorted oxide surface shown in Figure 95.

6) Tests 7 and 9: Presence of "JM-20" firebrick in the oxidizing zone increases the scaling rate of the metal. The microstructural characteristics of the oxide produced during test 9, however, remained very similar to those produced during test 7. The accelerated scaling behavior is thought to be due to volatile impurities in the brick which alter the transport properties of the oxide. This impurity was not detected by either X-ray or metallographic techniques.

7) Tests 9, 10, 11, and 12: Both the amplitude and wave shape of the thermal fluctuation appear to be important factors in oxide growth. As in the case of



(a)



(b)

Figure 94: Photomicrograph (a) and X-ray diffraction pattern (b) of the external surface of the scale formed on a cylindrical specimen of curvature 2 cm^{-1} oxidized for 16 hours at 1000°C . Environmental conditions: test 8 of Table 8. Magnification 500x (a).



Figure 95: Photomicrograph of the external surface of the scale formed on a cylindrical specimen of curvature 2 cm^{-1} oxidized for 16 hours at 1000°C . Environmental conditions: test 5 of Table 8. Magnification 500x.

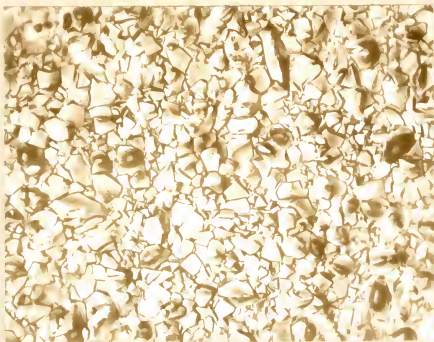
tests 2 and 3, tests 9 and 10 indicate that the thermal fluctuations on the order of $\pm 1\frac{1}{2}^{\circ}\text{C}$ do not alter the scaling behavior appreciably. Also, comparison of tests 10 and 11 shows that where the thermal fluctuation reaches an amplitude of approximately $3\frac{1}{4}^{\circ}\text{C}$, changes in oxide microstructure and scale thickness are observed. In this case, however, the changes are more drastic than those previously encountered and a portion of the resulting change should probably be attributed to the type-1 saw-tooth thermal wave (rise time $4\frac{1}{2}$ minutes, decay time 1 minute) associated with test 11. The change in oxide microstructure resulting from the differences in the time-temperature profiles of tests 10 and 11 may be seen by comparing the photomicrographs of Figure 96.

More convincing evidence that the amplitude of the thermal wave alone does not govern the scaling behavior is found in comparison of tests 10 and 12 wherein only the shape of the thermal wave is changed. The type-2 sawtooth wave associated with test 12 (rise time $2\frac{1}{2}$ minutes, decay time $6\frac{1}{2}$ minutes) produces both a thicker scale than either test 10 or 11 and the unusual microstructure shown in Figure 97.

8) Tests 11 and 13: Oxidation in stagnant air is again found to reduce the scale thickness as was the case in tests 6 and 7. Little change in the oxide microstructure was noted with this change in stagnation. The conditions of test 13 are identical to those used with the vertical furnace during preliminary oxidation studies.



(a)



(b)

Figure 96: Photomicrographs of the external surface of scales formed on cylindrical specimens of curvature 2 cm^{-1} oxidized for 16 hours at 1000°C . Environmental conditions: test 10 (a) and test 11 (b) of Table 8. Magnification 500x.



Figure 97: Photomicrograph of the external surface of the scale formed on a cylindrical specimen of curvature 2 cm^{-1} oxidized for 16 hours at 1000°C . Environmental conditions: test 12 of Table 8. Magnification 500x.

3.8 Oxidation-Creep Experiments

Three cylindrical creep specimens having nearly equal curvatures in their gage sections were simultaneously loaded axially in tension and oxidized in air for 64 hours at 900°C. The stress levels employed, based on the original specimen cross sections and the magnitude of the constant applied load, were varied from approximately 400 to 1600 psi. The thicknesses of scales developed on the gage sections of these specimens, together with that for an unstressed specimen, are presented in Table 9.

TABLE 9

SCALE THICKNESSES DEVELOPED ON OXIDATION-CREEP SPECIMENS

Specimen Curvature (cm ⁻¹)	Applied Stress (psi)	Scale Thickness (microns)
4.36	0	27.8 ± 3.2
4.24	412	27.3 ± 1.5
4.23	1020	27.7 ± 0.9
4.25	1576	*

*Specimen failed before completion of test.

These results indicate that the average thickness of the scale is unaffected by variations in tensile stress over the range investigated, while the roughness of the scale apparently decreases with increasing stress. The range of stress investigated is, of course, limited by the

ability of the specimen to resist deformation leading to failure. The maximum average strain rate encountered for those specimens which did not fracture was found to be approximately 4.4×10^{-6} in/in/min.

3.9 Elevated-temperature Creep Studies

Specimens of nickel and hot pressed nickel oxide powder were tested in compression at 1000°C using the apparatus shown in Figure 3. The deformation of these specimens as a function of time at constant stress is presented in the graphs of Figures 98 through 103. Stresses quoted for the oxide specimen are larger by a factor of 1.25 than those calculated on the basis of dimensional measurements and applied load. This correction was employed in order to account for the fact that the oxide specimen was hot pressed to a density of 80 per cent of its theoretical maximum. The curves for the metal, Figures 98 through 100, exhibit typical first and second stage creep behavior. The curves for the oxide show, in addition to these features, discontinuities which may be associated with recrystallization phenomena. This is especially apparent in the curve of Figure 102 for an effective stress of 1450 psi. The curve shape, in this case, was found to be qualitatively reproducible.

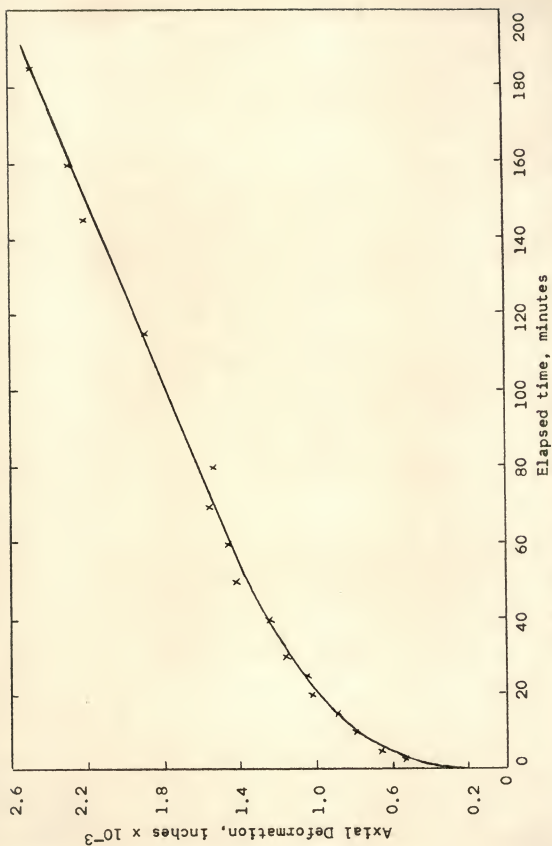


Figure 98: Axial deformation as a function of time for a specimen of Nickel-270 tested in compression at 1000°C. Stress level 754 psi.

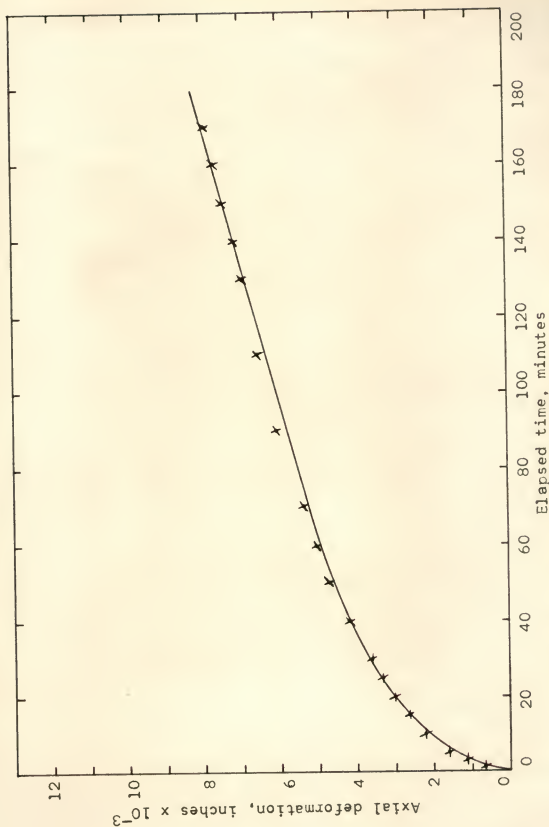


Figure 99: Axial deformation as a function of time for a specimen of Nickel-270 tested in compression at 1000°C. Stress level 1430 psi.

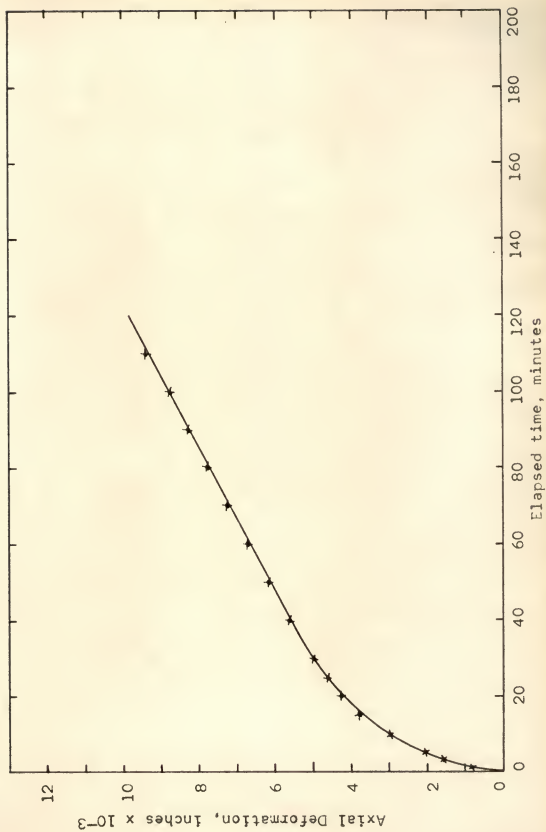


Figure 100: Axial deformation as a function of time for a specimen of Nickel-270 tested in compression at 1000°C, Stress level 1975 psi.

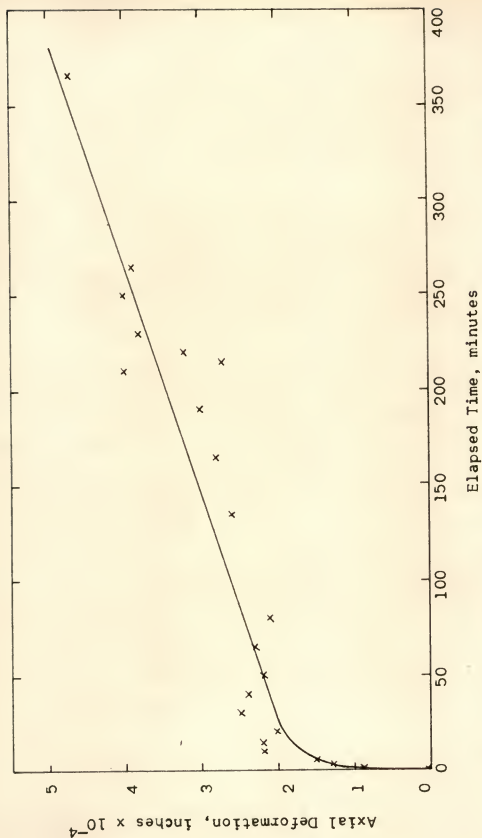


Figure 101: Axial deformation as a function of time for a specimen of hot-pressed nickel oxide tested in compression at 1000°C. Effective stress level 765 psi.

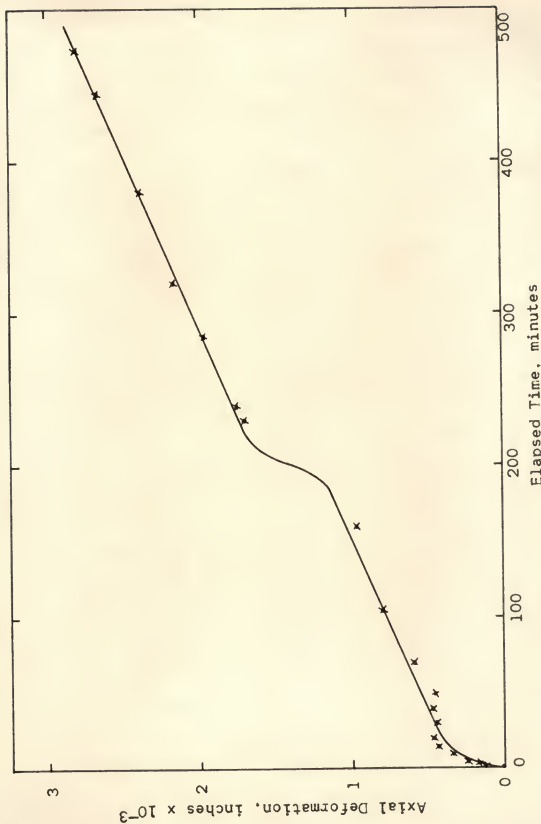


Figure 102: Axial deformation as a function of time for a specimen of hot-pressed nickel oxide tested in compression at 1000°C. Effective stress level 1450 psi.

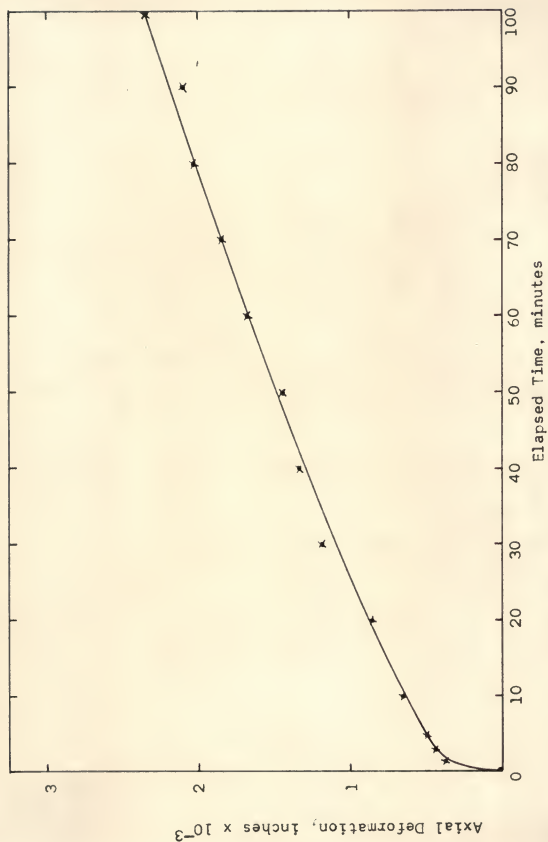


Figure 103: Axial deformation as a function of time for a specimen of hot-pressed nickel oxide tested in compression at 1000°C. Effective stress level 2060 psi.

The second stage creep rate was determined for each of the tests illustrated by determining the slope of the final portion of each graph, and dividing it by the appropriate gage length. Figure 104 illustrates that the logarithm of the second stage creep rate is proportional to the applied stress for both of these materials. Further, it is seen that, for a given stress, the metal deforms more readily than does the oxide. The data from which Figures 98 through 104 were drawn are presented in Tables 28 through 33 of Appendix 1.

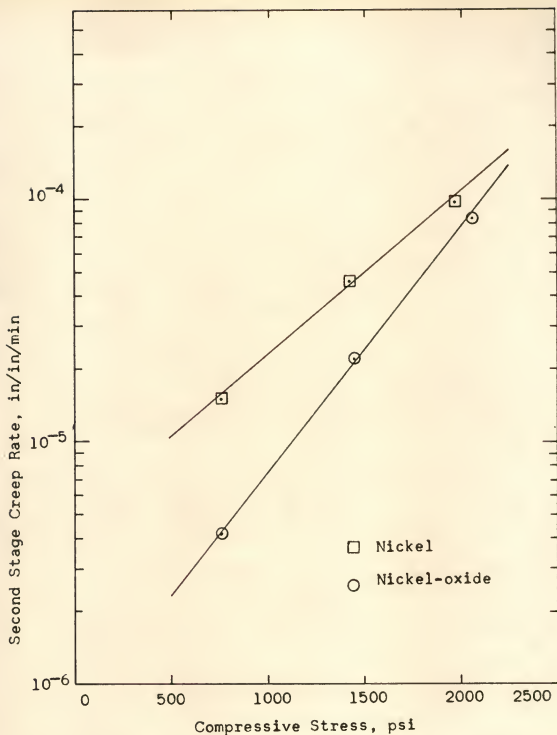


Figure 104: Second stage creep rate as a function of axial compressive stress for nickel and nickel oxide specimens tested at 1000°C.

CHAPTER IV

DISCUSSION

The results of this investigation indicated that the scaling behavior of nickel at elevated temperatures is dependent upon specimen size and shape and that deformation may in some cases occur as a result of the scaling process. A rather extensive search of the available literature has indicated that these effects are little known and, as a consequence, are without basis insofar as the present state of the science of oxidation is concerned. It is desirable, therefore, to postulate a single mechanism which will account for the apparently anomalous observed behavior and at the same time retain the classical framework of oxidation theory. In the sections which follow an attempt is made to first develop such a mechanism and then interpret the results of this investigation in terms of it.

4.1 Nature of the Scale Formed on Nickel

The oxidizing atmospheres employed in this study were basically either oxygen or air with very small quantities of carbon-, hydrogen-, and sulfur-bearing gases quite possibly present as contaminants. Under strong oxidizing conditions one would not expect these contaminants

to form stable compounds with the nickel metal since they have a greater affinity for oxygen (40). The nitrogen present, either in air or as a contaminant in the oxygen, is also incapable of stable compound formation with the metal in this type of environment (41). Thus nickel oxides appear to be the only stable condensed phases which form as a result of oxidation in air or oxygen.

At relatively low temperatures, thin films of nickel oxide have been found to assume a nickel-deficient spinel structure (42) and under conditions of high vacuum, suboxides of nickel have recently been observed (43, 44). However, the oxidation product normally found on oxidized nickel is NiO with a NaCl-type crystal structure. There is to the author's knowledge, no record of any oxide other than NiO forming on nickel as a result of extended oxidation. Limited X-ray examination of some of the specimens used in the subject research support this view. There is, however, a possibility that, under certain conditions, the oxide formed is actually a very dilute solid solution incorporating impurity elements within the nickel oxide lattice.

4.11 Transport of Matter Through the Scale

Nickel oxide is a classical p-type semiconductor and in the presence of oxygen at elevated temperature

exists in a non-stoichiometric form which is slightly deficient in nickel (45, 46, 47). The majority of studies concerning the bulk material and that formed on nickel by oxidation indicate that transport of matter through the oxide involves the interchange of nickel ions and nickel ion vacancies, while, to the limits of observation, oxygen appears to be immobile within nickel oxide crystals. Investigators who have assumed this scheme of transport have been able to account for:

- 1) The position of "inert" markers, originally placed on or near the metal surface, which were located near their original position subsequent to oxidation (48).
- 2) The effect of monovalent and polyvalent impurities on the scaling rate (49).
- 3) The effect of monovalent and polyvalent impurities on the electrical conductivity of nickel oxide (45, 49, 50).
- 4) The oxygen pressure dependence of the scaling rate (39, 51).
- 5) The magnitude of the scaling rate constant as calculated on the basis of transition-state theory (7, 50).

Evidence to the contrary has been claimed by other investigators who observed two distinct layers of oxide which appear to form with the interface between them at the site of the original gas-metal interface indicating inward

diffusion of oxygen (9, 53, 54, 55). This effect has been rationalized both on the basis that it arises as a result of impurities present in the nickel (48) and that it is a natural consequence of extended outward diffusion of nickel (56). The former explanation implies some third element plays an active rôle in the scaling process which may involve the production of a second oxide phase. The latter is based on the concept that new oxide is created at void sites on the interface by dissociation of the pre-existing scale.

Although, to the limits of detection oxygen is immobile in bulk crystals of nickel oxide, experimental evidence exists which indicates that oxygen may diffuse through the grain boundaries of nickel oxide (45). It is believed, however, that the presence of oxygen in these boundaries cannot, in itself, lead to a general thickening of the scale because of the large energy barrier associated with the formation of new oxide at the metal-oxide interface. The consensus to date is that nickel oxide forms during oxidation almost exclusively by transport of nickel through the scale.

An entirely equivalent description of the transport process may be stated in terms of the motion of nickel ion vacancies which, of course, must diffuse in the opposite direction. It will prove convenient to consider the oxidation process from both points of view.

4.2 Consequence of Unidirectional Transport

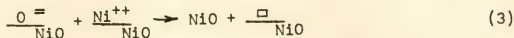
Consider a metallic specimen whose entire surface is at constant temperature and is in contact with an oxidizing gas. The oxidation process may be represented in simplified form by the following equations (52).

1) Oxygen adsorption on the outer surface of the oxide:



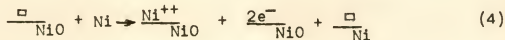
wherein the underscored quantities represent those in solution.

2) Formation of oxide at the gas-oxide interface

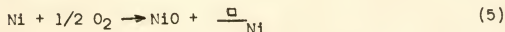


wherein the symbol (\square) is employed to represent a cation vacancy.

3) Solution of nickel at the metal-oxide interface:



The summation of these reactions gives:



The diffusion process, involving transport of nickel across the oxide, is determined by the concentration (activity) gradient of nickel in the oxide which, in turn, is the "mirror image" of the vacancy concentration gradient. Since the rate of oxidation is generally believed to be determined by the diffusion of nickel ion vacancies through the scale, most investigations of the scaling process have been concerned with the generation and motion of the nickel ion vacancy in the oxide. However, equation 5 shows that for each molecule of nickel oxide formed, one vacancy is generated in the nickel substrate near the metal-oxide interface. The effect of vacancies so positioned have received little consideration in the classical description of the oxidation process thus far, and it is their role which will now be discussed.

The major problems associated with the vacancies so formed in the metal are to determine first, how they are partitioned, and second what the effects of specific modes of partitioning would produce. Equation 5 indicates that the volume occupied by vacancies is significant, and to a first approximation, is equal to 60 per cent of the volume occupied by the scale (since the Pilling-Bedworth ratio for the system nickel-nickel oxide is about 1.66). Possible limiting modes of partitioning include positioning the vacancies: within the metal, at the metal-oxide interface, within the scale, and at the gas-oxide interface.

The latter two choices appear to be untenable in view of the fact that they require vacancies to diffuse in a direction opposite that normally associated with the vacancy gradient in the scale; i.e., "uphill" diffusion is required. In addition, the first of these implies that the oxide forms as a porous body (with a maximum of 60 per cent void space), which is not observed. The second process, applied in a limiting sense, would destroy all of the oxide which had formed by removing nickel ions from their sites in the oxide surface. It therefore appears that the vacancies found within the metal must either remain in the bulk or collect at the metal-oxide interface.

The first of these choices may, in turn, be subdivided into two limiting possibilities: either void formation by coalescence of vacancies or production of a "smeared" distribution of vacancies throughout the bulk of the material. Although void formation has been observed in the case of alloy oxidation, the existence of voids within oxidized pure metals is not generally found (57). In the case of nickel, this has never been observed to the author's knowledge. The existence of a "smeared" vacancy distribution and an associated hydrostatic stress has been postulated in the case of the oxidation of copper as one step in explaining certain deformation behavior; however, so far as is known there has been no direct determination

of the existence of such a distribution arising as a result of oxidation (30). In addition, density measurements made on the underlying metal of specimens oxidized in the course of this research showed that the theoretical density was maintained within ± 0.2 per cent indicating, along with metallographic evidence, that the metal did not contain the necessary bulk concentration of vacancies to account for those produced during oxidation. These considerations lead one to conclude that at least a major fraction of the vacancies produced in the metal, as a result of outward diffusion of nickel, must reside near the metal-oxide interface unless they are removed from this position by some mechanism other than diffusion.

Some clarification of the consequences of vacancy precipitation at the metal-oxide interface may be gained from studies other investigators have made on unalloyed iron (57, 58). Iron, unlike nickel, may exhibit as many as three stable oxides when exposed to the proper environmental conditions. In such cases, the sequence of condensed phases observed on an oxidized specimen is: Fe, FeO, Fe₃O₄ and Fe₂O₃. Under other oxidizing conditions it is possible to produce only FeO, a metal-deficient p-type semiconductor which is a homolog of NiO (49). Iron specimens, oxidized to completion under conditions wherein all three oxides form, tend to be hollow and show

evidence of loss of contact between metal and oxide at their interface, whereas those specimens oxidized under conditions such that FeO forms alone tend to be solid. It is believed that these apparently contradictory results are due to the effect of the higher oxides of iron producing a rigid "cage" of oxide in the former case while their absence in the latter case allowed the more plastic FeO to follow the retreating metal (58).

In the case of nickel, the behavior of NiO would be expected to parallel that of FeO . cursory examination of a thin sheet of nickel which was oxidized to completion revealed that it did, in fact, exhibit this behavior and, in general, it was shown that the oxidation process was not halted by loss of contact at the metal-oxide interface. Thus, it appears at first that the void space generated in the metal by oxidation may be eliminated by the oxide uniformly following the retreating metal. There are, however, certain restrictions associated with such a concept. Specimens normally used in oxidation studies, such as those of this research, are oxidized on all surfaces so that inward motion of the oxide is restricted by neighboring segments of oxide. Further, motion of the oxide implies that the void space, generated within the metal, is in some manner passed through the oxide layer to the outermost surface of the specimen. These considerations indicate that unidirectional diffusion through the scale layer should result

in stress generation and subsequent deformation of oxide specimens.

It is postulated that the observed collapse of the scale upon its retreating substrate is due to the effects of forces arising from the surface energy of voids or vacancies produced at the metal-oxide interface. Since phases do not generally separate at their interface per se, but rather in a region adjacent to it, the apparent adhesion between metal and oxide so generated might be more properly stated in terms of the cohesion of the weaker phase. Experimental evidence indicates that when separation occurs it does so within the scale layer at distances from the interface which are usually less than one micron.

The presence of voids or vacancies at the metal-oxide interface could produce the forces necessary for collapsing the oxide inward provided that the surface energies associated with the metal and oxide surrounding such a discontinuity were in excess of that associated with the void-free metal-oxide interface. The precise mechanism associated with the inward collapse of oxide is not known; but it appears that it would be at least partially dependent upon the (unknown) structure of the metal-oxide interface.

It has been suggested that scale-to-metal contact may be maintained by the motion of a step of atomic dimensions moving along the metal surface beneath the oxide layer

(11). As long as there is no geometric constraint associated with the inward motion of the scale, it is feasible that this process could supply the necessary continuity between scale and metal without generating major stresses in the scale. Such a process could apply near the central positions of large, flat specimens. However, if the specimen possesses curvature, then the scale must subsequently deform plastically in order to maintain intimate contact between metal and oxide.

In order that such plastic flow might occur in the oxide, it seems reasonable to postulate that there must be some degree of pre-alignment of vacancies at the interface prior to plastic deformation as essentially suggested above. If this were the case, then deformation could proceed by a stepwise-continuous process of generation, motion and annihilation of this alignment at the interface in which the void space is passed to the external surface of the specimen by means of shears through the scale layer.

4.3 Consideration Pertaining to the Existence of Stresses in Scales

The necessity for an inward collapse of the oxide layer results in an immediate classification of specimens on the basis of their geometry. The scales formed on specimens of finite curvature may support hoop stresses while

those developed on flat specimens probably cannot. Flat iron specimens, when oxidized under conditions such that the higher oxides form, exhibit a "pulling-away" of the scale in the immediate neighborhood of edges and corners (31, 59). Thus, it appears that the long-range normal stress due to the oxide layer following the retreating metal-oxide interface may be assumed to be zero in the central zone of a large, flat specimen while it is non-zero in the case of those specimens exhibiting either constant or smoothly changing curvatures. A method for calculating the elastic component of the stresses arising from this source has been developed for the case of cylindrical specimens and is presented in Appendix 2.

The results of the calculations based on this Appendix indicate that the dominant stresses in the scale will be a large hoop compression and a radial tension which cause an overall axial contraction of the specimen. Calculated values of stress are dependent upon the ratio of scale thickness developed to original specimen radius which is equivalent to the product of scale thickness and specimen curvature. Higher stresses and large axial contractions are predicted as a result of increases in either scale thickness or specimen curvature.

4.31 The Concept of a Grain Boundary Pressure

The observed length changes for both flat and cylindrical specimens indicate that stresses in the scale layer are of sufficient magnitude to cause deformation of the entire specimen. However, the observed deformations infer that stresses must arise from sources other than those associated with the motion of the scale layer as a whole normal to the metal-oxide interface. In the case of flat specimens, the observed bulk extensions should not have occurred if the stress effects associated with corners and edges were truly short-range in character as indicated above. In addition, calculations for cylindrical specimens, based on the development of Appendix 2, indicate axial contraction should occur in opposition to the generally observed extension. Although the model used in these calculations is based on elastic properties, it should have predicted the direction of the observed plastic deformation if all stresses were properly taken into account. In order to provide a basis for the observed extension of both flat and cylindrical specimens the existence of a lateral compressive stress within the scale is postulated.*

*The stress envisioned acts within the scale and parallel to the plane of the scale. In this sense, it may be considered as a "two-dimensional hydrostatic pressure."

In the oxidation of nickel, a two-dimensional layer of oxide is formed on a surface which is normal to the diffusion "streams" of oxygen and nickel and its orientation and position is fixed basically by the concentration product of nickel and oxygen. For metals, such as nickel, which oxidize by a metal-ion transport mechanism, this surface is usually considered to be at or near the gas-oxide interface and parallel to it; but, oxide deposition at such a surface could not produce the required lateral compressive stress. If, on the other hand, a small quantity of new oxide were formed on the boundaries of pre-existing columnar grains, such as those shown in Figure 55, then a lateral compressive stress would arise. This process would require that oxygen and nickel approach the two-dimensional grain boundary system normally and form oxide thereon.

It is proposed, therefore, that oxide growth occurs in a manner similar to that shown schematically in Figure 105; the major portion of the scale being formed by diffusion of nickel to the region of the metal-oxide interface, while some lesser amount is formed by diffusion of nickel through the oxide crystals toward the grain boundary region. There it unites with oxygen to form oxide "wedges," providing a "grain boundary pressure," which in a columnar grain structure appears as a lateral compression. It must be

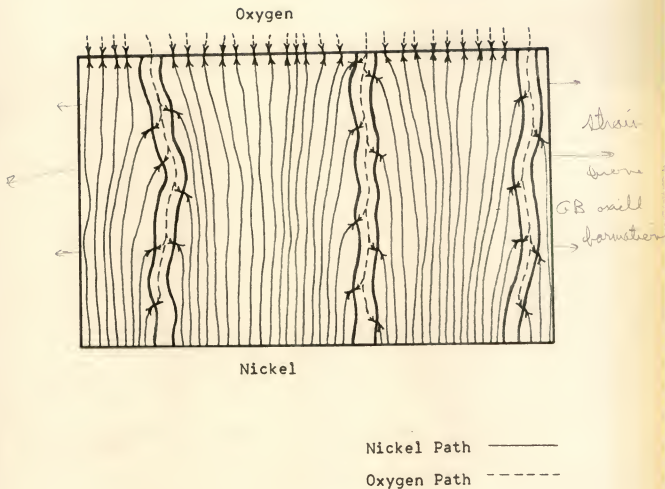


Figure 105: Schematic diagram of the proposed diffusion paths of nickel and oxygen prevailing during the formation of nickel oxide.

emphasized that the postulated process demands either that, in the main, oxygen alone be mobile in the bulk of the grains, or the converse. The former condition is believed to be the applicable one. Violation of this condition would lead to the formation of oxide on surfaces parallel to the scale interfaces which could in no way produce the requisite pressure.

The origin of lateral compressive stresses in scales formed by outward diffusion of the metal ion has not yet been subjected to intensive investigation; however, effects attributed to the existence of such stresses have been observed in the oxidation of both nickel and other metals (1, 60, 61). The formation of nickel oxide within crystals of the pre-existing scale seems highly unlikely in view of the accepted defect structure of the oxide. Assuming that oxygen could in some manner enter the oxide lattice, it then becomes difficult to envision the sequence of events necessary for chemical combination and growth of new oxide within the old. Further, this process would most probably provide oxide at a surface parallel to the scale interfaces and would therefore be incapable of giving rise to the requisite lateral stress. It therefore appears more likely that the compressive stress must result from oxide growth on pre-existing oxide grain boundaries by addition of material at the oxide lattice sites.

The existence of a grain boundary pressure is analogous to the concept of crystal pressure which was studied most intensively in the early part of this century (62, 63). This concept contains the implicit assumption that two crystals growing together do not cease growing upon contact; but rather, continue to grow toward one another until some limiting pressure is attained. This is not a particularly untenable position since we feel intuitively that adjacent crystals of oxide growing on a metallic surface do meet. Further, it could only be an ad hoc assumption that they meet in such manner as to be stress free; i.e., the true choice seems only to be whether the crystals meet with zero or finite pressure. As in the present case, such pressures appear to be associated with the creation of a new phase from some pre-existing one. The forces which arise may, in both cases, be thought of as resulting from the effects of capillarity with new materials being added at crystal interfaces.

There are three primary requirements necessary to any mechanism proposed for this mode of oxide formation:

- 1) Transport of oxygen to the reaction site.
- 2) Transport of nickel to the reaction site.
- 3) Existence of oxide surfaces upon which growth may take place.

Experimental evidence that oxygen is capable of penetrating boundary region of nickel oxide exists (45). Since the oxygen concentration in the scale is highest at the gas-oxide interface and lowest at the metal-oxide interface, it seems reasonable that grain boundary diffusion of oxygen may be capable of fulfilling the first requirement. Two modes seem to be available for the transport of nickel to the reaction site: grain boundary diffusion and bulk diffusion through the oxide. The latter process appears to be more favorable both on the basis of geometric considerations and the fact that it alone can produce the requisite pressurizing effects.

Although the structure of the grain boundary is not known in detail, it is assumed that sites for oxide formation are available in the form of facets or similar discontinuities at the grain boundaries. In any event, formation of new oxide appears to be more probable at the boundaries than within the grains.

In summary, it has been postulated that during the course of oxidation some oxide forms at pre-existing oxide grain boundaries, by means of lateral diffusion, and thus gives rise to a lateral compressive stress in the oxide layer. The magnitude of this stress, calculated from the elongation of flat specimens and compressive creep data, by the method of Appendix 3, is found to be of the order of 1500 psi, at 1000°C. Calculations based on

microstructural evidence and elongation data indicate that the average thickness of material deposited in this manner is of the order of thirty lattice parameters of the oxide per grain boundary, in 16 hours at 1000°C.

4.32 Plastic Deformation of the Scale

The applicability of an elastic model for the description of stresses and strains which occur during the oxidation process is necessarily limited. A primary consideration is the fact that there is no clear definition of the terms "elastic limit" or "yield stress" for a material subjected to loading at relatively high temperatures. In the vicinity of 1000°C, which is in excess of one-half of the Kelvin melting temperature for both nickel and nickel oxide, these terms necessarily carry with them the connotation of the short-time measurement. Further, although the metallic surface appears smooth upon metallographic inspection, it must in fact contain small-scale discontinuities. Thus, the oxidation process must proceed to such an extent that a coherent oxide film is formed whose thickness is large compared to the size of existing surface discontinuities before the elastic stress model may be utilized. In practice, this state of the process is reached within the first few minutes of oxidation at 1000°C.

An elastic analysis may be applied subsequent to the attainment of these conditions, but only until such time as the onset of plastic deformation occurs. Calculations

based on short-time mechanical behavior indicate that this occurs, for the scales formed on cylindrical specimens, very early in the oxidation process. In addition, the existence of the lateral stress associated with grain boundary pressure is large enough to cause early plastic deformation of scales formed on both flat and cylindrical specimens. It, therefore, appears that any stress-based effects must be interpreted in terms of the plastic behavior of the scale layers. It is generally conceded that plastic deformation requires the presence of dislocations. The most common dislocation found in ionic crystals of the NaCl structure is the $\langle 110 \rangle \{110\}$ -type, and it is believed that nickel oxide exhibits these (64).

In previous sections it has been proposed that stresses arise in the scale due to: 1) the oxide following the retreating metal-oxide interface under conditions of geometric constraint, and 2) the existence of a pressure, or compressive stress, at the oxide grain boundaries. Oxides developed on flat specimens are assumed to be, for the most part, subject only to stresses arising from the latter source. However, both sources of stress must be dealt with in the case of cylindrical specimens.

The scale formed on specimens of either geometry must necessarily be subjected to translation which allows contact to be maintained between metal and oxide. For the

range of specimen sizes investigated herein, each segment of oxide must be so transported, normal to the specimen surface, a distance equal to approximately 60 per cent of the scale thickness. Scales formed on cylindrical specimens must, however, have associated with their formation additional amounts of deformation. These arise from the lateral constraint imposed by maintenance of scale-metal contact.

The radial rate of metal consumption imposed by the oxidation process per se fixes the magnitude of the lateral compressive stress so generated. For a diffusion controlled process these stresses are highest in the initial stages of oxidation where the rate of "following" is greatest. At a fixed time and scale thickness, this stress increases with increasing specimen curvature. Its magnitude may be calculated from the strain rate-stress relation if the parabolic scaling rate constant is known. A more detailed application of these considerations is reserved for one of the following sections.

In the transposition of considerations from the elastic to the plastic case, it should be noted that radial plastic deformation of hollow cylinders does not lead to axial deformation. This effect has been demonstrated experimentally for the case of thick-walled steel tubing (65). Thus, it remains necessary to postulate the existence of a grain boundary pressure in order to comply with the observed axial extension of specimens.

4.4 Consideration Pertaining to the Structure of Scales

To this point, the scale layer has been treated as a homogeneous body with the exception that pressure sources have been introduced at the sites of grain boundaries. The purpose of this section is to delineate the consequences which arise as a result of the interaction of plastic deformation with the details of the structural features of the scale. The effects which arise from such interactions are believed to be of major importance in the mechanism of scale formation.

4.41 The Grain Boundary Network of the Scales

The processes which take place between the time of oxygen adsorption on the metal and the time at which the first detectable oxide is formed are essentially unknown. Observations of oxidizing metals at low magnification indicate that oxide patches, herein termed crystallites, quickly form and merge to produce the initial coherent scale (1, 3). This behavior indicates that the nucleation process involves at least one high-energy step and that the details of the surface structure, i.e., imperfection and impurities thereon, may play a major role in the nucleation process. This lends credence to the concept that the presence of oxygen in the grain boundaries of the scale is in itself not a sufficient condition for nucleation of oxide at the metal-oxide interface.

Subsequent to the formation of stable oxide crystallites at the metal surface, lateral growth of the oxide is assumed to ensue until the crystallites meet. The remaining "empty" space on the metal surface is then filled by the addition of material to the pre-existing growth sites and a "two-dimensional mosaic" of oxide is formed which separates the oxidizing gas and the metal. Similar schemes for the formation of the initial oxide layer on nickel have been advanced by others (66, 67, 68). After this layer has thickened, by transport of nickel through the oxide to the oxidant-oxide interface, it may be considered in terms of an oxide grain boundary network.

If this network is considered to be composed of cylindrical surfaces, normal to the metal surface, then the structure so defined contains:

- 1) Volumes, representing grains, which are bounded by the metal-oxide interface, the gas-oxide interface, and the surfaces of neighboring volumes.

- 2) Surfaces, both external and internal, which bound the volume occupied by the grains.

- 3) Lines of intersection of three oxide grains, hereafter referred to as "triple lines."

- 4) Points of intersection of the triple lines with the metal-oxide and gas-oxide interfaces, hereafter referred to as "external quadruple points."

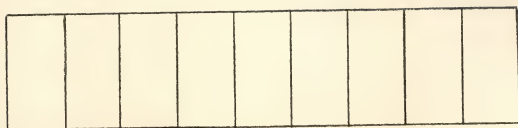
This concept of the grain boundary network is oversimplified, basically, in that the generators of the cylindrical surfaces involved are not precisely normal to the metallic surface due to the fact some grains are better oriented for growth than their neighbors. As a consequence, certain of the cylindrical surfaces intersect, which, in the case of oxide growth leads to the "cutting off" of some of the grains by their neighbors and introduces the possibility of providing the scale with internal quadruple points.

The distance from the metal-oxide interface at which internal quadruple points are first formed is dependent upon several conditions. If it is assumed that the first stable oxide grains are positioned regularly in space, but randomly in orientation, with respect to the metallic substrate, then an average rate (or angle) of lateral spreading may be defined for those grains of favored orientation. The relative preference for growth will determine the degree to which single grains may grow laterally. In the case that no growth preference exists, a purely columnar structure forms on a flat specimen and the internal quadruple points are located at infinity; i.e., they do not exist within the scale structure. This case is illustrated in Figure 106a. As the relative degree of preference between crystals of various orientation becomes more accentuated, these quadruple points approach the metal-oxide interface

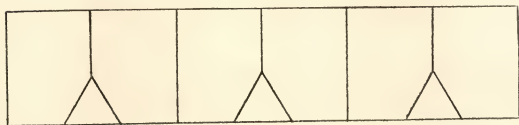
more closely and may become located within the scale layer. A two-dimensional schematic representation of the effect is illustrated in Figure 106b. Since these points exist in the space of the scale they are rarely encountered and never identifiable in single cross sections of the real scales.

The lateral dimension of the stable oxide grains at the metal-oxide interface also affects the location of the loci of quadruple points. Figures 106b and 106c show that as these grains become larger, the internal quadruple points are located further from the metal-oxide interface. This schematic drawing was constructed employing the same degree of growth preference as that used in Figure 106b.

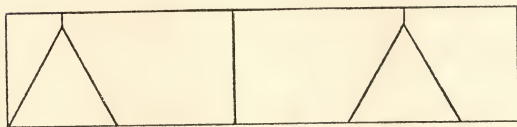
In the case of real scales, the above idealized description is slightly altered; however, the effects indicated remain qualitatively unchanged. The major alterations arise from differences between the assumed and the true distributions of initial oxide grain size and spacing. Non-uniform distributions in size and position resulting from non-uniform oxide nucleation will ² effect the local rate (or angle) of lateral spreading of oxide grains. This, in turn, will cause variation in distance between the internal quadruple points and the metal-oxide interface of the scale. Thus, the sharply defined loci of quadruple points, illustrated in the schematic drawings, become the



(a)



(b)



(c)

Figure 106: Schematic representation of oxide crystal growth; no favored orientation, (a); some favored orientation, (b); and favored orientation coupled with large grain size, (c).

centerlines of "bands" containing quadruple points in the real structure.

The concept of lateral spreading is further complicated by interaction arising between grains of preferred orientation and their neighbors during the growth process. As the initial lateral growth proceeds, the stable grains impinge, and those of favored orientation tend to cover their neighbors. If it is assumed that the grains possessing favored orientation must derive their supply of nickel from a diffusion path passing directly from the growing surface to the metal-oxide interface through their own volume, then the lateral growth will diminish as the path length increases because there is no passage of nickel across the oxide grain boundaries. This causes the grains of preferred orientation to take on a convex form near their bases when viewed from the metal-oxide interface. Since an oxide grain boundary is created between the covering and covered grains, the lateral growth of preferred grains may be further retarded while their normal growth is accentuated due to the effect of grain boundary pressure. The observed paraboloid-like grain shape, noted in the case of the dominant grains of certain scales, is thought to be due to this type of growth process. Other evidence for the opacity of oxide grain boundaries to nickel will be cited later.

cf electroplating

?

Quadruple points are generated in the scale when the growth process has continued long enough to allow grains of favored orientation to cover or "cut-off" their neighbors. In the case of air oxidation, wherein the grains at the metal-oxide interface are relatively small, this happens rather early. Specimens oxidized in oxygen, on the other hand exhibit much larger grains at this interface so that very few grains are "cut-off." However, these structures are believed to be different in degree rather than kind. If the oxidation process were extended to long enough times, it is believed that all structures would exhibit internal quadruple points generated by the preferred growth process, since barring "perfect" orientation, some grain-to-grain growth preference must always exist.

The paraboloid-like grain shape, in this case, becomes rather important to the final scale structure. The specimens examined indicate that the fraction of favorably oriented grains is relatively high; thus, quadruple points are essentially generated by the establishment of contact between three of the faster-growing grains. Since the degree of lateral spreading is small at the time such contact is made, the quadruple points do not form until an appreciable amount of scale is developed. The angle of lateral spreading, just prior to this event, is strongly diminished with respect to its initial value. This will tend to accentuate the width

of the zone of quadruple points within the scale. It may be noted that the specimen curvatures, such as those employed herein, probably cannot measurably alter the distance between the quadruple points and the metal-oxide interface.

4.42 Deformation-Induced Alterations of the Grain Structure

It has been postulated that mechanical deformation of the scale accompanies the oxide growth process. The shears associated with this deformation are, however, not necessarily constrained solely to certain crystallographic directions within the oxide grains of scale. In the case of polycrystalline materials subjected to plastic deformation, a portion of the deformation may pass through a region immediately adjacent to the grain boundaries. This type of deformation has been associated with materials which are subjected to plastic flow at temperatures in excess of their recovery temperatures. The oxidation temperatures employed herein are believed to be in excess of the recovery temperature of nickel oxide and a portion of the deformation is believed to be relegated to the grain boundary regions. The overall process involved, termed grain boundary shearing, has been discussed by others (69).

In the case of boundary networks which contain no internal quadruple points, such as a purely columnar structure, the major effect of this phenomenon is simply to produce a surface step in the oxide structure. If scales

do, however, contain internal quadruple points, then grain boundary shearing may promote mechanical defects within the scale. Under conditions of preferred crystal growth, quadruple points are introduced into the scale layer by the normal thickening process per se. Therefore, it is believed that grain boundary shearing, and the effects which arise from it are of greater importance in the later stages of the oxidation process.

Examination of certain of the specimens indicated that oxygen, as well as nickel, may have been transported through the scale layer. The oxide grains located beneath the apparent position of the metal-oxide interface, henceforth termed "undergrowth," are believed to thicken as a result of this type of transport. Examples of undergrowth formation may be recognized most easily in the photomicrographs of Figures 44, 53 and 66.

Since this mode of oxide formation has been found to be associated primarily with cylindrical specimens and only rarely with flat specimens, it must arise, basically, from geometrically-controlled effects. This observation seems to rule out the possibility of continuous underlayer formation by diffusion-controlled transport of oxygen through the oxide boundaries (or grains) of the scale since specimen geometry per se would be expected to alter only the degree and not the mode of transport. Therefore,

it is believed that the oxide grains associated with underlayer formation are supplied with oxidant by some type of mechanical defects which traverse the scale from the gas-oxide to the metal-oxide interface.

It is postulated that grain boundary shearing, in the scale layer, is responsible for the creation of void space at internal quadruple points and its subsequent propagation along triple lines of the oxide grain boundary network. If the rate of propagation of void space is greater than that of addition of material by normal and lateral growth, then the void space could supply the scale traversing defect necessary to admit oxygen to the metal-oxide interface. The void distributions present in the photomicrographs of Figures 51 through 53 support this concept.

In the case of flat specimens, the major driving force available for the activation of this mechanism is the lateral stress created by grain boundary pressure. Further, if one considers the lateral growth derived from the addition of material at pre-existing oxide grain boundaries, the mechanism postulated for the production of grain boundary pressure, then it is seen that each oxide grain is augmented in size and that it is necessarily under constraint; i.e., the grains no longer fit properly into the network. This type of constraint would tend to

act most strongly in the region of triple lines and quadruple points. It is feasible that the grain structure would, therefore, "pull apart" or more precisely be "wedged apart," with the subsequent formation and propagation of void space.

The wedging process, applied to the region of the oxide immediately adjacent to the metal-oxide interface, could conceivably provide the conditions necessary for formation of undergrowth crystals. It is postulated that the shears associated with addition of material to oxide grain boundaries is more severe in the region of scale immediately adjacent to this interface. A localized tilting of the oxide lattice may then ensue, causing subgrain boundary formation. Aggravation of this process, by continued local shearing, could then lead to the oxide grain boundary formation observed as undergrowth. This process is believed to continue until a coherent undergrowth, one oxide crystal in thickness, is produced. Normal growth of the crystals so formed would be enhanced by oxidant supplied through opened triple lines of the scale.

With the formation of new quadruple points between the undergrowth and the original oxide, further oxidation (and deformation) would again form and propagate void space at the triple lines of the undergrowth. This, in turn, could lead to a "third generation" of oxide crystals beneath the undergrowth. However, this repetitive process is thought to be extremely slow in the case of nickel oxidation due to a

deficiency of oxygen beneath the original oxide crystals and the attendant low rate of scale deformation.

In the case of specimens possessing positive curvature, the lateral stresses due to grain boundary pressure would be augmented by those due to geometric constraint. Early in the oxidation process, deformation may be so severe that the grain boundary region associated with grain boundary shearing widens to a point where it becomes indistinguishable from the grain itself. Under these conditions, one may expect bulk deformation of oxide grains which essentially takes the form of extrusion. Subsequent reduction of the state of stress, or rate of deformation, which accompanies the scale thickening process, would tend to reestablish the identity of the grain boundary shearing mechanism. As a result, the process of void formation and propagation necessary to undergrowth thickening could ensue.

Other investigators have found that a "two-layered" scale forms on nickel and it has been pointed out that this effect may be due to the presence of impurities in the material used. The purity of material employed in this research is, however, much in excess of the composition limit set for dividing the scaling behavior into one- and two-layer classes. It is therefore felt that the production of the second layer is intimately associated with the details of the oxidation mechanism per se, as postulated above.

4.43 Rearrangement of the External Surface of Oxide Grains

It has been postulated that, during the oxidation process, nickel is delivered to both the external surface of the scale and to the oxide grain boundary region. This feature of the process requires that the system of growing oxide crystals be regarded as an entity different from a similarly arranged group of crystals which are not growing, if surface rearrangement is considered. The faceting process is envisioned as a competitive one wherein the rate of surface rearrangement must be balanced against the rate of oxide formation. In order to proceed from this point, it is therefore expedient to first consider the behavior of a static system (not growing) and then apply the modifications induced by transport of material from the underlying metal.

Rearrangement of the crystals of a columnar scale, in the form of faceting, may occur as a result of effects arising from interfacial energies if the supply of nickel from their substrates is removed. The general principles involved in such rearrangement, under conditions wherein the volume of material is nearly constant, have previously been applied to polycrystalline materials (70, 71).

A region surrounding the external surface of the oxide may be considered to contain two phases: the oxidizing gas and the oxide. Areas of the surface, wherein an oxide grain is in contact with the gas, have associated

with them the gas-oxide interfacial energy. Lines on the external oxide surface, which represent the termination of grain boundaries, have associated with them three interfacial energies: gas-oxide₁, gas-oxide₂, and oxide₁-oxide₂.^{*} Similarly, six interfacial energies may be enumerated for the quadruple points of the surface. The relative magnitudes of these interfacial energies will, in part, determine the equilibrium distribution of material under conditions of adequate surface mobility.

If the gas-oxide interfacial energy is much lower than that associated with the oxide-oxide surface, as is thought to be the case, then the oxide-oxide surface will be destroyed in favor of the creation of gas-oxide interfaces. Further, if this surface transport process is allowed to continue until the surface of the scale approaches equilibrium, then one would expect to observe effects due to the directional anisotropy of the oxide crystal's surface energy (71). In particular, the production of faceted grain surfaces or grains exhibiting idiomorphic shapes such as those shown in Figure 85 would be predicted to result from this driving force for rearrangement.

^{*}The subscripts used here denote different oxide grains.

Quadruple points of the oxide surface provide favorable sites from which facets may grow. At the beginning of the faceting process, one faceting surface of each of the three associated oxide grains may be developed by the transport of a relatively small amount of material, with the expenditure of little energy. As the process continues, the volume of the pyramidal facet pit is believed to increase by surface transport of material from each of the relatively stable crystal facets to the outermost surface of their grains. Under conditions of material conservation, this would lead to a thickening of the scales. It should be noted that the external quadruple point which recedes along a triple line of the oxide structure is at all times the point of deepest intrusion of the gaseous phase.

In the case of growing oxide crystals the description of surface rearrangement just presented is modified by considerations of the rate of delivery of material to various crystal surfaces. Thus, the existence of a columnar oxide grain structure which fills all space in the region of the scale indicates that the effects due to growth have overshadowed those due to the anisotropic nature of the crystal surface energy. Such structures are believed to arise from the lateral growth of oxide crystals under conditions of relatively high rates of nickel delivery to their surfaces.

If complete contact of the scale is maintained, both internally and at the metal-oxide interface, then the rate of delivery of nickel to the external surface is as high as possible and one might expect that the rate of delivery of material to the surface would exceed that of surface rearrangement. However, some specimens exhibit faceted surfaces in spite of the fact that the scales formed are adherent and appear to be relatively free of mechanical defects which would act as diffusion barriers. Such specimens usually exhibit some degree of undergrowth formation. It is, therefore, proposed that transport of nickel from the substrate takes place only through single, columnar oxide grains which are in direct contact with the metallic phase.

Thus, although nickel is free to move through the metal-oxide and gas-oxide interfaces, it is believed that transport of nickel through the oxide-oxide interfaces (grain boundaries) is highly restricted. This concept is supported by the observation that the lateral dimension of oxide grains is apparently unchanged by increasing the duration of oxidation. Such dimensional stability is, in turn, indicative of a lack of lateral transport through columnar grain boundaries. Faceting of the external surface is, therefore, believed to arise only for those scales (or portions of scales) which have lost direct

contact with the metal-oxide interface. Under such conditions it is postulated that nickel can no longer be delivered to the gas-oxide interface of the grain, because it would have to cross the oxide-oxide boundary to get from the metal phase into the oxide crystal.

4.5 A Proposed Mechanism for the Oxidation of Nickel

It has been proposed that deformation, in the form of shears passing through the scale layers, necessarily accompanies the continued oxidation of nickel. In the previous sections, concepts involving the interaction of this deformation with the microstructural features of the scale were introduced. The purpose of this section is to unify these concepts into a single mechanism of the scaling process for nickel which is compatible with the experimental observations of this research.

Subsequent to the initiation and production of oxide crystallites, the oxide grains grow to form a three-dimensional grain boundary network. Attendant with the formation of this network is the proposed grain boundary pressure which is large enough to cause plastic deformation of the oxide crystals. The state of stress in the scale is determined by the mechanical response of the oxide to this pressure and the stresses which arise as a result of the constraint developed by the scale (as a unit) attempting to follow the retreating metal.

In the case of flat specimens, this latter source of stress is believed to be negligibly small; however, in the case of specimens possessing curvature it must be taken into account. Scales developed on convex specimens will thus be subjected to greater stresses and suffer more severe deformation than those developed on flat specimens, while scales developed on concave specimens may be subject to reduced circumferential compression. Since results of investigations concerning deformation-enhanced transport processes are, to date, inconclusive; it is assumed that these stresses cause only mechanical, as opposed to physicochemical effects.

At the oxidation temperatures employed herein, this mechanical deformation is believed to lead to grain boundary shearing except in the case of very high scale stresses where this process degenerates to extrusion. Prior to the time at which the growth of crystallites possessing preferred orientation produce quadruple points within the scale, effects due to this mode of deformation are believed negligible. However, after quadruple points have been developed, voids may form at these sites as a result of grain boundary shearing and the void space may subsequently be propagated along the associated triple lines. It is proposed that this mode of deformation provides a defect or "channel" which completely traverses the scale and which is capable of providing a relatively

easy path for oxygen transport to a region of metal-oxide interface.

It has been postulated that a localized rearrangement of the structure of individual columnar oxide crystals also arise as a result of concentrated shearing in the region of the metal-oxide interface. This deformation initially takes the form of lattice bending which, when sufficiently severe, provides an oxide grain boundary within the original columnar grain. The small grain so formed, immediately adjacent to the metal-oxide interface, is one crystal of several which are collectively termed undergrowth.

The thickening of this layer of crystals may proceed by the flow of oxygen from the outermost surface of the specimen. Two classes of oxygen transport through the scale are thought to exist:

(1) Restricted transport wherein oxygen arrives at the undergrowth crystals via oxide grain boundary diffusion.

(2) A less-restricted form of transport wherein oxygen enters via void space associated with triple lines of the scale.

In the latter case, thickening of the undergrowth once again involves grain boundary diffusion; however, the path length would be diminished.

It is further postulated that the electrostatic character of the (ionic) nickel oxide grain boundaries is such that transport of nickel through the boundary region is severely restricted. In view of the condition on the transport of nickel, it is believed that undergrowth formation is accompanied by a reduction in the rate of overall scale thickening.

Since the oxide grain boundaries are assumed to be opaque to nickel transport, formation of the undergrowth removes the supply of nickel from the overlying grains and faceting of them may commence. As faceting proceeds, it is believed that intergranular matter is transported by essentially surface paths from high- to low-energy sites of individual grains. In addition, the lack of nickel supply removes the source of grain boundary pressure in the original scale, so that stresses are relegated to the region of the undergrowth. It is proposed that the cycle of events becomes complete when faceting of the primary layer is so aggravated that the older grains fall away and the supply of oxygen to the undergrowth is equivalent to that of the surrounding environment.

4.6 Interpretation of Results of This Investigation

The quantity of scale formed on nickel specimens during oxidation at elevated temperatures has been found to

be dependent upon both the duration of oxidation and the particular specimen geometry employed. Further, it has been found that the quantity of scale produced is not, in general, simply related to the oxidation time or the specimen shape; rather, it appears that these parameters are interrelated. The proposed scaling mechanism predicts that there will exist an effect of specimen geometry on the scaling behavior provided specific structural features obtain in the scale. For this reason, the results of the present investigation will be compared to those predicted by the proposed mechanism in that both the degree of scale development and the degree of deformation will be considered.

It will be seen that the proposed mechanism provides a reasonable and consistent explanation of the scale thickening effects, oxide microstructures, and macroscopic specimen deformations observed herein as a result of oxidizing high-purity nickel. The principles involved are, however, believed to be applicable to the field of high-temperature oxidation of metals as a whole. The applicability of the proposed scaling mechanism to other oxidation studies is reserved for a later section of this work.

The results of this research, which should be forecast by the proposed mechanism may be broadly classified into five major categories: rate of oxygen consumption

scale thickening characteristics, microstructural features of the scale, macroscopic deformation behavior and special experiments. It will prove expedient to discuss the first and last of these as separate entities, while scale thickening and oxide microstructure are so closely related that they must be discussed as a unit. The material which follows is in the form of a point-to-point assessment of the data in terms of the proposed scaling mechanism. This analysis follows the organization of Chapter III as far as is practicable.

4.61 Oxygen Consumption

So long as the thickness of scale is small, few quadruple points exist within it and, for this case, the proposed scaling mechanism predicts that the scaling rate should remain parabolic, independent of both oxidation time and the degree of oxide constraint. The parabolic scaling rate indicated by the linear relation between oxygen consumption and the square root of oxidation time, as shown in Figures 9 through 13, is in accord with the proposed mechanism. Since the oxidation times involved are relatively short (about 2 hours), the scales developed would be expected to be thin (of the order of 5 microns) and almost entirely free of quadruple points. Under these conditions, plastic flow of the scale could not generate

the defects necessary for undergrowth formation and parabolic scaling would be expected to persist, as observed.

In order to interpret properly some aspects of the results of the volumetric experiments, certain features of the structural character of both metal and oxide must be recognized. The Mond Process nickel spheroids used in this series of experiments are fabricated by continuous deposition of nickel on nickel "seeds" by the decomposition of gaseous nickel carbonyl. This mode of production provides a material, which, though free of other metallic contaminants, is not perfectly dense. Metallographic inspection of these specimens indicated that the internal voids are probably in the form of disk-like areas which are oriented nearly parallel to the surface of large specimens and nearly normal to the surface of smaller ones. In addition, the external surfaces are not even approximately smooth as evidenced by their matte-grey color.

The lack of an initially smooth metal surface is believed to be responsible for the initial deviations from "pure" parabolic behavior shown in Figures 9 through 13. Thus, fluctuation in the values of the initial scaling rate constant, K_{V1} , are believed to merely represent a type of complex surface readjustment which tends to provide an effectively smooth surface which then oxidizes parabolically.

Inspection of specimens prior to oxidation did not reveal any systematic difference in the surface roughness of prepared specimens.

The observed trend of increasing final rates of reaction, (K_{V2}), with increasing specimen curvature, Figure 15, is believed to be due to the particular manner in which the porosity of the Mond Process nickel spheroids change with specimen size. As the specimen diameter is decreased, the probability that a channel of porosity intercepts the specimen surface increases. Metallographic inspection of the specimens indicated that these channels do not oxidize completely; i.e., after oxidation they remain essentially voids rather than sites of deep oxide penetration.

Inspection of the scale layers showed that the scales which formed contained less than one-tenth the volume fraction of void space originally present in the metal. This suggests that the void space is closed by lateral plastic flow of the oxide as the scaling process progresses. Since a larger fraction of the original surface of smaller specimens is composed of void channels, the scales formed on them would be capable of more lateral plastic flow than those developed on larger specimens. As a result, the thickness of the scale, which is inversely proportional to the rate of oxidation, would be less for smaller specimens. Therefore, the scaling rate, as measured

by oxygen consumption per unit of projected surface area, would be greater for smaller specimens, as is observed.

The phenomenon involving lateral plastic flow of the scale, employed above, is not contrary to the basic ideas involved in the proposed scaling mechanism; rather, it supports them. The observed lateral flow, in place of the predicted scale extrusion under conditions of constraints, is believed to be merely a consequence of the specially-distributed porosity. This behavior indicates that some scale extrusion, normal to the specimen surface, would have probably occurred under conditions of stronger lateral constraint; i.e., the absence of pores.

4.62 Scale Thickening and Oxide Microstructure

The Nickel-270 bar stock used in all but the oxygen consumption experiments of this investigation, was pore-free and found to exhibit the theoretical density of nickel, within experimental error. The metallic surfaces provided were metallographically smooth and mirror-like so that the ratio of geometric to true surface area was probably very nearly unity. Thus, effects arising from lateral constraint of the oxide may be expected to appear under these circumstances where they are predicted by the proposed scaling mechanism.

One of the most striking features of the scale thickening studies is the persistence of the geometric

dependence of this feature of the oxidation process, independent of oxidation temperature, oxygen pressure, or other environmental factors. Figures 16 through 25 and 32 indicate that solid cylindrical specimens developed thicker scales than do flat specimens when oxidized under isochronic, isothermal conditions. This behavior is in accord with that predicted since the lateral yielding of the oxide is larger in the case of cylindrical specimens than it is in flat specimens.

The general features of the scale developed on cylindrical specimens are believed to be represented, qualitatively, by the three-dimensional graph of Figure 31. The observed time dependence of the effect of specimen curvature illustrated therein is in accord with the concept that certain structural features must obtain in the scale prior to the development of a curvature-dependent scaling rate. The precise form of the plotted surface will, of course, depend upon the specific environmental conditions which prevail during oxidation; however, it is felt that such a difference will basically alter only the elevation and not the overall shape of this surface.

The oxide microstructures were, of course, developed at elevated temperatures whereas metallographic inspection was carried out at room temperature. Although evidence of the mechanical deformation of the oxide structure was obtained

at room temperature, it is believed that the deformation had occurred at the oxidation temperature and did not result during the cooling of specimens. This view is supported by the fact that measurements of the thermal coefficients of expansion of nickel and nickel oxide indicate that their average values are so nearly equal that the differential strain due to cooling from 1000°C would not exceed 0.05 per cent (35). Strains of such magnitude could hardly account for most of the observed deformations in oxide surface structure.

Microscopic evidence for the existence of stresses and attendant deformation in oxide scales include observations of void and blister formation and a general roughening of the surface structure in the form of protrusions at points of grain-to-grain contact, the apparent extrusion of oxide grains beyond the general level of the scale layer, and deformation markings present at the external surface of certain oxide grains. Many of these features may be best explained when considered from the viewpoint of the proposed scaling mechanism. Thus, oxide protrusions at points of grain-to-grain contact and the observation of elevated grain boundary regions are believed to arise from the existence of a grain boundary pressure, while tilted or warped oxide grain surfaces are believed to be due both to this pressure and shear deformation necessary to the maintenance of scale contact at the metal-oxide interface.

Oxidation in Air for 16 Hours at 1000°C - The various features of the surface of Figure 31 may be best explained using the 16-hour, 1000°C data as a model since they represent a relatively advanced degree of oxidation in terms of the proposed scaling mechanism; i.e., quadruple points are believed to be present in all of the scales produced. The total scale thickness, including undergrowth, is shown in the graph of Figure 16 and corresponding microstructures may be seen in Figures 45 through 53. The initial increase in scale thickness with increased curvature is believed to represent the addition of increasing amounts of undergrowth to a layer of fixed thickness (about 26 microns) of original columnar scale. It should be emphasized that the measuring process employed averages individual determinations of scale thickness. Thus, either a greater thickness of isolated units of undergrowth or a more uniform distribution of undergrowth having some lesser thickness would produce the same average value of total scale thickness.

The cross-sectional view of the flat specimen, Figure 51a, shows voids located on the grain boundary network and a very small degree of undergrowth formation. In terms of what has been proposed, the voids are interpreted as sections through triple lines along which void space has been propagated. An oblique section through the scale

indicated that these voids are in fact a section through a zone of connected porosity which appears to be centered within a stratum roughly parallel to the surface of the specimen. This zone is believed to contain the outermost quadruple points of the scale.

The presence of these voids plus the small amount of undergrowth, shown in Figure 51a, for the case of a flat specimen, indicates that the grain boundary pressure alone is able to both nucleate void space and to propagate it to form a scale-traversing channel. This latter event probably occurred late in the process since no faceting of the external surface and a very small amount of undergrowth were noted. The observed scale thickening and microstructural features of the scale are those which would be expected on the basis of the proposed scaling mechanism.

Further increases in curvature, to a value of approximately 6 cm^{-1} are believed to promote an increasing number of patch-like undergrowth formations having nearly the same thickness (about 4 microns). This behavior is expected on the basis of the postulated increased scale deformation associated with specimens of higher curvature. Such enhanced deformation is thought to increase the number of channels formed as the curvature is increased, and thereby promote increased underlayer growth.

Since the deformation suffered by the oxide is strongly dependent upon the specimen curvature, larger amounts of surface upheaval would be expected as a result of relatively small increases in curvature. Figures 45 and 46a illustrate this effect. They also indicate that undergrowth formation is relatively recent since no appreciable degree of faceting has taken place. However, the increasing number of large cavities shown in Figure 52a, for the specimen curvature 6.4 cm^{-1} , indicates that this scale is more friable than those developed on specimens of lower curvature. This behavior is interpreted as being due to mechanical weakening of specific portions of the scale at the onset of faceting. The electron photomicrograph of the surface of this specimen, Figure 48a, illustrates a faceted portion of the scale which implies local stoppage of nickel transport into the first-formed crystals. This behavior also indicates that the nickel supply to the surface was interrupted earlier in the case of this specimen than it was for those specimens of lower curvature. Thus, the observed behavior for curvatures less than approximately 6 cm^{-1} is precisely that predicted by the proposed scaling mechanism.

As the curvature is increased to a value in excess of approximately 7 cm^{-1} , the circumferential stress level is apparently large enough to cause severe deformation of

the oxide in the region immediately adjacent to the metal-oxide interface. As a result, the bases of some of the columnar grains appear to be highly distorted, as if they had been fragmented. According to what has been proposed, additional deformation, caused by those grains which have maintained contact, would provide few scale-traversing channels necessary for the admission of air to the metal-oxide interface and subsequent undergrowth thickening.

Air, once admitted to the region of the metal-oxide interface, is thought to be not only capable of promoting further development of the undergrowth, but also of faceting those grains which are not directly connected to the metallic substrate. It is believed that this process provides the friable, nearly continuous dark band of faceted oxide formed at the innermost zone of the original scale shown in Figure 52b. In addition, since the supply of air is limited by the closely-packed overlying grains, there is only a small amount available for undergrowth development and this layer is subsequently relatively thin.

The proposed mechanism would predict that there is more time for facet formation and structural weakening of the oxide since the supply of nickel to the original columnar grains is disrupted relatively early in the process. Deep faceting of the surface, illustrated in Figure 46b, and the sensitivity of the oxide to mechanical

and/or thermal shocks, evidenced by the cracking shown in Figure 52b, both suggest early removal of the nickel supply. This, in turn, is believed to be responsible for the relatively thin outer layer of columnar oxide and the decrease in total scale thickening near the midrange of specimen curvature investigated, illustrated in Figure 16.

A further increase in curvature, to approximately 12 cm^{-1} , would be predicted to increase the amount of deformation in the scale which would cause, in addition to the effects noted above, a measurable lengthening of the first-formed oxide crystals by extrusion. This mode of deformation is believed to obviate lattice bending in the columnar crystals. The time of undergrowth formation would therefore be delayed due to the plastic extension of oxide grains, with respect to that predicted on the basis of curvature-induced deformation alone. The "grain-straightening" process, caused by extrusion, and the larger channels also apparently provide easier paths for oxygen transport, as evidenced by the thicker undergrowth layer and the large, dark zone of faceted crystals shown in Figure 53a. The same process appears to aggravate surface faceting in that the external quadruple points appear to have intruded to a greater depth causing a general weakening of the structure as evidenced by its extreme friability. The degree of surface faceting

illustrated in Figure 47b, however, is less marked than that of the scale described immediately above. This indicates that the faceting process occurred later in time for the scale developed on the specimen of higher curvature, and that, therefore, when channels do occur after extrusion they are relatively massive.

The scale developed on the specimen of highest curvature. Figure 53b, exhibits certain areas, roughly in the shape of triangles, which consist of grains which appear to be fragmented. It is proposed that these areas were initially occupied by grains similar in shape to their neighbors, but less well oriented for radial plastic flow than they. The very large circumferential stress postulated to exist in the scale of the high-curvature specimen is believed to be responsible for this type of grain structure. In addition, the larger combined stresses are thought to have caused considerable lengthening of those grains more suitably oriented for extrusion.

It has been postulated that, under the influence of the higher stresses involved, the grain boundary region associated with grain boundary shearing becomes diffuse and bulk extrusion prevails. If this were so, it would tend to delay the onset of grain boundary shearing and subsequent channel formation. The irregularity of the undergrowth formation, Figure 53b, and the relatively

small degree of external faceting, Figure 50, both indicate that the undergrowth formation has been delayed relative to some of the specimens possessing lower curvature. The trend for slightly decreased oxide adhesion, Figure 86a, near the midrange of curvature investigated further supports the idea of delayed undergrowth formation in that the scales formed on the specimen, of highest curvature are apparently not mechanically weakened by subsequent faceting.

Further evidence for grain extrusion during oxidation of this specimen may be seen in the photomicrograph of Figure 47b which shows oxide protrusions at points of grain-to-grain contact. In addition, the photomicrographs of Figures 53b and 54 show axial and longitudinal sections, respectively, indicating that grains are essentially in the form of flat pie-shaped wedges - the form expected for radial extrusion by the proposed dominant circumferential compression. This latter feature may, however, also arise as a result of other phenomena.

The tendency for preferential alignment of oxide grains in the scales, although most probably arising as a result of microscopic alteration of the growth mode, may be qualitatively described on the basis of the proposed scheme of macroscopic scale deformation in spite of the fact that this deformation is smaller than that

usually associated with the production of textures. X-ray examination of flat specimens oxidized in dried oxygen, which are believed to have possessed growing scales at the termination of the treatment, showed that the $\{220\}$ -reflection was abnormally strong. This indicates that, for the oxide, the preferred direction of growth is $\langle 110 \rangle$. If the largest principal (compressive) stress in the scale of a cylindrical specimen is considered to be the circumferential stress, as postulated, then there should be a tendency for the slip plane to contain the specimen axis. Since the slip system in the oxide is most probably $\langle 110 \rangle \{110\}$, the predicted wire texture would be approximately a $\langle 111 \rangle$ -type. Upon the addition of stress in other principal directions, one may expect a "rotation" of this spatial relation which is dependent upon the ratio of the stresses involved.

Tests in which the amplitude of the thermal wave was varied indicate that such rotation is possible. Since the scales of the specimens employed in these tests exhibited faceting, it would be predicted that the supply of nickel, and therefore the grain boundary pressure, is absent in the outermost (reflecting) grains. If there has been introduced a small-amplitude thermal variation, then one would expect that the oxide grains would retain the growth-

induced wire texture provided basically by the postulated circumferential stress originally present. Figure 93 is believed to show the results representative of this case. If, on the other hand, a large-amplitude thermal variation were present, then the alignment effects, due to circumferential and axial deformations would be expected to be more nearly equal. The relatively weak $\langle 100 \rangle$ wire texture, shown in Figures 58 and 94, appears as if it had been produced by such deformation induced alignment. The fact that the oxide exhibits a weak $\langle 111 \rangle$ -type texture in the absence of the small superimposed thermal stress (approximately 200 psi), also is in accord with the apparent "rotation" suggested above.

The scales developed on specimens of higher curvature occasionally exhibited blisters such as those shown in Figures 56 and 57. These photomicrographs indicate that the oxide crystals tend to act in a cooperative, rather than independent, fashion in that the blisters illustrated therein are composed of several oxide grains. This observation supports the idea of treating the scale as a homogeneous band of material; a concept implicit in the considerations involving the existence of a circumferential constraint. In addition, the photomicrographs of Figures 56 and 57 illustrate the following important features in the scaling process:

1) The apparent radial displacement of the blister "cap" away from the metal-oxide interface as well as the curvature of the original shearing surfaces indicates that the oxide crystals which form upon the "floor" of the blister cavity are capable of exerting a thrust on those associated with the detached portion of the scale. These observations are in accord with the proposed existence of a grain boundary pressure since, after sintering, the surface joining old and new grains is essentially a specially-oriented oxide grain boundary.

2) The blister "cap" is porous, thus further scaling processes may take place by the passage of oxygen through the outermost surface of the blister and subsequent reaction at the "floor" of the blister cavity. In both cases shown, the thickness of the columnar oxide, at the time of blister formation, was approximately one-third that finally developed, while the thickness of the oxide at the "floor" of the cavity is more nearly twice this amount. This indicates that a critical thickness, or time, may be associated with blister formation. In terms of the proposed oxidation mechanism, this would correspond to a time just subsequent to quadruple point generation in the scale. It therefore appears that the combined effects of relatively high circumferential

compression and the nucleation of the undergrowth may in some cases cause local blistering of the first-formed oxide.

3) The tapered thickness of the original scale zone, shown in Figure 57b, lends credence to the concept that the undergrowth is capable of a rather slow "sideways" propagation. It is suggested that this may arise as a result of the bending of crystals by their neighbors as the initial sites of undergrowth thicken. The tapering of the scale thickness above the underlayer is believed to be indicative of variations in length of time contact between the original crystals and the metal-oxide interface has been maintained. It is thought that the progressive differences in thickness arise basically from the fact that the grain boundary between the original crystals and the undergrowth is opaque to nickel transport.

It is proposed that the formation of an underlying oxide layer may, in some cases, promote subsequent blister formation. Because nickel transport is blocked by the boundaries of the underlying scale, its supply to the outer layer of oxide is diminished and faceting with attendant mechanical weakening of the external portion of the scale would be predicted. Subsequent outward buckling of the weakened scale by the residual lateral compressive stresses is believed to constitute the actual act of

blister formation. It is thought that this occurs rather suddenly, perhaps by the propagation of a crack near the interface common to older and newer oxide grains. This mechanism for blister formation is strongly suggested by the presence of the relatively large oxide crystals at the floor of the blister cavity shown in Figure 56.

The blister depicted in the photomicrograph of Figure 57, however, does not exhibit this feature as markedly. Thus, it appears that more than one mechanism for blister formation may be operative. It is suggested that local discontinuities in the surface of the metal, such as minute slag inclusions for example, may also act as blister-promoting agents much in the same manner as would a crystal of the undergrowth.

Flat specimens, unlike cylindrical ones, are assumed to have no stresses arising from the motion of the scale as it follows the retreating metal-oxide interface. Thus, the upper bound of the lateral stresses present is set by the magnitude of the postulated grain boundary pressure. Stresses this small are evidently insufficient to produce the scale distortion necessary for massive undergrowth formation during the course of the 16-hour, 1000°C oxidation treatment. The scale thickening of the series of cylindrical specimens just discussed supports this idea.

Determinations of the scale thickness developed on flat specimens revealed that in all cases the overall

scale thickness was less than that developed on similarly oxidized cylindrical specimens as predicted, Figure 22. This is believed to be due to: (1) the lack of undergrowth thickening, and (2) the relatively small amount of grain extrusion which can be caused by the smaller lateral stresses. The minor trend for decreasing scale thickness with decreasing specimen thickness is attributed, in part, to the fact that lateral stresses in scales developed on thinner specimens may be partially relieved by the extension of the metallic substrate. It is proposed that by partitioning a small amount of the deformation to the metal, the lateral stress is slightly diminished and so, according to what has been proposed, is oxide grain extrusion. Comparison of Figures 51a and 61b, representing the scales formed on the thickest and thinnest specimens, respectively, support this contention.

Secondary effects, due to the mode of specimen preparation may also play a role in the thickening process. Since the flat specimens were fabricated by cold-rolling and annealing, a (100) recrystallization texture has quite probably been produced in the metal (72). Further, it is expected that such a texture would be more pronounced for the thinner specimens which were subject to larger amounts of deformation. It has been found that thin films of nickel oxide tend to orient themselves crystallographically with

respect to the metal, and in particular the (111)-plane of the oxide tends to align parallel to the (100)-plane of the metal (73). If this original preferred growth persisted, then one might expect thinner layers of the oxide to form on more highly textured flat surfaces since the direction of growth, $\langle 111 \rangle$, requires that alternating layers of nickel and oxygen be provided. Thus, some portion of the apparent size effect noted for flat specimens may arise simply as a result of the degree of texture induced in specimen preparation.

The scale microstructures involved, Figures 59 through 61, exhibit relatively flat external oxide surfaces and columnar grains, generally without visible undergrowth. A single exception, Figure 59b, shows some degree of faceting which, in turn, indicates that undergrowth exists in the scale of this specimen. In view of this observation and the amount of scatter found in the scale thickness data of thicker metallic specimens, it is believed that there exists some relatively minor, non-systematic specimen-to-specimen differences in the initial size and orientation distributions of the oxide grains which may cause similarly treated specimens to exhibit slightly different degrees of oxidation.

Oxidation in Air at 900°C - Comparison of Figures 17 and 18 shows that while the scale thickening process is

nearly insensitive to specimen curvature at short times, there is a curvature dependence of the scale thickness for longer oxidation times. As in the previous case, this effect is attributed to the thickening of undergrowth during the course of the long-time treatments and its absence at shorter times. Figure 40 illustrates the nearly "pure" columnar structure produced during exposure for 16 hours. In contrast, after oxidation for 64 hours, a specimen possessing approximately the same curvature exhibits marked undergrowth formation accompanied by voids on the grain boundary network of the original columnar structure which are interpreted as sections through triple-line void space, Figure 44. Further, this figure illustrates the radial thrust associates with undergrowth formation in that the oxide is bowed outward above each segment of undergrowth formation. The general features illustrated indicate that grain boundary shearing is operative in polycrystalline nickel oxide at 900°C . However, the apparent intrusion of the undergrowth into the metal, shown in Figure 44, lacks explanation.

The large initial slope of the specimen curvature-scale thickness plot, Figure 17, indicates that the stresses induced by geometric constraint are more effective in providing the scale-traversing channels than was the case at 1000°C , Figure 16. This effect is thought to be due to

the lower overall plasticity of the oxide at 900°C which, in turn, concentrates the deformation in the grain boundary regions thus accentuating the role of grain boundary shearing. The low slope of the thickness-curvature plot associated with those specimens oxidized for lesser times indicates that grain boundary shearing in a purely columnar structure has little effect on the scaling behavior, as expected.

Both the appearance of undergrowth on specimens oxidized for 64 hours and the protrusions at points of grain-to-grain contact, for both the long- and short-time oxidation treatments, indicate that a grain boundary pressure also exists in the scale at 900°C. The effect of the curvature-induced constraint on the external structure of the scale is not as marked in the case of the specimens oxidized for 16 hours as it is for those oxidized for 64 hours, although both series of specimens exhibit a trend for increased scale roughening with increasing specimen curvature. Figures 41 and 42 show an increase in both the number and size of oxide protrusions as the curvature is increased from approximately 2 to 10 cm⁻¹. This effect has been predicted on the basis of the increase in constraint, and subsequent acceleration of plastic flow, as the curvature is increased.

At curvatures in excess of approximately 12 cm⁻¹, the external surface of the scale becomes faceted, Figure 43,

and the total scale thickness remains nearly constant. In terms of the proposed mechanism, this behavior indicates that, for curvature in excess of 12 cm^{-1} , a complete layer of undergrowth forms earlier (due to the larger amounts of deformation) and that the attendant removal of the nickel supply allows faceting. In addition, the photomicrographs of Figure 43 show that the degree of faceting increases with increasing specimen curvature, reinforcing the idea that undergrowth occurs earliest on specimens of highest curvature.

In contrast to the 16-hour, 1000°C behavior, there is apparently no drastic extension of the oxide grains by extrusion on the specimen of highest curvature. Thus, no marked "dip" was developed in the scale thickness-curvature plot. However, this is to be expected both on the basis of the lower rate of scaling (and deformation) and the lower ductility of the oxide at reduced temperatures. In agreement with the 16-hour 1000°C behavior, it was found that the scale thickness developed on flat specimens was less than that found on cylindrical specimens oxidized under similar conditions, Figure 23. As before, this behavior is attributed to the lack of measurable undergrowth formation on flat specimens and its presence on cylindrical ones.

The general loss of scale adhesion exhibited by cylindrical specimens possessing curvature in excess of

approximately 10 cm^{-1} is most probably due to the void formation associated with a nearly complete layer of thick undergrowth. Figure 86 shows that scales formed upon high-curvature specimens oxidized for 64 hours tend to exfoliate, while those formed upon either cylindrical specimens oxidized for shorter times or flat specimens oxidized the same amount of time tend to be adherent. Neither of the latter class of specimens exhibit large quantities of undergrowth.

In the case of hollow cylindrical specimens, the proposed model predicts that scales formed on the inner surfaces may be subjected to diminished circumferential compression resulting from the motion of the oxide. Examination of oxidized specimens indicates that the grain structure developed on these surfaces remains basically columnar in nature so that the main effects which arise would be those due to the grain boundary pressure. The precise stress state is determined by the relative rates of pressurizing the grain boundaries and the reduction of this pressure caused by the oxide following the retreating metal-oxide interface.

It is believed that the scales formed on the concave surfaces were subjected to smaller circumferential compressive stresses than the scales formed on the convex surfaces. In terms of the proposed scaling mechanism such decreased stresses would be predicted to produce smaller

quantities of undergrowth and therefore smaller total scale thicknesses. The data of Table 5, for the specimens oxidized at 900°C , are in accord with this prediction. The effect of oxide extrusion, which would act in the same sense, is not believed to contribute because of the reduced ductility of the scale at this temperature.

Oxidation in Air for 64 Hours at 1000°C - The thickness of the scales formed on specimens oxidized for 64 hours at 1000°C are nearly independent of curvature as shown in Figure 19. It should be emphasized that these scales were formed in an environment which differs from that employed in 16-hour, 1000°C treatment (i.e., degree of atmosphere stagnation and amplitude of temperature oscillation). Comparison of tests 7 and 13 of Table 9 shows the pertinent differences involved and indicates that the rate of oxidation is approximately twice as fast under the 16-hour conditions (test 13). This indicates that the relatively small scale thickness developed upon those specimens oxidized for 64 hours may be due almost entirely to supposedly minor differences in environment.

While the general level of the curve of Figure 19 may be attributed to environmental conditions, its shape cannot. It is, however, believed that the scale thickening, which is nearly independent of specimen curvature may be accounted for by the proposed oxidation mechanism.

Inspection of a number of the specimens oxidized for 64 hours in air at 1000°C indicated that measurable amounts of undergrowth had formed. Further, since this feature was noted in the case of those specimens oxidized for 16-hours at 1000°C , it is highly probable that undergrowth formations occurred on every cylindrical specimen subjected to 64-hour oxidation. The faceted oxide surfaces shown in Figures 62 through 64, which would be predicted under such circumstances, indicate that this has, in fact, happened. Thus, only a relatively minor variation of scale thickness with specimen curvature is expected, as is observed.

The idiomorphic oxide crystals, appearing as sharply defined rectangles or squares in the surface structure, indicate that the cessation of nickel transport into the outermost crystals occurred relatively early in the oxidation of all specimens. The undergrowth formed on one of these specimens illustrated in the photomicrograph of Figure 66, is similar to that shown previously for the specimens subjected to 16 hour, 1000°C oxidation. In addition, the friability of the scale indicates that the undergrowth formed early in the course of oxidation.

The minor trend for an increased degree of surface faceting with increasing specimen curvature indicates that specimens of higher curvature formed undergrowth earlier

in the process. This behavior, which is in accord with the proposed scaling mechanism, is supported by the observation that specimens of higher curvature have less adherent scales, as illustrated in Figure 87c. The preceding observation, coupled with the trend for increased thickness of scale accompanying specimens of higher curvature, indicates that some extrusion of the oxide grains may have occurred in the case of the more constrained scales. These observations are also in accord with the proposed scaling mechanism.

The diffraction patterns shown in Figure 67 indicate that a $\langle 111 \rangle$ -type wire texture though weak, does tend to develop. As in the case previously discussed, the texture is associated with a closely-controlled oxidizing temperature.

Oxidation in Dried Oxygen at 1000°C - The thicknesses of scales developed on cylindrical specimens exposed to dried oxygen at 1000°C have been determined as a function of both specimen curvature and oxidation time. It was found that these scales exhibit certain characteristics which set them apart from those produced in air and which must be taken into account in explaining the observed oxidation behavior.

One such characteristic of primary importance is the fact that the stable oxide crystallite size developed

in oxygen is apparently much larger than that developed in air. The reason for this difference in the size of the first stable crystals is not known; however, it is surmised that the smaller oxide grain size associated with air oxidation which arises as a result of "impurities," such as nitrogen or water vapor, in some manner lowers the energy barrier associated with the nucleation of oxide crystallites. Evidence that the nucleation process is a difficult step in oxide formation has been cited previously.

As a direct result of the larger stable oxide grain size at the metal-oxide interface, there is less lattice bending in the columnar crystals due to addition of material at oxide grain boundaries. Thus, the onset of undergrowth formation is necessarily delayed. The results of scale thickness determinations are summarized in Figure 31, which is believed to illustrate the effect of delayed undergrowth formation. The curvature-thickness sections of this surface for the oxidation time of 4 hours, shown in Figure 24, indicates that there is almost no variation in scale thickness with specimen curvature. This result is expected on the basis that the oxide grain boundary network is insufficiently deformed to produce appreciable thicknesses of undergrowth. In addition, because of the large stable oxide grain size the crystals must be

relatively long before the scale can develop a meaningful number of internal quadruple points. Therefore, it appears that the variation in circumferential constraint can only produce varying degrees of oxide extrusion. The minor but consistent trend of increasing scale thickness with increasing specimen curvature is believed to arise from this mode of deformation. Thus, the predicted and observed behaviors are parallel.

The microstructures shown in Figures 68 through 78 support the foregoing analysis, based on scale thickening. The upper photomicrographs of each figure, representing the scales developed on specimens oxidized for 4 hours, indicate that there is, in general, only a minor systematic curvature dependence of the external structure of the oxide. The appearance of less-distorted structures, centered about the specimen curvature value of 8 cm^{-1} , indicates the onset of faceting and, therefore, the onset of undergrowth formation. Such formation, however, was probably not accompanied by the production of scale-traversing channels and therefore the undergrowth did not contribute markedly to the scale thickening. This is in accord with the idea that only a very limited number of quadruple points exist in the scale at times as early as 4 hours.

As the oxidation time is increased to and beyond 16 hours, more quadruple points become available and the

production of oxygen channels and subsequently undergrowth thickening is possible. The effects which make themselves evident are thought to be, for the most part, analogous to those discussed in the case of the specimens oxidized in air for 16 hours at 1000°C . The lower photomicrographs of Figures 68 through 78 show that at this time faceting has become more advanced on the range of specimen curvatures centered about the value of 8 cm^{-1} . However, the total surface rearrangement has not yet been achieved and it is therefore believed that the overlying crystals still serve as an effective barrier to oxygen. Thus, the effect of the undergrowth can only be to diminish the total scale thickness due to its own limited thickness. The decrease in scale thickness illustrated in the thickness-curvature plot of Figure 25 is believed to arise from this barrier effect. At still higher specimen curvatures, oxide extrusion would be predicted, accompanied by an increase in scale thickness. This is observed.

It should be noted that the use of dried oxygen as an oxidant also apparently retards the degree of surface rearrangement with respect to that afforded by air. Thus, though the surface of the specimen shown in Figure 70b appears to be distorted by the growth-induced deformation, Figure 79b indicates that faceting has indeed begun. The latter figure clearly indicates the "pushing-out" of

material in regions adjacent to oxide grain boundaries. Comparison of the photomicrographs of Figure 90 shows that the addition of water vapor alone to oxygen accelerates the rate of surface rearrangement. Since water vapor is always present in the case of air-oxidized specimens, it becomes difficult to establish a one-to-one correspondence between the external surface structures formed in air and those formed in dried oxygen.

Figure 30 shows a summary of the oxidation time-scale thickness section of Figure 31. It is seen that as the specimen curvature is increased, there is a regular increase in the initial rate of the process (as indicated by the initial slopes of the lines). In terms of the proposed scaling mechanism, this effect is attributed to the larger amounts of deformation, in the form of oxide extrusion, associated with the larger constraints of the high-curvature specimens. Figure 30 also shows that flat specimens retain their initial parabolic scaling behavior throughout the duration investigated, while specimens of higher curvature deviate earlier from their initial parabolic rate. This (negative) deviation is believed to be due to the formation of undergrowth. Such behavior is also in accord with the proposed scaling mechanism in that it predicts earlier formation of undergrowth as the degree of deformation is increases. The

thickening of undergrowth, on specimens of low curvature is illustrated in the photomicrographs of Figure 80.

The scale adhesion curves of Figure 89 indicate a trend for increases "tearing away" of the scale both at short times and higher specimens curvatures. Under these conditions, the scales formed would be most highly stressed and upon being subjected to added mechanical stresses involved in the cooling and preparation operations would therefore be most susceptible to exfoliation. Scales formed over longer periods of time would, on the other hand, be subject to less severe stresses; especially in the advent of undergrowth formation. The trend for increased scale adhesion at longer times, apparently independent of specimen curvature is, therefore, believed to be a natural result of the reduced state of stress.

The retrograde behavior of the scaling rate shown for the specimen of curvature 12 cm^{-1} in Figures 29 and 30, is believed to be due to a special mode of scale failure associated with the high degree of its constraint. Metallographic examinations of the scale produced after one hour of oxidation indicated that small, apparently empty blisters formed on the specimen surface. In terms of the proposed mechanism, this circumstance would remove the lateral constraints, thereby precluding oxide grain extrusion until such time as the blister caps faceted

and the oxygen supply was returned to the floor of the blister cavities. Subsequent scale growth at those sites could then essentially repair the continuity of the scale and provide the possibility of further extrusion; however, a delay in thickening would be noted, as is observed.

The thickness of the scales developed on flat specimens of various thickness was, as in the case of other oxidizing conditions, found to be smaller than that developed on cylindrical specimens. The curve of Figure 32 indicates that the scale thickness goes through a shallow minimum as the sheet thickness is decreased. The initial decrease in scale thickness, for larger specimens, is believed to arise as a result of partitioning a portion of the deformation to the underlying metal, a concept discussed earlier.

The explanation of the trend for increased scale thickness on the thinnest specimens investigated is based on the assumption that three-dimensional curvature may have been induced in them as a result of the localized action of stresses which arose during the oxidation process. If such deformation took place, then the scale on one surface would have to deform not only its share of the metal, but also a portion of the oxide on the opposite surface of the specimen. Thus, the metallic phase would appear

anomalously strong. Such strengthening would be expected to arise only in the case of thinner specimens and would increase the stress in the scales formed on them, thereby increasing the rate of oxide extrusion.

The decrease in scale adhesion with decreasing specimen thickness shown in Figure 88c may be due in part to the larger effects of thermal or mechanical shock which attends the bent specimens. This bending is, in turn, thought to be due to a change in the mode of oxide formation.

Figures 81 and 82 illustrate that, as the thickness of the metallic specimen is decreased to a point where the reciprocal thickness of the metal has a value of approximately 30 cm^{-1} , its external appearance is relatively unchanged. However, scales formed on thinner specimens exhibited the relatively thin "islands" of oxide shown in Figure 83a. Their distribution on the specimen surface, shown at lower magnification in Figure 83b, suggests localized bending of the scale may well occur due to oxide deformation occurring more readily between the "islands" than in the "islands" themselves.

The photomicrographs of Figures 83 and 84 further indicate that the "islands" may be strongly-oriented overgrowths or single crystals of nickel oxide. The crystallographic deformation markings present in the photomicrograph of Figure 84b, support this view. Since

this thinnest specimen was drastically deformed during fabrication (98 per cent by cold rolling) it is believed that a strong texture has been developed in the metal prior to oxidation. Under such conditions, the development of an oriented overgrowth of nickel oxide by subsequent oxidation seems plausible.

The stress state predicted for the case of hollow cylindrical specimens has been discussed earlier and the possibility of reducing the circumferential compressive stress in the scale formed on the concave surface has been introduced. At 1000°C the rate of retreat of the oxide may be sufficiently high to produce enlarged oxygen channels. If this occurred it would result in rapid transport of both nickel and oxygen through the scale region and production of a thick undergrowth. Both the increased amount of scale formed, shown in Table 5, and the oxygen-rich character of the scale, as determined metallographically by coloration, support the hypothesis that the rate of oxygen transport is abnormally high.

4.63 Macroscopic Deformation

Deformation, which was believed to have occurred as a direct result of oxidation was noted in the case of

cylindrical and flat specimens, as well as those fabricated into special shapes. In all instances, the overall results obtained may be interpreted in terms of the postulated scaling mechanism. It should be noted that these observed deformations cannot be attributed to the effect of oxygen solution in the metal due to both the extremely low solubility of oxygen in nickel (36) and the fact that the commercial grade of material used was probably already saturated with oxygen.

Cylindrical Specimens - It was found that specimens fabricated from hot-rolled Nickel-270 rod changed in length upon heating in dried oxygen for 5 minutes at 1000°C. This dimensional change, shown in Figure 33, is believed to have arisen solely as a result of relaxation effects associated with the residual stress distribution. Calculations indicated that such deformation could not have occurred as a result of stresses developed in the metal by the postulated grain boundary pressure since, for the short time involved, deformation arising from this cause would have been nearly unobservable with the measuring techniques employed herein.

Figure 34 shows that there is, in general, an axial extension of cylindrical specimens, with respect to the length change incurred after the first 5 minutes of oxidation at 1000°C, when the oxidation time is extended

to periods of the order of hours. The magnitude of these extensions is commensurate with that which would be predicted on the basis of the existence of a grain boundary pressure of 1500 psi. Measurement of specimens oxidized for 4 hours showed that the lengthening was somewhat erratic in that both very large expansions and a few contractions were noted. The reason for this behavior is uncertain; however, it may be associated with some type of metallic grain rearrangement (growth) process. The elongations noted for the 16-hour specimens correspond more closely to the values predicted by calculations based on the general method of Appendix 3. The degree of agreement, shown in Figure 107, is thought to be satisfactory in view of the possible effects in specimen-to-specimen variation which may have arisen.

The interrupted oxidation tests, which were performed using single specimens, with the idea of eliminating such variations, exhibited elongations which are in very good agreement with the calculated values of extension. The calculated and observed values are shown superimposed in Figures 108 and 109 for specimens of curvature 6 and 8 cm^{-1} , respectively. Liberty has been taken to shift the ordinate of the theoretical curve shown in Figure 109 in order to discount the initial short-term variation of unknown origin. The divergence of the experimental points for the theoretical curves at longer oxidation times is

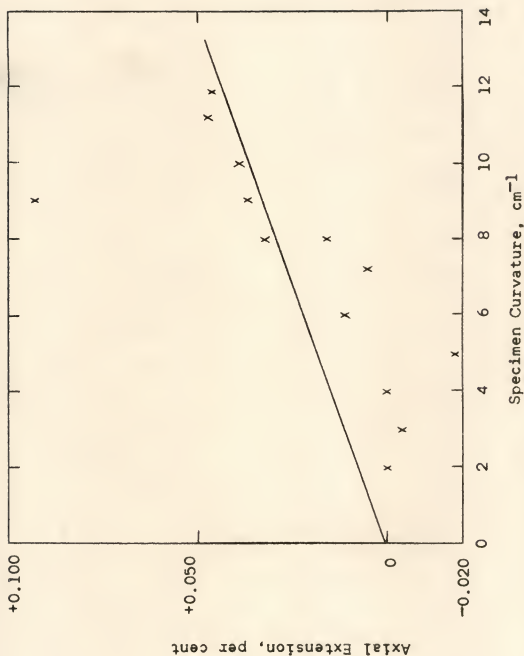


Figure 107: Comparison of observed and calculated values of the axial extension of cylindrical specimens oxidized for 16 hours at 1000°C in dried oxygen.

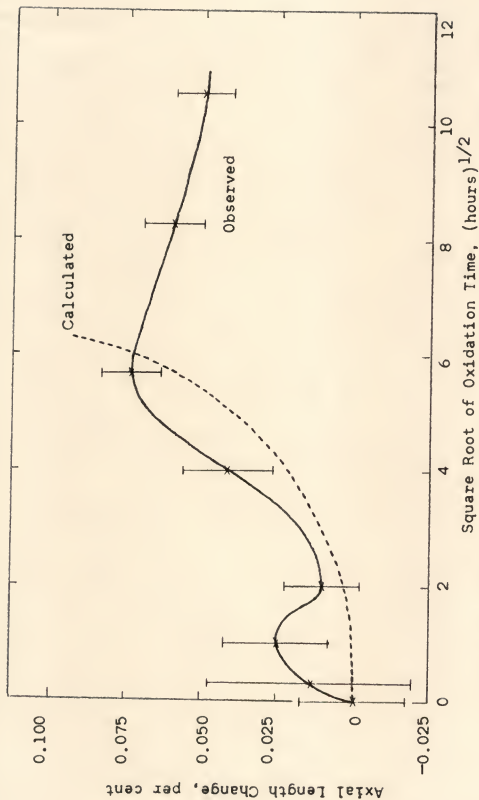


Figure 108: Comparison of calculated and observed axial length change as a function of time for a cylindrical specimen of curvature 6 cm⁻¹ subjected to interrupted oxidation at 1000°C.

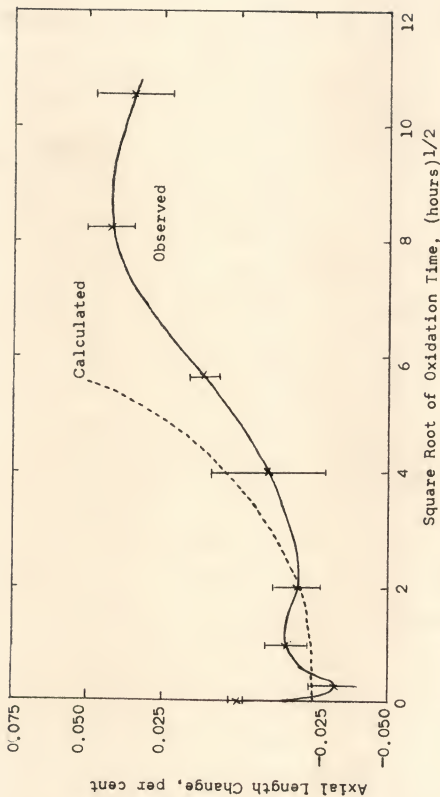


Figure 109: Comparison of calculated and observed axial length change as a function of time for a cylindrical specimen of curvature 8 cm^{-1} subjected to interrupted oxidation at 1000°C .

to be expected on the basis of undergrowth formation since, after its occurrence, the outermost crystals no longer may provide the grain boundary pressure necessary for continued extension. The calculations upon which the theoretical curves are based did not take into account the effects due to this phenomenon. It may be noted that the divergence between calculated and observed elongation values occurs earlier in the case of the specimen possessing higher curvature. This behavior is interpreted in terms of the proposed scaling mechanism as being due to earlier undergrowth formation on the specimen of higher curvatures.

Flat Specimens - The flat specimens oxidized for 16 hours at 1000°C in dried oxygen also exhibited extension upon oxidation subsequent to a short-time vacuum heat treatment at 1000°C . The thickness dependence of their extension was employed in the calculation of the magnitude of the grain boundary pressure. The values of extension, given in Table 6, are believed to be most reliable in the case of the two specimens of intermediate thickness. The possibility of bending of the smaller specimen, due to its unique mode of scale formation, is believed to cause an anomalous reduction in its extension. Measurement of the thickest specimen used is less certain due to difficulties associated with the

alignment of its reference holes with the axis of the optical comparator.

Helical Specimens - The deformation data for helical specimens, oxidized at 1000°C in air, are given in Table 7. Their tendency to decrease in diameter or "wind-up" is in qualitative agreement with the proposed stress state in the oxide. The external surfaces of the helices are essentially segments of convex cylinders, while their inner surfaces are concave. Thus, the stresses due to constraint would be expected to be compressive on the outer surface and tensile on the inner surface. The addition of a constant compressive stress, due to the grain boundary pressure, to this system of stresses does not change their relative values. The couple so formed would tend to wrap the helices tighter as is observed.

Right-Angle Bend Specimens - The observed tendency for bent sheet stock to deform during air oxidation at 1000°C so as to diminish the angle between its unbent portions is explained on the same basis as was employed in the case of helical specimens. Since the scale thickness developed on these specimens is roughly independent of sheet thickness, the observed tendency for increased bending with decreased sheet thickness is also expected. The time dependence of this bending, shown in Figure 37 for the case of a single specimen oxidized in air at 1160°C , indicates that the scaling process alone is

responsible for the deformation since the deformation suffered follows a parabolic law just as the scale formation would be expected to do.

4.64 Special Experiments

Several oxidation experiments of limited scope were performed in order to gain supplementary information about the oxidation process. Each of these involved either the addition of some new variable to the procedure or the extension of a previously used parameter. Experimental techniques included: mechanical application of loads during oxidation, varying the time-temperature profile of the environment, and varying the secondary constituents of the oxidizing gas. For those cases wherein an interpretation is possible in terms of the proposed scaling mechanism, there is found to be a qualitative agreement between predicted and observed behavior.

Mechanical Loading - Application of an axial load during oxidation would be expected to decrease the magnitude of the axial compressive stress (due to grain boundary pressure) and increase the magnitude of the circumferential stress in the scales formed on solid cylindrical specimens. Thus, the octahedral stress in the scale, which determines the degree of plastic flow, remains nearly constant. No drastic change in the scaling behavior is to be expected

from this mode of loading as long as the magnitude of the applied stress is less than the magnitude of the grain boundary pressure. The data of Table 9 indicate that steady application of superimposed axial tensile stresses of up to 1000 psi have little effect on the scale thickening process at 900°C. An attempt to exceed this level of stress resulted in failure of the metal by stress-rupture before the required oxidation time could be attained.

Thermal Loading - A more positive demonstration of the effect of stress on the scale thickening process may be found in an analysis of the results of the environmental tests given in Table 8. In these cases, stresses whose origin was thermal in nature were added to those already present as a result of the oxidation process. Data concerning the linear thermal coefficients of expansion of nickel and nickel oxide indicate that at 1000°C they differ by approximately $3 \times 10^{-6} \text{ in/in/}^\circ\text{C}$, with the coefficient for the metal being larger (33, 35). If it is assumed that all of the deformation due to differential thermal expansion occurs in the scale, then a change of one degree centigrade will produce a stress of approximately 60 psi in the scale. Upon cooling, this stress will increase the magnitude of those compressive stresses postulated to be present in the oxide due to the oxidation process; whereas heating will decrease their magnitude.

It was found that sinusoidal thermal fluctuations did not affect the scaling behavior in air at 1000°C unless their amplitude was greater than approximately 2°C , corresponding to an approximate alternating stress of 120 psi. Thus, it appears that relatively rapid variations in stress may be absorbed if their amplitude is small and if little time is allowed for deformation to take place. The results of tests 10 through 12 shown in Table 8, however, indicate that prolonged cooling accelerates scale growth even when the amplitude of the fluctuation is as small as $1\frac{1}{2}^{\circ}\text{C}$, while prolonged heating has a smaller effect when the amplitude is twice as great. These observations, which emphasize the importance of the role of deformation in the scaling process, may be rationalized on the basis of the postulated stress system.

Under conditions of slow cooling, the magnitude of all stresses are increased and some additional deformation evidently takes place in this case, whereas it did not in the case of the more rapid sinusoidal fluctuations. If an accelerated rate of scale deformation is, in turn, associated with an earlier formation of undergrowth and an increased supply of oxygen to it, then the observed increase in scale thickness would be expected. The slow heating and rapid cooling of the $3\frac{1}{4}^{\circ}\text{C}$ -amplitude wave would be expected to first slowly decrease the magnitude

of the stresses and then rapidly increase them. Thus, the first portion of the thermal wave has no accelerating effect on the scaling process because it is reducing stresses and the second (cooling) portion has a smaller than proportional effect because only a short time is allowed for deformation phenomena to act.

It should be noted that calculations based on heat transfer equations indicate that the thermal phase lag is negligible with respect to the period of the thermal oscillations employed. Thus, the implicit assumption used here that the metal and oxide are thermally "in phase" is valid to a very good approximation.

Composition of the Oxidizing Gas - One of the more striking features associated with the oxidation of nickel is the variation in the size of the initial stable oxide grains which may be produced by secondary constituents present in the oxidizing atmosphere. The reduction in size, promoted by the presence of water vapor and/or nitrogen has been cited previously.

In terms of the proposed scaling mechanism, a reduction in grain size should lead to earlier formation of the undergrowth layer due to the increased severity of the deformation associated with the addition of material at oxide grain boundaries. Relatively early undergrowth formation in air-formed scales, with respect

to oxygen-formed scales has been observed. The photomicrographs of Figures 51b and 80a, for air- and oxygen-formed scales, respectively, illustrate this effect. It may be noted that these different oxide microstructures were developed under conditions which were nearly identical except for the presence of the secondary constituents associated with the oxidation in air.

Impurities in the atmosphere surrounding the specimen may also either be dissolved into the oxide lattice or may in some manner alter the rate of reaction at the oxide surface. Since the rate of transport of nickel through the oxide is determined by the vacancy concentration within it, which is, in turn, strongly dependent on the presence of impurities, both the surface structure and thickness of the scale could be altered by impurities. Results of the environmental tests indicate that for the case of specimens oxidized in air at 1000°C one or more rate-accelerating impurities, associated with the "JM-20" firebrick were present. The relatively large values of scale thickness support the contention that the observed behavior is due, in part, to effects of impurities. Others have noted that normally encountered impurities usually accelerate the oxidation of nickel (9, 32).

Comparison of the oxide surface structures developed on specimens during oxidation in air and dried oxygen, as well as results of the environmental tests showed that water and vapor and/or nitrogen also play an important role in accelerating the production of an equilibrium surface structure. In most cases, specimens oxidized in air exhibit faceted oxide grains, while those treated in dried oxygen usually exhibit surface distortion. This indicates that the "impurity" gases associated with air tend to accelerate the transport of material on the surface of nickel oxide with respect to the transport which is associated with the presence of oxygen alone.

4.7 Interpretation of Results of Other Investigations

The proposed mechanism for the thickening of scales during the oxidation of nickel must, of course, be compatible with results obtained by other investigators who have studied this material. In addition, it should apply to the oxidation of other single metals which form scales by transport of the metallic species through the oxide layer. Thus, one would expect that the scaling of cobalt, iron, and copper, for example, would be amenable to description by this mechanism if differences in the mechanical and physicochemical properties of the metal oxides involved are taken into account. Beyond this, however, there appears

to be limited amount of evidence which indicates that the proposed scaling mechanism has fairly general applicability.

The purpose of this portion of the discussion is therefore to attempt to demonstrate the overall applicability of the mechanism which has been suggested. There are certain difficulties which attend the performance of such an analysis due to the fact that most of the available information is in the form of volumetric or gravimetric data. The nearly universal practice of using flat sheet material for oxidation specimens is, however, one simplifying factor. In view of the lack of specific observations concerning oxide composition, plasticity, and microstructure, part of what follows is necessarily speculative in nature.

4.71 The Oxidation of Nickel

In the early stages of oxidation and subsequent to the occurrence of certain short-time effects, the scale developed on nickel specimens exposed to either oxygen or air, at temperatures ranging from 400 to 1200°C, has been found to grow parabolically (51, 74, 75). However, as the time of oxidation is extended to the order of tens of hours, several aspects of the scaling behavior appear which seemingly cannot be explained on the basis that the only process occurring is the unidirectional transport of nickel.

Several investigators have found that two layers of scale developed on nickel when the duration of oxidation is sufficiently long at temperatures of 800 to 1200°C (2, 53, 55). Further, it was noted that the rate of scale formation which attends the production of this layer is lower than the initial rate (55). In terms of the proposed scaling mechanism, the appearance of the second oxide layer, noted by these investigators, corresponds to undergrowth formation, while the reduction in scaling rate is a natural consequence of the dormant overlying crystals acting as a barrier to the oxygen supply of the undergrowth crystals.

The appearance of platinum markers, in some cases found between the scale layers (48, 55), is also interpretable on the basis of what has been proposed herein. Prior to undergrowth formation, a marker would be expected to be located at the metal-oxide interface since the oxide initially forms by relatively rapid diffusion of nickel in regions immediately surrounding it. However, the proposed slow lateral growth of the underlayer would tend to allow time for oxygen penetration through and beneath the marker and subsequently could thrust it from the metal surface. Alternatively, the marker could be bodily lifted from the metal surface by the first-formed crystals as they were being thrust away from the metal surface by

the lateral motion of the undergrowth.* In either case, the marker would appear between the two zones of oxide, as observed.

Measurements of activation energies for the oxidation of nickel also tend to support the proposed viewpoint that oxygen penetration of the scale layer is time dependent. The results of several studies concerning the air oxidation of nickel indicate that the activation energy for the process varies from approximately 60 to 30 k-cal/mole (32) while careful measurements of the diffusion of nickel through nickel oxide crystals show that the activation energy is approximately 60 k-cal/mole (76). These data indicate that the diffusion of nickel sets the upper bound of the activation energy which describes the oxidation process. It, therefore, appears likely that the proposed entrance of oxygen through the scale is responsible for the observation of lower activation energies. Thus, the variation in observed activation energies may be interpreted on the basis of varying amounts of undergrowth formation. Commonly used rate-determining techniques, such as those based on gravimetric or volumetric measurements, which integrate the scaling

*The first-formed crystals, being thus separated from the metal could exert no growth thrust (pressure) on the marker.

behavior over the entire specimen surface, would therefore be especially prone to provide misleading information.

Other observations concerning the nature of the scale are more readily explained on the basis of the postulated grain boundary pressure. Thus, the wrinkling of thin oxide scales, upon careful chemical removal of the nickel substrate, has been attributed to compressive stresses in the film (25). In addition, the observation that scales formed on nickel sheet, subsequently bent at room temperature exfoliate from the compression side of the bend zone, but not from the tension side (35), indicates that a lateral compression exists in the scale. Since the thermal stresses associated with cooling are small, both of these observations are in qualitative agreement with the existence of a grain boundary pressure.

The grain boundary pressure may be diminished, or eradicated if the external supply of oxidant is suddenly removed subsequent to the development of a scale composed of columnar oxide grains. It is postulated that, under such conditions, material may be transported more readily across oxide-oxide grain boundaries resulting in an increased oxide grain size. Upon return of the oxidant, the restabilized grain boundary area served by it would have been reduced, and according to what has been proposed previously, the rate of oxygen consumption by the

scale would similarly be reduced (since oxygen is necessarily consumed in establishing the grain boundary pressure).

In a recent experiment, the oxidation of a nickel-copper alloy at 800°C was interrupted by evacuating the surroundings and, upon return of the oxidant, it was found that the rate of oxidation was diminished (77). Although an alloy other than pure nickel was used in this investigation, the surface scale was found to be nickel oxide; therefore, the rate of decrement should be explicable on the basis of the behavior of nickel oxide. It is believed that the consideration involving a decrease on the grain boundary area, presented above, may be applicable in this case. Similar experiments, involving other oxidizing metals, will be cited later in the text.

There are, as might be expected, certain observations which appear to be more difficult to justify in terms of what has been proposed. Thus, although the observation of oxide whiskers or platelets growing normal to the surface of scales is suggestive of extrusion via lateral compression of the oxide; their development at temperatures near 500°C (78) by this mechanism is questioned, since oxide extrusion at 500°C seems improbable. The proposed mechanism does, however, offer a qualitative

explanation of some of the more widely observed, and heretofore anomalous, consequences of scale formation on unalloyed nickel. Further, and most important, it retains the time-proven concept that the earlier stages of oxidation may be described by the parabolic rate law.

4.72 The Oxidation of Other Metals

It appears that the proposed scaling mechanism may have rather general applicability in the field of high-temperature oxidation of metals if one considers the oxidation of all metals to proceed basically by metal-ion transport through the oxide lattice. This concept, which is contrary to the consensus existing at this date, implies that observations indicative of lattice diffusion of oxygen are, in fact, due to the consequences of extended metal-ion diffusion. In terms of the proposed mechanism, such observations may be rationalized on the basis of undergrowth formation and the presence of oxygen in the grain boundary network of the scale. In the discussion which follows, it will be assumed that the specimen geometry is planar and that the scales involved are composed of columnar oxide-crystals, as was observed herein. The latter assumption is probably valid in all but very special instances since the necessary anisotropic growth persists in most crystalline substances.

In terms of the proposed scaling mechanism, the precise physical or geometric form of the reaction product, which subsequently may govern the rate of reaction, depends upon the degree of advancement of the scaling process. This, in turn, may be artificially divided into three major classes:

1) A small degree of advancement would characterize scales which either did not contain quadruple points or scales which, though containing quadruple points were insufficiently deformed such that undergrowth did not occur. In either case, one would expect to observe a protective, parabolic scaling behavior.

2) A medium degree of advancement would describe those scales wherein undergrowth formation had occurred; but, to the exclusion of severe faceting. Under such conditions, one would expect to observe some slower-than-parabolic scaling rate law and the nature of the scale would be expected to remain protective.

3) A large degree of advancement would describe those scales wherein faceting was so severe that the supply of the oxidant to the undergrowth was equivalent to that of the surroundings. Under such conditions, one would expect to find a faster-than-parabolic rate law and oxide formation would probably be observed to proceed in a linear, or non-protective manner.

In order to extend the scaling mechanism proposed for nickel to other metals, one must take into consideration various qualities associated with the scale. Each of the following would be of major importance:

- 1) The size of the initial stable oxide crystallites.
- 2) The degree of opacity of the oxide-oxide grain boundary to metal transport.
- 3) The relative ability of oxygen to penetrate into the grain boundaries.
- 4) The magnitude of the grain boundary pressure.
- 5) The mechanical properties of the oxide.

Although this list may be somewhat formidable with respect to quantitative prediction of behavior, there is a single qualitative trend which is believed to persist throughout. That is, any given metal-oxide system should exhibit a scale which increases in its degree of advancement as the oxidizing temperature is increased. Such a trend has, in fact been found in that most oxidizing metals exhibit protective scaling behavior at low temperatures while their scales become non-protective at higher temperatures. A tabular summary of the temperature dependence of the protectivity is given in Table 34 of Appendix 1.

The remainder of this section is devoted to a short summary of the scaling behavior of several metals, interpreted on the basis of an extension of the proposed scaling mechanism for nickel. Most of the information about to be presented has been taken from summary articles in the field of oxidation (3, 17). The references cited below have been employed to supplement them as deemed necessary.

Alkali Metals - Most of the data available on the oxidation of the alkali metals appear to be qualitative in nature. All of the Group I A metals have been observed to oxidize linearly in air at room temperature, and for many years this behavior has been ascribed to the fact that the Pilling-Bedworth ratio for these metal-oxide systems is less than unity. More recent investigations, however, have shown that protective oxides may be formed upon sodium, potassium, and rubidium if the oxidation reaction is carried out at lower temperatures.

It has been found that impurities in the metal apparently play a major role in the oxidation behavior. Sodium, for example, will oxidize in a protective manner in moist, room-temperature air if the metal is sufficiently pure; but, will oxidize linearly if less pure. In addition, it has been found that purified sodium will form an initially protective scale in an atmosphere of dry oxygen

at temperatures as high as 48°C , whereat bulk diffusion appears to be the rate-controlling process (10).

In terms of the proposed scaling mechanism, these observations indicate that the oxide grain size is probably very small and that it is reduced by the presence of impurities. The long-time "break-away" behavior exhibited by thin scales formed on sodium (10), suggests that relatively high concentrations of oxygen are available in the grain boundaries of the scale. It is postulated that the "break-away" stage represents a thickening of the undergrowth and subsequent exfoliation of the first-formed crystals accompanied by formation of a new layer undergrowth. Such a process, if it occurred at different times on different portions of the specimen surface, would lead to the observed non-protective behavior.

Copper - The oxidation of copper is believed to proceed by the transport of copper through a scale composed basically of Cu_2O which may possess an outermost layer of CuO . At temperatures between 200 and 1000°C the oxidation of copper proceeds by an essentially parabolic process; however, it has been noted that a cubic (slower) rate law may also apply. In addition the scale thickness developed on copper has been found to increase parabolically at temperatures between 600 and 800°C for approximately 20 hours and subsequently approach a limiting value of

thickness (79). This behavior is analogous to that exhibited by nickel and it is therefore believed that the slowing of parabolic growth indicates that undergrowth formation has been initiated as would be predicted by the proposed scaling mechanism.

Observations concerning the deformation of copper helicies may be interpreted in terms of either a lateral stress in the scale layer or a hydrostatic tension in the metallic phase arising from a "smeared" vacancy distribution (29, 30). The postulated grain boundary pressure is believed to provide the stress responsible for the observed deformations. Further evidence for applicability of the proposed scaling mechanism to copper lies in the observation that the rate of oxidation is diminished as a result of "aging" copper oxide scales in inert atmospheres (80). As in the case of nickel oxide, a recrystallization or "healing" of the scale appears to occur.

Beryllium - The scaling of beryllium is believed to proceed by the outward diffusion of the metal through BeO. Parabolic oxidation is observed for times up to 2 hours for temperatures in the range 350 to 950°C. At temperatures between 500 and 750°C the rate of reaction was found to decrease if the oxidation time was extended to the order of hundreds of hours (81). On the basis of

what has been proposed, this is interpreted as being due to the onset of undergrowth formation. At 750°C , a minor amount of "break-away" behavior in the scaling rate was noted (81). It is suggested that this is due to local exfoliation of the first-formed crystals and subsequent enrichment of the oxygen supply to the crystals of the undergrowth lying directly beneath them.

Magnesium - The scaling behavior of magnesium is generally believed to proceed by diffusion of magnesium through MgO and protective oxidation behavior has been noted at temperatures up to approximately 400°C . At temperatures in the neighborhood of 450°C , parabolic oxidation has been noted. In terms of what has been proposed, this indicates localized undergrowth formation and exfoliation of the original oxide crystals. Above approximately 500°C , oxidation proceeds in a non-protective (linear) fashion and at approximately 575°C the initial linear rate increases markedly after approximately 2 hours of oxidation (82). Others have attributed this latter behavior to sublimation of the metal through scale-traversing cracks in the oxide and subsequent ignition. However, cracking per se would seemingly require the production of lateral stresses in the scale which cannot arise simply from outward diffusion of the metal.

In terms of the proposed mechanism for scaling, the linear scaling behavior of magnesium is interpreted as being the alternate formation of undergrowth and ex-foliation of the previously formed oxide crystals occurring in a rapid, cyclic fashion. The observations which indicate that ignition of magnesium occurs are rationalized on the basis that scale-traversing defects, caused by addition of material at the grain boundaries of MgO , may be capable of producing channels large enough to allow transport of gaseous magnesium.

Calcium, Strontium, and Barium - It appears that the degree of protectivity afforded by the scales formed on the Group II A metals decreases as the period with which they are associated is located further down in the Periodic Table. Thus, calcium oxidizes protectively at temperatures on the order of $350^{\circ}C$ for approximately 1 hour and thereafter oxidizes linearly; while barium oxidizes linearly at room temperature.

In terms of what has been proposed, this trend may be due to the oxide plasticity, as indicated by the metal oxide melting temperatures. Since the oxides of the heavier elements melt at lower temperatures, their plasticity at a given temperature would be expected to be greater than that of the oxides of the lighter elements. This, in turn, may facilitate undergrowth formation in the

heavy-metal oxides. As a result, one would expect the degree of advancement of the scaling process to increase as the melting temperature of the oxide decreased. In the case of the Group IIA metals, wherein the magnitude of the oxide plasticity is assumed to be small, this is observed.

Zinc and Cadmium - The scales formed on both zinc and cadmium are apparently protective so long as the materials are sufficiently pure. As in the case of the Group II A metals, these oxides are believed to form at higher temperatures by transport of metal through the scale. The extremely low rates of scale formation, found in the case of both of these metals is indicative of a small degree of advancement of the scaling process.

In terms of the proposed scaling mechanism, it appears that the grain boundary network of each of these oxides is nearly impermeable to oxygen. As a result, the lateral deformation is small, and the time of undergrowth formation is very much delayed. One would therefore expect that, subsequent to undergrowth formation, the rate of oxidation would be drastically diminished. This has been observed in the case of the oxidation of cadmium at 300°C.

Yttrium, Lanthanum, and Cerium - Oxidation of the Group III A elements appears to parallel that of the alkaline earths, though only limited information is available. Cerium exhibits what appears to be an advanced scaling behavior with respect to either lanthanum or yttrium. Between 20 and 60°C, it oxidizes in an initially protective manner while at temperatures between approximately 100 and 300°C, the protective period is short and a linear rate of oxidation subsequently prevails. A conversion (oxidation) of Ce_2O_3 to CeO_2 has been postulated by others to be the rate controlling step in the scaling process. Lanthanum, on the other hand, exhibits limiting value of weight gain (or scale thickness) at 300°C. The apparently divergent behaviors are, however, believed to arise as a result of differences in degree, rather than kind.

In terms of the proposed scaling mechanism, the behavior of lanthanum may be interpreted in terms of scale development with a small degree of advancement; i.e., the limiting value of scale thickness would arise as a result of undergrowth formation coupled with a small degree of oxygen mobility in the oxide grain boundaries. Conversely, the scaling of cerium indicates a large degree of advancement involving undergrowth production and growth. The observed oxidation of Ce_2O_3 to CeO_2 is interpreted to be

a direct result of the removal of the metal supply from the outermost oxide crystals by the intrusion of oxide grain boundary barriers which arise as a result of undergrowth formation. Similar processes appear to occur in the scaling of tungsten and uranium.

Aluminum - The oxidation of aluminum is unique in that the oxide Al_2O_3 acts as an extremely effective barrier to diffusion at temperatures up to and beyond the melting point of the metal. Temperature dependent changes in the rate of scaling have been noted. At moderate temperatures, there is an initial rapid oxidation of aluminum until a scale thickness of a few hundred angstroms is developed; thereafter the oxidation process ceases for all practical purposes. As the temperature is increased to 400°C , parabolic oxidation is observed to persist several hours. Further increases in temperature, to 600°C , give rise to scaling rates which have been described as parabolic; however, as the time of oxidation is increased, the rate of scale formation decreases. Oxidation of molten aluminum, at temperatures in excess of 700°C , proceeds by a parabolic rate law.

The above information indicates that the high-temperature scaling of aluminum proceeds at a rate which, in general, diminishes with time, in the case of the solid

metal. It is proposed that this behavior is due to the formation of undergrowth by the shear mechanism postulated earlier. An investigation concerning oxygen diffusion in polycrystalline and single crystal Al_2O_3 indicated that diffusion of oxygen along oxide grain boundaries, necessary to the production of lateral stresses, does occur (83). Further, the parabolic thickening of oxide formed on liquid aluminum, which cannot support a shear, indicates that undergrowth does not form thereon. It therefore appears that the proposed scaling mechanism may be able to qualitatively account for some of the observed features in the scaling of aluminum.

Titanium - At temperatures below 550°C , the oxidation of titanium proceeds by a relatively slow process which has been described by both the cubic and logarithmic rate laws. It is proposed that this behavior is due to the formation of undergrowth in the scale region. For temperatures in the range from 550 to 850°C , the process proceeds in a parabolic fashion, and markers have been found both on the external surface of and within the scale. This behavior has been attributed to the diffusion of oxygen through the scale layer. However, in terms of the proposed mechanism it indicates that the scale structure has achieved a moderate to large degree of advancement. The motion of markers away from the interface is believed to be due to

channel formation in the first-formed crystals which facilitates entry of oxygen to the region of the undergrowth. Subsequent growth of the underlying crystals would push the markers away from the metal-oxide interface as is observed.

The paralinear oxidation of titanium at temperatures in excess of 850°C , and the observation of porous scales consisting of the higher oxides of titanium formed thereat, is in accord with the concept that metal diffusion across the oxide grain boundaries is highly restricted. The observed porosity may have been developed by the volume change associated with the formation of the higher oxides.

Zirconium and Hafnium - The oxidation of both of these metals initially proceeds at a parabolic rate on the temperature range from approximately 300 to 700°C . Oxygen diffusion, through the oxide lattice, has been postulated in the case of hafnium oxidized in this temperature range. The observation of "inert" markers consisting of other oxides, at the gas-oxide interface appears to support this contention. Other than this evidence, however, the scaling process may be described in terms of what has been proposed herein.

It has been found that the oxidation of these metals may be described by slower-than-parabolic rate expression in the above temperature range if the long-time scaling

behavior is considered. This observation suggests that undergrowth formation may occur in the scales. Further, for temperatures in excess of approximately 900°C , the initially parabolic behavior becomes linear as the oxidation time is increased and the external scales change in character, becoming white and powdery. It is proposed that this behavior represents a high degree of advancement in the scale structure with the observed linear scaling behavior arising from a summation of local parabolic growths, in turn, due to exfoliation of the outermost crystals and rapid parabolic growth of the underlying crystals.

Silicon and Germanium - Oxidation of both silicon and germanium appears to be protective up to the temperatures at which the effects of gaseous oxides become important. No information was found to indicate that other than parabolic scaling occurs for silicon or germanium at temperatures as high as 1300 and 500°C , respectively. As in the case of zinc, this behavior is interpreted in terms of what has been proposed herein, as being due to the low permeability of the grain boundary network to oxygen.

Tin and Lead - The mechanism associated with the oxidation of tin appears to be rather complex and, to date, there appears to be no general agreement on the temperature ranges in which specific scaling rate laws apply. There

appears to be a low-temperature protective scale of SnO which becomes porous upon continued oxidation, thus reducing the macroscopic scaling rate. This implies that there is either a metal-oxide interface control of the tin diffusion or that the grain boundaries of the oxide act as diffusion barriers, as suggested herein. In either case, it appears that the flow of oxygen via oxide grain boundaries is highly restricted.

At temperatures, near 500°C whereat SnO_2 is the stable oxide, there is disagreement as to the exact composition of the scale. The rate of scaling increases and appears to proceed at a parabolic rate in this temperature range, suggesting a large degree of advancement in the scale structure. In addition, "cracking" of the scale is observed. It is suggested that gaseous oxides may play an important role at this temperature. The analysis of the mechanism of the oxidation of lead is similarly obscured due to uncertainties in the role played by the higher oxides.

Niobium and Tantalum - Oxidation of these metals is normally considered to occur by oxygen diffusion. At temperatures below approximately 500°C , oxidation proceeds in a parabolic fashion and the sub-oxides NbO and TaO form. Continued oxidation in this temperature range leads to the formation of the M_2O_5 -type oxides and a linear rate of

oxidation ensues. It is proposed that the observed time-dependent changes in rate are due to the formation of undergrowth in the NbO and TaO crystals. The subsequent removal of the supply of metal from the metallic substrates would then permit the oxidation of the sub-oxides to the M_2O_5 forms, as is observed. It is further proposed that the degree of advancement of the scale structure is very large in that several cycles of undergrowth formation and sub-oxide oxidation take place in the case of normally encountered specimens, giving the impression that oxygen transport through the oxide lattice had occurred.

Chromium - Chromium is considered to oxidize by transport of metal through the scale. The rate of oxidation has been found to be parabolic at temperatures below approximately 900°C . At higher temperatures, the initial protective behavior gives way to a linear oxidation which is thought to be associated with evaporation of chromium. Metallographic inspection of scales formed at elevated temperature indicated that lateral compressive stresses were present in the scale at the oxidizing temperature (61).

In terms of the proposed scaling mechanism, it appears that the Cr_2O_3 scale is deformed by the addition of material at oxide grain boundaries. The loss of protection, evidenced by the evaporation-controlled rate of oxidation suggests that scale-traversing channels may be formed as a result of such deformation.

Molybdenum and Tungsten - At temperatures in the neighborhood of approximately 600°C , an initially parabolic rate of scaling was observed and marker studies indicated oxygen transport through the scale. After continued oxidation the rate becomes linear and the scale porous and non-protective. The oxides normally observed, both before and after the rate transition, are the MO_3 -type; however, there is some evidence that the MO_2 -type sub-oxides lie between these and the metal. It has been proposed by others that, in the case of tungsten, the linear rate is controlled by the rate of transformation of the sub-oxide to the oxides. In terms of what has been proposed herein, the above observations arise from the formation of sub-oxide undergrowth and subsequent oxidation of the overlying crystals. This description of the scaling process is analogous to that presented earlier for the case of niobium oxidation.

Iron - The oxidation of iron may produce as many as three chemically different oxide phases. At oxidizing temperatures below 570°C , only Fe_3O_4 and Fe_2O_3 form under normal conditions and the scaling rate is usually found to be parabolic. At temperatures in excess of 570°C , the FeO phase appears, and is situated between the metal and the Fe_3O_4 layer. While scaling is initially parabolic, cavities may develop if the higher oxides are present (27).

Cavity formation is associated with a loss of contact between metal and oxide. The resulting oxidation of the lower oxides (near the points whereat metal-oxide contact is lost) indicates that metal transport through columnar grain boundaries of the FeO is restricted, as proposed herein. The apparent lack of evidence for massive undergrowth formation in FeO-bearing scales is attributed to the large grain size associated with this oxide.

Cobalt - Cobalt exhibits three stable oxides: CoO , Co_3O_4 , and Co_2O_3 . Air oxidation of this metal at temperatures in excess of approximately 850°C precludes the formation of all oxides except CoO , while oxidation at lower temperatures produces a CoO scale layer immediately adjacent to the metal. This oxide is similar to NiO in defect structure, crystallographic form, and melting point.

The initial oxidation of cobalt, at temperatures between 400 and 1200°C , has been found to be parabolic. At temperatures in excess of approximately 800°C , and a two-layered scale within the CoO phase has been observed. Further, there is a sharp increase in the activation energy for oxidation (at 700°C) near this same temperature. With the exception of the direction of the change in activation energy the scaling behavior appears to be entirely analogous to that observed for nickel. The formation of undergrowth

in the CoO layer, apparently plays a major role in the scaling behavior of cobalt, and like nickel, the degree of advancement of the scaling process remains small.

CHAPTER V

CONCLUSIONS

1. The rate of oxidation of nickel has been found to be essentially parabolic at 1000°C for oxidation times less than approximately 2 hours.

2. The thickness of scales and the oxide microstructure developed during isochronic oxidation at both 900 and 1000°C has been found to be nearly independent of specimen geometry for oxidation times less than 16 and 4 hours, respectively.

3. The thickness of scale and the oxide microstructure developed during isochronic oxidation at both 900 and 1000°C has been found to be strongly dependent upon the specimen geometry for oxidation times of 64 and 16 hours, respectively.

4. The thickness of scales developed during oxidation at elevated temperatures appears to be dependent upon the interaction of mechanical deformation with the grain boundary network of the scale which causes a decrement in the rate of scale thickening.

5. The lengths of both cylindrical and flat specimens have been found to increase slightly as a result of oxidation at 1000°C and more gross

dimensional changes, resulting from oxidation, have been noted for specimens of special geometric form.

6. The concepts of grain boundary pressure and undergrowth formation have been introduced and incorporated into a mechanism for the oxidation of nickel which appears to account for the overall scaling behavior observed herein.

7. An extension of the proposed scaling mechanism applied to the results of other oxidation studies, indicates that it may have rather general applicability in the field of high-temperature oxidation metals.

APPENDICIES

APPENDIX I

TABULAR DATA

TABLE 10

Oxygen Consumption as a Function of Time for a Spherical Specimen of Curvature 2.75 cm^{-1} oxidized at 1000°C

Oxidation Time (Minutes)	Square Root of Oxidation Time (Minutes) ^{1/2}	Volume Consumed (cc)	Volume Consumed Per Square Centimeter of Specimen Surface (cc/cm ²)
4 1/2	2.120	2.3	0.331
5 3/4	2.316	4.5	0.643
7 1/4	2.670	5.3	0.758
8	2.828	6.2	0.889
8 3/4	2.890	7.0	1.00
9 1/2	3.081	7.8	1.12
10	3.162	8.3	1.19
10 3/4	3.275	8.9	1.27
11 1/2	3.390	9.5	1.36
12 3/4	3.565	10.7	1.53
14	3.740	11.4	1.63
15	3.870	11.7	1.68
15 3/4	3.963	12.1	1.73
16 1/2	4.060	12.3	1.76
17 1/4	4.150	12.3	1.76
18 1/3	4.280	12.3	1.76
19 1/2	4.410	12.8	1.83
20 2/3	4.550	13.2	1.89
23 1/4	4.820	14.1	2.02
24 1/3	4.928	14.4	2.06
25	5.000	14.8	2.12
25 2/3	5.065	15.0	2.15
26 1/2	5.145	15.2	2.17
27 1/4	5.215	15.6	2.23
28 1/4	5.315	15.9	2.27
28 3/4	5.360	16.1	2.30
29 1/2	5.430	16.5	2.36
30 3/4	5.545	16.4	2.35
31 1/2	5.610	16.7	2.39
32 1/2	5.700	16.8	2.41
33 1/4	5.760	17.0	2.43

TABLE 10 (Continued)

Oxidation Time (Minutes)	Square Root of Oxida- tion Time (Minutes) ^{1/2}	Volume Consumed (cc)	Volume Consumed Per Square Centimeter of Specimen Surface (cc/cm ²)
35	5.910	17.3	2.48
38 3/4	6.220	18.2	2.60
39 1/2	6.280	18.4	2.63
40 3/4	6.385	18.9	2.70
42	6.478	18.9	2.70
43	6.560	18.9	2.70
43 1/2	6.590	18.8	2.69
44 1/4	6.650	18.8	2.69
45 1/4	6.725	18.9	2.70
46 1/4	6.800	19.1	2.73
47	6.855	19.2	2.75
48	6.925	19.4	2.78
48 3/4	6.980	19.6	2.80
49 3/4	7.050	19.8	2.83
50 1/2	7.110	20.1	2.88
51	7.140	20.3	2.90
52 1/2	7.240	21.3	3.05
53 1/4	7.300	21.5	3.08
54 1/4	7.360	21.6	3.09
55	7.41	21.8	3.12
55 3/4	7.46	21.8	3.12
56 1/4	7.50	21.9	3.13
57	7.55	21.8	3.12
58 1/4	7.63	21.6	3.10
60	7.74	21.8	3.12
66	8.12	22.8	3.26
67	8.18	23.0	3.29
67 1/2	8.21	23.2	3.32
68 1/3	8.26	23.3	3.33
69 1/2	8.34	23.4	3.34
70 1/2	8.39	23.6	3.37
71 1/3	8.44	23.6	3.37
72 1/4	8.50	23.6	3.37
72 3/4	8.52	23.6	3.37

TABLE 10 (Continued)

Oxidation Time (Minutes)	Square Root of Oxida- tion Time (Minutes) ^{1/2}	Volume Consumed (cc)	Volume Consumed Per Square Centimeter of Specimen Surface (cc/cm ²)
74	8.60	23.7	3.39
79	8.88	24.7	3.53
79 1/2	8.91	24.8	3.54
80 1/4	8.95	24.9	3.56
81	9.00	25.1	3.59
82 1/2	9.08	25.2	3.60
85	9.21	24.9	3.56
86	9.26	25.0	3.57
87	9.32	25.2	3.60
90 1/2	9.51	26.1	3.73
91 1/2	9.56	26.6	3.81
92 1/2	9.61	26.9	3.84
93 1/2	9.66	27.0	3.86
94 1/2	9.71	27.0	3.86
95 3/4	9.78	26.9	3.84
97 1/2	9.87	26.9	3.84
104 1/2	10.2	27.9	3.99
105 1/4	10.3	28.1	4.01
106 1/4	10.3	27.8	3.98
107 1/4	10.3	27.8	3.98
108	10.4	27.8	3.98

TABLE 11

Oxygen Consumption as a Function of Time for a Spherical Specimen of Curvature 3.40 cm^{-1} Oxidized at 1000°C

Oxidation Time (Minutes)	Square Root of Oxidation Time (Minutes) ^{1/2}	Volume Consumed (cc)	Volume Consumed Per Square Centimeter of Specimen Surface (cc/cm ²)
4 1/4	2.06	1.5	0.34
5 1/4	2.40	3.3	0.758
7 1/2	2.74	4.8	1.10
9	3.00	5.8	1.33
10	3.16	6.5	1.49
12 1/4	3.50	7.3	1.68
14 3/4	3.84	8.3	1.91
17	4.12	9.1	2.09
18 3/4	4.32	9.7	2.22
21 3/4	4.65	10.1	2.32
24 1/2	4.95	11.0	2.52
27 1/2	5.25	11.0	2.52
29 3/4	5.45	11.8	2.71
33	5.75	12.8	2.93
35 3/4	5.97	13.2	3.03
41 3/4	6.45	14.0	3.21
46 1/2	6.82	15.5	3.56
53	7.28	15.8	3.62
56 3/4	7.52	16.3	3.74
63	7.94	17.4	3.99
71 1/2	8.45	18.3	4.20
77 1/2	8.80	19.1	4.38
82 1/2	9.09	19.6	4.50
90	9.49	20.3	4.66
96 1/2	9.81	20.7	4.75
99 1/2	9.97	21.4	4.91
108 1/2	10.40	22.1	5.03
122 1/4	11.06	23.0	5.28

TABLE 12

Oxygen Consumption as a Function of Time for a Spherical Specimen of Curvature 3.99 cm^{-1} Oxidized at 1000°C

Oxidation Time (Minutes)	Square Root of Oxidation Time (Minutes) ^{1/2}	Volume Consumed (cc)	Volume Consumed Per Square Centimeter of Specimen Surface (cc/cm ²)
1 1/4	1.12	0.5	0.158
2 1/2	1.58	1.1	0.349
4	2.00	2.3	0.730
5 1/4	2.29	3.2	1.01
6 1/2	2.55	3.8	1.21
8	2.83	4.4	1.40
10	3.16	5.1	1.62
11 3/4	3.43	5.6	1.78
13 1/2	3.67	6.0	1.90
15 1/2	3.94	6.4	2.03
17 1/4	4.16	6.8	2.16
20 1/4	4.50	7.4	2.35
22 3/4	4.77	7.9	2.51
25	5.00	8.2	2.60
26 3/4	5.17	8.2	2.60
29 1/2	5.43	8.2	2.60
31	5.57	8.8	2.79
35	5.92	9.3	2.95
37 1/4	6.11	9.7	3.08
39 1/4	6.26	10.2	3.24
42 1/2	6.50	10.3	3.27
46 1/4	6.80	10.4	3.30
51 3/4	7.19	10.8	3.43
54 1/2	7.38	11.4	3.61
62	7.87	11.9	3.78
69 1/4	8.32	12.7	4.03
75	8.66	13.4	4.250
80 1/4	8.96	13.3	4.215
88 3/4	9.42	13.8	4.375
96 1/4	9.81	14.4	4.570
101 1/4	10.1	14.9	4.730
106	10.3	15.2	4.820
113 3/4	10.7	15.5	4.915
125 1/4	11.2	16.2	5.130

TABLE 13

Oxygen Consumption as a Function of Time for a Spherical Specimen of Curvature 4.67 cm^{-1} Oxidized at 1000°C

Oxidation Time (Minutes)	Square Root of Oxidation Time, (Minutes) ^{1/2}	Volume Consumed (cc)	Volume Consumed Per Square Centimeter of Specimen Surface, (cc/cm ²)
1.0	1.00	0.6	0.26
3.0	1.73	1.2	0.52
4.5	2.12	1.7	0.73
6 1/4	2.50	2.6	1.12
7 3/4	2.78	3.4	1.47
9 1/4	3.04	3.9	1.68
11	3.32	4.2	1.81
12 3/4	3.57	4.6	1.98
14 3/4	3.84	4.6	1.98
16 3/4	4.09	5.1	2.20
18 3/4	4.33	5.6	2.41
20	4.47	5.0	2.16
22 3/4	4.77	4.9	2.12
25 3/4	5.07	5.2	2.24
30 1/4	5.50	5.4	2.33
35 1/4	5.94	6.6	2.85
39 1/4	6.26	6.4	2.76
45 1/4	6.73	6.2	2.67
47 3/4	6.91	7.9	3.41
54 3/4	7.40	8.0	3.45
60 1/4	7.76	8.4	3.62
66	8.12	8.8	3.79
70 3/4	8.40	8.8	3.79
74 3/4	8.65	9.2	3.96
79 3/4	8.92	9.7	4.18
87 1/2	9.35	9.9	4.27
94 1/4	9.71	10.2	4.50
105 1/4	10.3	10.5	4.53
110 1/4	10.5	11.0	4.75
118 1/4	10.9	11.2	4.83
123	11.1	11.5	4.96

TABLE 14

Oxygen Consumption as a Function of Time for a Spherical Specimen of Curvature 5.23 cm^{-1} Oxidized at 1000°C

Oxidation Time (Minutes)	Square Root of Oxidation Time (Minutes) ^{1/2}	Volume Consumed (cc)	Volume Consumed Per Square Centimeter of Specimen Surface (cc/cm ²)
2 1/2	1.58	0.7	0.38
3	1.73	1.7	0.93
3 3/4	1.94	2.5	1.37
5	2.22	2.6	1.52
6 1/2	2.52	3.2	1.75
8	2.81	3.3	1.80
9 1/4	3.02	3.5	1.91
10 3/4	3.28	3.6	1.97
11 3/4	3.42	3.8	2.08
13	3.61	3.9	2.13
14	3.74	4.25	2.32
15 1/2	3.94	4.45	2.43
17	4.12	4.8	2.62
18 1/4	4.27	4.9	2.68
19 3/4	4.44	5.4	2.95
21	4.58	5.3	2.90
22 1/2	4.74	5.5	3.00
25	5.00	5.5	3.00
26 1/2	5.15	5.5	3.00
38 1/4	6.18	5.9	3.22
34 1/2	5.87	6.2	3.39
37 3/4	6.14	6.35	3.47
41	6.41	6.45	3.52
47	6.85	7.3	3.99
49	7.00	7.45	4.07
54	7.35	7.6	4.15
61	7.81	8.15	4.46
69 1/4	8.32	8.1	4.43
76 1/2	8.75	8.5	4.65
84	9.16	8.8	4.81
89 1/2	9.46	9.2	5.02
97 1/2	9.87	9.2	5.02
104	10.4	9.5	5.19
111 1/2	10.6	9.95	5.43

TABLE 15

Parabolic Rate Constants Derived from Volumetric Data as a Function of Specimen Curvature for Spheroids Oxidized at 1000°C in Oxygen at a Pressure of One-quarter Atmosphere.

Specimen Curvature (cm^{-1})	Initial Value ($\text{cc}/\text{cm}^2\text{-min}^{1/2}$)	Final Value ($\text{cc}/\text{cm}^2\text{-min}^{1/2}$)
2.75	0.799	0.369
3.40	1.07	0.477
3.99	0.929	0.429
4.67	1.11	0.410
5.23	2.05	0.481

TABLE 16

Scale Thickness as a Function of Curvature for Cylindrical Specimens Oxidized in Air at 1000°C for 16 Hours

Specimen Curvature (cm^{-1})	Scale Thickness (microns)	Probable Error (microns)
0.00	27.6	± 1.1
1.99	29.1	± 1.6
4.00	31.3	± 1.6
6.40	32.2	± 1.7
7.90	27.1	± 1.5
8.92	27.2	± 1.8
9.0	26.9	± 0.7
10.2	30.1	± 1.1
11.1	36.0	± 1.5
12.6	38.1	± 0.9
15.4	39.5	± 2.8

TABLE 17

Scale Thickness as a Function of Curvature for Cylindrical Specimens Oxidized in Air at 900°C for 64 Hours

Specimen Curvature (cm^{-1})	Scale Thickness (Microns)	Probable Error (Microns)
0.00	17.8	± 2.6
1.64	21.6	± 1.9
1.81	25.1	± 2.7
2.10	24.6	± 2.1
2.54	26.9	± 3.8
3.16	25.9	± 3.2
4.36	27.8	± 3.2
6.46	34.9	± 4.3
8.22	34.9	± 2.0
9.68	34.4	± 1.7
11.0	20.8	± 1.0
11.1	41.7	± 2.0
12.2	32.3	± 2.1
12.9	31.0	± 1.9
17.8	31.1	± 2.6

TABLE 18

Scale Thickness as a Function of Curvature for Cylindrical Specimens Oxidized in Air at 900°C for 16 Hours

Specimen Curvature (cm^{-1})	Scale Thickness (microns)	Probable Error (microns)
0.00	15.6	± 0.7
1.98	13.7	± 1.9
3.94	15.8	± 1.1
6.40	16.9	± 1.2
8.96	16.6	± 0.7
11.3	15.9	± 1.1
12.9	17.5	± 1.6
15.6	11.9	± 1.6

TABLE 19

Scale Thickness as a Function of Curvature for Cylindrical Specimens Oxidized in Air at 1000°C for 64 Hours

Specimen Curvature (cm^{-1})	Scale Thickness (microns)	Probable Error (microns)
2.00	25.0	± 1.4
4.02	27.6	± 0.8
6.02	27.2	± 1.1
7.20	28.1	± 1.1
7.88	27.3	± 0.8
8.94	27.0	± 1.5
9.96	30.9	± 1.7
11.0	30.5	± 1.9
13.9	26.5	± 1.5

TABLE 20

Scale Thickness as a Function of Specimen Thickness for
Flat Specimens Oxidized in Air at 1000°C for 16 Hours

Reciprocal Thickness (cm^{-1})	Scale Thickness (microns)	Probable Error (microns)
1.04	21.7	± 1.9
2.23	25.3	± 4.8
3.08	13.4	± 2.3
4.10	18.2	± 2.3
6.21	18.3	± 1.3
8.29	18.1	± 1.6
10.1	21.2	± 3.6
13.0	25.0	± 3.5
15.0	19.6	± 2.5

TABLE 21

Scale Thickness as a Function of Specimen Thickness for
Flat Specimens Oxidized in Air at 1000°C for 16 Hours

Reciprocal Thickness (cm ⁻¹)	Scale Thickness (microns)	Probable Error (microns)
1.17	27.1	± 1.4
2.31	21.4	± 1.1
3.19	24.7	± 1.4
4.33	21.9	± 1.4
6.52	24.5	± 1.2
8.93	25.4	± 1.4
10.2	21.7	± 1.4
14.8	21.7	± 2.5
16.8	19.9	± 1.7

TABLE 22

Scale Thickness as a Function of Curvature for Cylindrical Specimens Oxidized in Dried Oxygen at 1000°C for 4 Hours

Specimen Curvature (cm^{-1})	Scale Thickness (microns)	Probable Error (microns)
0.00	8.66	± 0.82
2.00	8.59	± 0.92
2.99	8.61	± 1.1
4.00	9.61	± 0.88
4.04	9.79	± 0.91
5.00	10.0	± 1.1
5.07	10.8	± 1.6
6.00	9.31	± 1.1
6.94	9.31	± 1.5
8.08	10.5	± 1.5
9.15	10.0	± 0.78
10.2	10.7	± 0.49
11.1	11.7	± 2.0
12.0	8.7	± 1.5

TABLE 23

Scale Thickness as a Function of Curvature for Cylindrical Specimens Oxidized in Dried Oxygen at 1000°C for 16 Hours

Specimen Curvature (cm^{-1})	Scale Thickness (microns)	Probable Error (microns)
0.00	15.7	± 2.4
2.00	20.3	± 2.0
2.94	17.5	± 2.0
3.99	21.0	± 1.5
4.97	20.1	± 1.6
5.00	22.0	± 1.9
6.01	18.8	± 1.7
7.13	17.0	± 0.9
7.93	15.1	± 1.7
8.07	18.8	± 1.3
8.96	21.8	± 1.4
9.16	21.2	± 1.6
10.1	22.0	± 2.2
11.1	22.9	± 1.8
11.7	20.5	± 2.1

TABLE 25

Axial Length Change as a Function of Curvature for Cylindrical Specimens Oxidized for Five Minutes in Dried Oxygen at 1000°C

Specimen Curvature (cm^{-1})	Axial Length Change (per cent)
1.62	+ 0.0116
1.71	- 0.0346
1.81	- 0.116
2.00	- 0.0345
2.00	- 0.0322
2.20	+ 0.0365
2.25	+ 0.0622
2.50	+ 0.0682
2.95	+ 0.0265
3.09	+ 0.0155
3.29	- 0.0270
3.59	- 0.0821
3.79	- 0.0747
4.01	- 0.0007
4.18	+ 0.0321
4.68	+ 0.0239
5.01	+ 0.0065
5.98	- 0.0235
7.15	- 0.0386
8.25	- 0.0485
9.05	+ 0.0078
9.06	- 0.0273
10.2	- 0.0590
14.4	+ 0.0004

TABLE 26

Axial Length Change as a Function of Curvature for Cylindrical Specimens Oxidized for Various Times in Dried Oxygen at 1000°C

Specimen Curvature (cm^{-1})	Oxidation Time (hours)	Axial Length (per cent)
8.24	1	- 0.0586
12.3	1	+ 0.0121
1.99	4	- 0.0364
2.99	4	+ 0.0332
4.00	4	- 0.0829
4.04	4	- 0.0335
5.00	4	+ 0.0073
5.07	4	+ 0.0036
6.00	4	- 0.0691
6.94	4	- 0.0814
8.08	4	+ 0.0576
9.05	4	+ 0.0145
10.2	4	+ 0.0171
11.1	4	- 0.0536
12.0	4	+ 0.187
2.00	16	- 0.0281
2.94	16	+ 0.0013
3.99	16	- 0.0496
4.98	16	- 0.0113
5.00	16	- 0.0131
6.01	16	- 0.0135
7.13	16	- 0.0364
7.93	16	- 0.0165
8.07	16	- 0.0339
8.96	16	+ 0.102
9.16	16	+ 0.0454
10.1	16	- 0.0143
11.1	16	+ 0.0060
11.8	16	+ 0.0213
4.00	36	+ 0.0760
12.3	36	+ 0.121
3.99	64	+ 0.0069

TABLE 27

Axial Length as a Function of Oxidizing Time for Two Cylindrical Specimens Subjected to Interrupted Oxidation at 1000°C in Dried Oxygen

Test I: Original Specimen Curvature 5.95 cm^{-1}

Total Oxidation Time (hours)	Gage Length (inch)
0	0.43939 ± 0.00007
1/12	0.43945 ± 0.00013
1	0.43949 ± 0.00007
4	0.43944 ± 0.00005
16	0.43956 ± 0.00006
32	0.43968 ± 0.00004
68	0.43963 ± 0.00004
111 1/2	0.43959 ± 0.00004

Test II: Original Specimen Curvature 7.96 cm^{-1}

Total Oxidation Time (hours)	Gage Length (inch)
0	0.42022 ± 0.00001
1/12	0.42009 ± 0.00003
1	0.42016 ± 0.00003
4	0.42014 ± 0.00003
16	0.42018 ± 0.00007
32	0.42027 ± 0.00002
68	0.42039 ± 0.00003
111 1/2	0.42036 ± 0.00005

TABLE 28

Axial Deformation as a Function of Time for a Specimen of Nickel-270 Tested in Compression at 1000°C - Stress Level 754 psi

Time (minutes)	Axial Deformation in 0.500-inch Gage (inches x 10 ⁻³)
0	0.00
1	0.28
3	0.53
5	0.65
10	0.79
15	0.88
20	1.02
25	1.04
30	1.16
40	1.25
50	1.41
60	1.46
70	1.55
80	1.53
115	1.89
145	2.21
160	2.30
185	2.49
200	2.60

TABLE 29

Axial Deformation as a Function of Time for a Specimen of Nickel-270 Tested in Compression at 1000°C - Stress Level 1430 psi

Time (minutes)	Axial Deformation in 0.500-inch Gage (inches $\times 10^{-3}$)
0	0.00
1	0.68
3	1.13
5	1.61
10	2.23
15	2.67
20	3.03
25	3.35
30	3.65
40	4.19
50	4.71
60	5.06
70	5.37
90	6.04
110	6.57
130	6.97
140	7.16
150	7.49
160	7.67
170	7.91

TABLE 30

Axial Deformation as a Function of Time for a Specimen of Nickel-270 Tested in Compression at 1000°C - Stress Level 1975 psi

Time (minutes)	Axial Deformation in 0.470-inch Gage (inches x 10 ⁻³)
0	0.00
1	0.82
3	1.59
5	2.02
10	2.98
15	3.79
20	4.25
25	4.59
30	4.96
40	5.61
50	6.15
60	6.71
70	7.24
80	7.76
90	8.25
100	8.72
110	9.40

TABLE 31

Axial Deformation as a Function of Time for a Specimen of Hot-pressed Nickel Oxide Tested in Compression at 1000°C - Corrected Stress Level 765 psi

Time (minutes)	Axial Deformation in a 0.197-inch Gage Length (inches x 10 ⁻³)
0	0.00
1	0.09
3	0.13
5	0.15
10	0.22
15	0.22
20	0.20
30	0.25
40	0.24
50	0.22
65	0.23
80	0.21
135	0.26
165	0.28
190	0.30
210	0.40
215	0.27
220	0.32
230	0.38
250	0.40
265	0.39
365	0.47

TABLE 32

Axial Deformation as a Function of Time for a Specimen of Hot-pressed Nickel Oxide Tested in Compression at 1000°C - Corrected Stress Level 1450 psi

Time (minutes)	Axial Deformation in a 0.197-inch Gage Length (inches $\times 10^{-3}$)
0	0.00
1	0.14
3	0.16
5	0.25
10	0.34
15	0.44
20	0.47
30	0.45
40	0.48
50	0.47
70	0.60
105	0.80
160	0.97
230	1.71
240	1.75
285	1.97
320	2.17
380	2.38
445	2.66
475	2.79

TABLE 33

Axial Deformation as a Function of Time for a Specimen of Hot-pressed Nickel Oxide Tested in Compression at 1000°C - Corrected Stress Level 2060 psi

Time (minutes)	Axial Deformation in a 0.197-inch Gage Length (inches $\times 10^{-3}$)
0	0.00
1	0.38
3	0.45
5	0.51
10	0.67
20	0.86
30	1.19
40	1.34
50	1.45
60	1.68
70	1.85
80	2.03
90	2.10
100	2.35

TABLE 34

Degree of Protection Afforded by the Scales Formed on Several Metals as a Function of Oxidizing Temperature (17)

Metal	Temperature, (°C)						
	0	200	400	600	800	1000	1200
Na	Protective + Non-protective						
Cu	Protective						
Mg	Protective + Non-protective						
Ca	Protective + Non-protective						
Zn	Protective						
Al	Protective + Non-protective						
Ce	Protective + Non-protective						
Ti	Protective + Non-protective						
Zr	Protective + Non-protective						
Si	Protective						
Sn	Protective + Non-protective						
Nb	Protective + Non-protective						
Cr	Protective + Non-protective						
Mo	Protective + Non-protective						
W	Protective + Non-protective						
Fe	Protective						
Co	Protective						
Ni	Protective						

APPENDIX 2

APPENDIX 2

AN ELASTIC MODEL FOR THE PREDICTION OF STRESSES ARISING DURING THE OXIDATION OF NICKEL CYLINDERS

It is believed that stresses arise both in the oxide scale and in the metallic substrate due to geometric restrictions which prevail throughout the oxidation process. When these restrictions are coupled with a specific mechanism for oxide growth, the resultant stresses may be calculated provided that the assumptions introduced approximate the true state of affairs.

The development which follows is in part restricted both to a cylindrical geometry and to the nickel-nickel oxide system. These severe restrictions are not necessary; but rather, are introduced only to reduce the complexity of the algebra and simplify the numerical calculations involved. The general concepts are believed to apply to other geometries and metal-metal oxide systems, so long as the mechanism of oxidation is known with some degree of certainty.

It is extremely important to note that the work which follows is based only upon a simple elastic model. The implied assumption being that all other effects which may be taking place such as relaxation processes, solution

of oxygen gas in the metal, dissociation of the oxide at the gas-metal interface, vaporization of the oxide, etc. are considered to be second order in their effect upon the results of this analysis.

The approach taken herein is to assume that both the metallic and oxide phases of the specimen undergo elastic deformation only. This concept can be modified if the elastic equations predict stresses which are known to be in the plastic range; i.e., the elastic analysis is to serve as a first approximation to the truth.

Consider a right cylindrical nickel specimen of radius (r_0) having unit length. Let this specimen be subjected to an oxidizing atmosphere and let the reaction product (NiO) form exclusively by outward radial diffusion of the metallic ion through the resultant reaction product. It is readily seen that if both the metal and reaction product are non-deformable, then contact between metallic substrate and scale will be lost rather soon in the process; i.e., as soon as the first layer of metal (at radius r_0) has been transported away from its initial position. It is well known that the reaction does not in general stop at this point; but rather, it continues until the metal is consumed. The physical reason for the continuance of the reaction may be thought of in terms of a high degree of

adhesion between the metal and the scale. Because the reaction can not proceed without deformation of one or both phases, the consequences of a deformable metal and reaction product are discussed below. This treatment is essentially an extension of the analysis of elastic stresses in thick-walled cylinders.

If the metallic specimen initially has radius (r_0) and unit length (l_0) and is oxidized to produce a scale of thickness (x_*) on its surface, then the interface between metal and oxide must necessarily move inward from (r_0) some amount to radius (r_*). A schematic drawing is shown below:

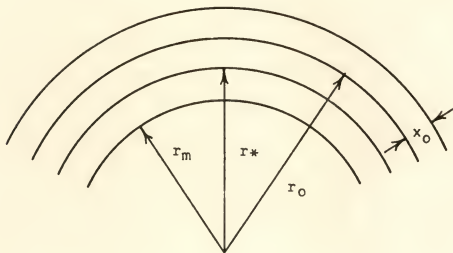


Figure 110: Schematic drawing of scale formation on a cylindrical section.

If the mechanical constraints were removed from this system, the inner surface of the oxide would elastically return to radius (r_0) and the outer surface of the metal would elastically shrink to some radius (r_m) $<$ (r_*). In this stress-free condition, the actual volumes of oxide produced (V^0) and the metal used (V^m) are related by the Pilling-Bedworth ratio (P) as follows:

$$V^0 = P V^m \quad (6)$$

Introducing the cylindrical geometry and notations of Figure :

$$\pi(r_0 + x_0)^2 l_u - \pi(r_0)^2 l_u = P[\pi(r_0)^2 - \pi(r_m)^2] l_u \quad (7)$$

therefore:

$$x_0 = -r_0^m \pm \left\{ (r_0^m)^2 + P \left[(r_0^m + r_m)(r_0^m - r_m) \right] \right\}^{1/2} \quad (8)$$

for (r_0) approximately equal to (r_m); i.e., (x_0) \ll (r_0):

$$\begin{aligned} x_0 &\approx -r_0 \pm \left\{ (r_0)^2 + P(2r_0)(r_0 - r_m) \right\}^{1/2} \\ &\approx -r_0 \pm r_0 \left\{ 1 + 2P \frac{(r_0 - r_m)}{r_0} \right\}^{1/2} \end{aligned} \quad (9)$$

expanding the term in brackets:

$$x_0 \approx -r_0 + r_0 \left\{ 1 + 1/2 \cdot 2P \frac{(r_0 - r_m)}{r_0} + \dots \right\} \quad (10)$$

therefore:

$$x_0 \simeq + P (r_0 - r_m) \quad (11)$$

Equation 11 is interpreted as follows: if the reaction proceeds to a point such that the stress-free thickness of the oxide formed is (x) then the metal must necessarily have lost a layer of thickness $(r_0 - r_m)$ at the metal-oxide interface. This description of oxidation process supplies the starting point for an elastic analysis of the stresses involved in the oxidation reaction.

Consider an artificial process which breaks down the motion of the metal-oxide interface into two components. The first component of the motion being that due to the consumption of the substrate nickel metal with the subsequent production of nickel oxide and the second being due to the elastic stresses of the system. Then the total motion of the interface described by the coordinates of the metal is given by:

$$r_0 - r_* = (r_0 - r_m) - u_m (r_m) \quad (12)$$

Where (u_m) is the radial displacement of the metal due to stresses in the system, measured positive in the outward direction. The quantity $(r_0 - r_m)$ may be evaluated by equation 11 :

$$r_0 - r_* = \frac{x_0}{P} - u_m (r_m) \quad (13)$$

However, for the oxide we have:

$$r_0 - r_* = -u_0(r_0) \quad (14)$$

Where $(u_0(r_0))$ is the radial deformation of the oxide layer at the interface.

Therefore:

$$u_0(r_0) = u_m(r_m) - \frac{x_0}{p} \quad (15)$$

We will now relate the deformations (u) with the stresses of the system.

In order to handle the mathematics associated with cylindrical geometries, it is convenient to adopt the cylindrical coordinate system with principle orthoginal directions denoted by (r, θ, z) . In this system, the strain relations are given by:

$$\epsilon_r = \frac{\sigma_r}{E} - \nu \left(\frac{\sigma_\theta + \sigma_z}{E} \right) \quad (16)$$

$$\epsilon_\theta = \frac{\sigma_\theta}{E} - \left(\frac{\sigma_z + \sigma_r}{E} \right) \quad (17)$$

$$\epsilon_z = \frac{\sigma_z}{E} - \left(\frac{\sigma_r + \sigma_\theta}{E} \right) \quad (18)$$

Where (ϵ_i) is the strain, (σ_i) is the applied stress, and (E) and (ν) are the elastic modulus and Poisson's ratio

of the material, respectively. Equations (16), (17), and (18) may be solved for the (σ_i) in terms of (ϵ_i) to yield:

$$\sigma_r = \frac{E}{(1+\nu)(1-2\nu)} \left[(1-\nu)\epsilon_r + \nu(\epsilon_z + \epsilon_\theta) \right] \quad (19)$$

$$\sigma_\theta = \frac{E}{(1+\nu)(1-2\nu)} \left[(1-\nu)\epsilon_\theta + \nu(\epsilon_r + \epsilon_z) \right] \quad (20)$$

$$\sigma_z = \frac{E}{(1+\nu)(1-2\nu)} \left[(1-\nu)\epsilon_z + \nu(\epsilon_\theta + \epsilon_r) \right] \quad (21)$$

Consider an element of volume $(r d\theta dr dz)$ of either material and apply a force balance. It proves convenient to join enough such elements to form a half-hoop as shown:

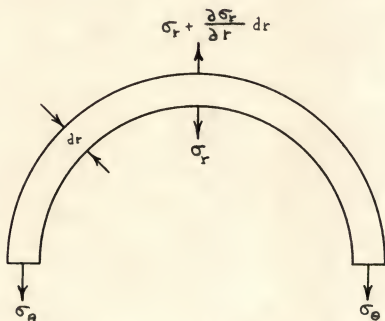


Figure 111: Forces acting on a cylindrical section.

The downward forces are given by:

$$1) \quad 1) F_1 = 2 \sigma_{\theta} \, dr dz \quad (22)$$

$$2) F_2 = \int_0^{\pi} \sigma_r \sin \phi \, r d\phi \, dz = r \sigma_r dz [-\cos \phi]_0^{\pi} \\ = 2r \sigma_r dz \quad (23)$$

The upward force is given by:

$$1) F_3 = 2(r+dr) \left(\sigma_r + \frac{\partial \sigma_r}{\partial r} dr \right) dz \\ = 2r \sigma_r dz + 2 \sigma_r dr dz + 2r \frac{\partial \sigma_r}{\partial r} dr dz \\ + 2dr \frac{\partial \sigma_r}{\partial r} dr dz \quad (24)$$

Neglecting higher order term, (24) may be written as:

$$F_3 = 2r \sigma_r dz + 2 \sigma_r dr dz + 2r \frac{\partial \sigma_r}{\partial r} dr dz \quad (25)$$

A force balance in the up-down direction requires that:

$$F_1 + F_2 - F_3 = 0 \quad \text{or}$$

$$2 \sigma_{\theta} dr dz + 2r \sigma_r dz - 2r \sigma_r dz - 2 \sigma_r dr dz - 2r \frac{\partial \sigma_r}{\partial r} dr dz = 0$$

$$\text{therefore:} \quad (26)$$

$$2 \sigma_{\theta} dr dz - 2 \sigma_r dr dz - 2r \frac{\partial \sigma_r}{\partial r} dr dz = 0 \quad (27)$$

therefore:

$$\sigma_{\theta} - \sigma_r - r \frac{\partial \sigma_r}{\partial r} = 0 \quad (28)$$

It should be noted that (9) is independent of (z) and that therefore it represents a differential equation of a "plane-strain" problem.

We may now relate equation (26) to the displacement (u) at a cylindrical surface of radius (r). This displacement may be thought of arising from stresses acting on the system. It follows that a radius ($r+dr$), the displacement ($u(r)$) is given by:

$$u(r) = u + \left(\frac{du}{dr} \right) dr \quad (29)$$

This is shown schematically below:

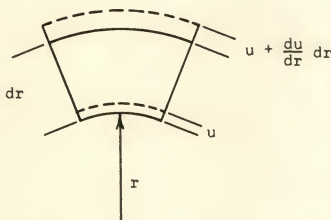


Figure 112: Displacements in a cylindrical element.

The radial strain due to the displacement (u) is then given by the expression:

$$\epsilon_r = \frac{(u + \frac{du}{dr} dr) - u}{(r + dr) - r} = \frac{du}{dr} \quad (30)$$

The tangential strain is:

$$\epsilon_\theta = \frac{2\pi(r+u) - 2\pi r}{2\pi r} = \frac{u}{r} \quad (31)$$

Assuming that the lack of curvature in the Z-direction implies that no Z-directed stress is necessary to produce the above radial deformation, the longitudinal strain may be calculated on the basis of a "plane-strain" model.

The equations of strain may be expressed as:

$$\epsilon_r = \frac{du}{dr} \quad (32)$$

$$\epsilon_\theta = \frac{u}{r} \quad (33)$$

$$\epsilon_z = \frac{dw}{dz} \quad (34)$$

where (w) is an axial deformation.

Let: $\alpha \equiv \frac{E}{(1+\nu)(1-2\nu)}$; then equations (19, 20, 21) become:

$$\sigma_r = \alpha \left[(1-\nu)\epsilon_r + \nu(\epsilon_\theta + \epsilon_z) \right] \quad (35)$$

$$\sigma_\theta = \alpha \left[(1-\nu)\epsilon_\theta + \nu(\epsilon_z + \epsilon_r) \right] \quad (36)$$

$$\sigma_z = \alpha \left[(1-\nu)\epsilon_z + \nu(\epsilon_r + \epsilon_\theta) \right] \quad (37)$$

and:

$$\frac{\partial \epsilon_r}{\partial r} = \alpha \left[(1-\nu) \frac{\partial}{\partial r} \epsilon_r + \nu \frac{\partial}{\partial r} \epsilon_\theta + \nu \frac{\partial}{\partial r} \epsilon_z \right] \quad (38)$$

therefore:

$$\frac{\partial \epsilon_r}{\partial r} = \alpha \left[(1-\nu) \frac{d^2 u}{dr^2} + \nu \left(-\frac{u}{r^2} + \frac{1}{r} \frac{du}{dr} \right) + \nu \frac{\partial^2 w}{\partial r \partial z} \right] \quad (39)$$

Inserting equations (35, 36) and (39) into equation (28):

$$\alpha \left[(1-\nu) (\epsilon_\theta - \epsilon_r) + \nu (\epsilon_r - \epsilon_\theta) \right] - r \alpha \left[(1-\nu) \frac{d^2 u}{dr^2} + \nu \left(-\frac{u}{r^2} + \frac{1}{r} \frac{du}{dr} + \frac{\partial^2 w}{\partial r \partial z} \right) \right] = 0 \quad (40)$$

therefore:

$$1(1-2\nu) \frac{u}{r} - (1-2\nu) \frac{du}{dr} - r(1-\nu) \frac{d^2 u}{dr^2} + \nu \frac{u}{r} - \nu \frac{du}{dr} - r \nu \frac{\partial^2 w}{\partial r \partial z} = 0 \quad (41)$$

therefore:

$$(1-\nu) \frac{u}{r} - (1-\nu) \frac{du}{dr} - r(1-\nu) \frac{d^2 u}{dr^2} = r \frac{\partial^2 w}{\partial r \partial z} \quad (42)$$

therefore:

$$\frac{d^2 u}{dr^2} + \frac{1}{r} \frac{du}{dr} - \frac{u}{r^2} = \frac{1}{(1-\nu)} \frac{\partial^2 w}{\partial r \partial z} \quad (43)$$

Since the condition of plane strain has been assumed:

$$\frac{\partial^2 w}{\partial r \partial z} = \frac{\partial}{\partial r} \left(\frac{\partial w}{\partial z} \right) = 0 \quad (44)$$

Therefore:

$$\frac{d^2 u}{dr^2} + \frac{1}{r} \frac{du}{dr} - \frac{u}{r^2} = 0 \quad (45)$$

This is the equation which governs the radial dependence of an arbitrary displacement (u). It applies, with the proper boundary conditions, to both the solid metallic cylinder and the hollow ceramic cylinder. Equation (45) is known as Euler's Equation, and is transformable into a linear second order differential equation with constant coefficients.

A general solution of equation 45 is:

$$u(r) = C_1 r + \frac{C_2}{r} \quad (46)$$

Let the solution for the deformation in the metal be expressed as:

$$u_m(r) = C_1 r + \frac{C_2}{r} \quad (47)$$

The physical condition that infinite stresses cannot exist

immediately demands that $C_2 = 0$; therefore:

$$u_m(r) = C_1 r \quad (48)$$

Let the deformation in the oxide be expressed as:

$$u^o(r) = C_3 r + \frac{C_4}{r} \quad (49)$$

The strains in each component of the system may be expressed in terms of their radial deformations:

$$\epsilon_r^m(r) = C_1; \quad \epsilon_\theta^m(r) = C_1; \quad \epsilon_z^m(r) = \frac{1}{E_m} [\sigma_z^m - \quad (50, 51, 52)$$

$$\nu (\sigma_r^m + \sigma_\theta^m)]$$

$$\epsilon_r^o(r) = C_3 - \frac{C_4}{r^2}; \quad \epsilon_\theta^o(r) = C_3 + \frac{C_4}{r^2}; \quad \epsilon_z^o(r) =$$

$$\frac{1}{E_o} (\sigma_z^o - \nu (\sigma_r^o + \sigma_\theta^o)) \quad (53, 54, 55)$$

By introducing physical conditions, the constants may be evaluated and the stresses may be found in terms of parameters of the system.

Condition 1 - The circumference of the metal-oxide interface is the same for both the metal and the oxide:

$$2\pi r_m (1 + \epsilon_\theta^m(r_m)) = 2\pi r_o (1 + \epsilon_\theta^o(r_o)) \quad (56)$$

therefore

$$r_m(1 + C_1) = r_o \left(1 + C_3 + \frac{C_4}{r_o^2} \right) \quad (57)$$

Condition 2 - The length of the metal-oxide interface is the same for both the metal and the oxide:

$$l_u (1 + \epsilon_z^m(r_m)) = l_u (1 + \epsilon_z^o(r_o)) \quad (58)$$

where l_u is a unit length.

therefore:

$$\epsilon_z^m(r_m) = \epsilon_z^o(r_o) \quad (59)$$

Since plane strain has been assumed, these values of strain are independent of (r) ; therefore;

$$\epsilon_z^m = \epsilon_z^o \quad (60)$$

Condition 3 - The sum of the radial deformation at the metal-oxide interface for the metal and the oxide, are equal to the amount of metal consumed:

$$+ u^m(r_m) - u^o(r_o) = + \frac{x}{P} \quad (61)$$

therefore:

$$C_1 r_m - C_3 r_o - C_4 \frac{1}{r_o} = \frac{x}{P} \quad (62)$$

Condition 4 - The sum of the radial forces at the metal-oxide interface are zero:

$$\sigma_r^m(r_m) [2\pi r_m l_u] - \sigma_r^o(r_o) [2\pi r_o l_u] = 0 \quad (63)$$

Condition 5 - The sum of the radial forces at the gas-oxide interface are zero:

$$\sigma_r^o(r_o + x_o) [\text{Interfacial area}] = 0 \quad (64)$$

Therefore:

$$\sigma_r^o(r_o + x_o) = 0 \quad (65)$$

Condition 6 - The sum of the z-directed forces are equal to zero; therefore:

$$\int_0^{r_m} \sigma_z^m(r) dA_{\text{metal}} + \int_{r_o}^{r_o+x_o} \sigma_z^o(r) dA_{\text{oxide}} = 0 \quad (66)$$

In order to facilitate calculations, all stresses and strains are first expressed in terms of the constants C_1 , C_3 , C_4 , and the axial strains ϵ_z , in the cases where this has not already been done. Finally, it will prove convenient to define the following combined parameters:

$$\alpha_m = \frac{E_m}{(1+\nu_m)(1-2\nu_m)} ; \quad \alpha_o = \frac{E_o}{(1+\nu_o)(1-2\nu_o)} \quad (67)$$

The stresses are then written in terms of the strains as prescribed by equations (19,20,21,50,51,52) and (53,54,55) recalling that condition (2) requires $\epsilon_z^0 = \epsilon_z^m = \epsilon_z$.

The physical conditions imposed on the system may now be expressed as follows:

$$\text{Condition 1: } r_m(1+C_1) = r_o \left(1 + C_3 + \frac{C_4}{r_o^2} \right) \quad (68)$$

$$\text{Condition 2: } \epsilon_z^m = \epsilon_z^0 = \epsilon_z \quad (69)$$

$$\text{Condition 3: } C_1 r_m - C_3 r_o - \frac{C_4}{r_o} = \frac{x_o}{P} \quad (70)$$

Equation (70) may be rearranged by employing the relation of equation (11):

$$x_o = P (r_o - r_m)$$

This operation results in a restatement of equation (68); therefore equation (68) may be considered redundant.

$$\begin{aligned} \text{Condition 4: } \alpha_m \left[C_1 + \nu_m \epsilon_z \right] r_m &= \alpha_o \left[C_3 - (1-2\nu_o) \right. \\ &\quad \left. + \frac{C_4}{r_o^2} + \nu_o \epsilon_z \right] r_o \end{aligned} \quad (71)$$

$$\text{Condition 5: } C_3 - (1-2\nu_o) \frac{C_4}{(r_o+x_o)^2} + \nu_o \epsilon_z = 0 \quad (72)$$

Condition 6:

$$\begin{aligned} \alpha_m \left[(1-\nu_m) \epsilon_z + 2\nu_m C_1 \right] (r_m^2) + \alpha_o \left[(1-\nu_o) \epsilon_z + 2\nu_o C_3 \right] \\ \times (2r_o x_o + x_o^2) = 0 \end{aligned} \quad (73)$$

It is convenient to define a new set of parameters which will help simplify equations (70) through (73).

Let them be defined as follows:

$$K = \frac{r_m}{r_o}; \text{ therefore, from equation (11): } K = (1 - \frac{x_o}{Pr_o}) \quad (74)$$

$$L = (1 + \frac{x_o}{r_o})^2; \text{ therefore } Lr_o^2 = (r_o + x_o)^2 \quad (75)$$

$$M = (2 \frac{x_o}{r_o} + (\frac{x_o}{r_o})^2); \text{ therefore } M = L - 1, \text{ and}$$

$$Mr_o^2 = (2x_or_o + x_o^2) \quad (76)$$

Substitution of these parameters into equations (70) through (73) permits the axial strain, (ϵ_z), to be expressed in terms of the scale thickness-specimen radius ratio, $\frac{x_o}{r_o}$. Upon carrying through the algebra, it is found that:

$$\epsilon_z = \frac{\alpha_m(1-K) \left[\frac{T}{S} - 2 \nu_m K \right]}{\left[U - \alpha_m \frac{T}{S} (K \nu_m - \nu_o) \right]} \quad (77)$$

Where the symbols S, T, and U represent quantities which include the material parameters and, implicitly, the ratio $\frac{x_o}{r_o}$. Thus:

$$S = \alpha_m \left[1 + \frac{(1-2\nu_o)}{L} \right] + \alpha_o(1-2\nu_o) \frac{M}{L} \quad (78)$$

$$T = 2 \alpha_m \nu_m K \left(1 + \frac{(1-2\nu_o)}{L} \right) + 2 \alpha_o \nu_o M \frac{(1-2\nu_o)}{L} \quad (79)$$

$$U = \alpha_m K^2 (1 - \nu_m) + \alpha_o M (1 - \nu_o) - 2 \alpha_m \nu_m \nu_o K - 2 \alpha_o \nu_o^2 M \quad (80)$$

The stresses and strains in both the metal and oxide may be calculated by choosing fixed values of the ratio $(\frac{x_0}{r_0})$ and subsequently determining the magnitude of (C_1) , (C_3) , $(\frac{C_4}{r_0^2})$ and (ϵ_z) via equations (70) through (77).

If the elastic moduli (E_o) and (E_m) are assigned values of 20×10^6 and 10×10^6 psi, respectively, and Poisson's ratio for the oxide and metal are assigned values of 0.2 and 0.3, respectively, it is found that the ultimate strength of the oxide is reached for values of $(\frac{x_0}{r_0})$ of the order of 10^{-3} . For the range of specimen sizes employed herein, this value indicates relatively early failure of the oxide. Limitations of the applicability of this model are discussed elsewhere in the text.

APPENDIX 3

APPENDIX 3

ESTIMATION OF THE MAGNITUDE OF THE GRAIN BOUNDARY PRESSURE

The magnitude of the grain boundary pressure may be estimated from the data concerning elongation of flat specimens and that of the creep rate of Nickel-270 at 1000°C. It will be assumed that the grain boundary pressure, (σ_g^o), is constant throughout the oxidation process in analogy with the limiting values of pressure found in earlier experiments concerning crystallization pressure (84) . Since the grain structure of the oxide formed on flat specimens was found to be columnar, as illustrated for example by the photomicrographs of Figure 61b, the stress arising from the grain boundary pressure may be considered to act only in planes parallel to the specimen surface.

If the scaling rate is parabolic, as indicated by Figure 26 for the case of flat specimens, then the force developed on a unit cross section of the scale will also increase parabolically and may be expressed as:

$$F^o = \sigma_g^o x = \sigma_g^o K_x t^{1/2} \quad (81)$$

where (x) is the scale thickness, (K_x) is the parabolic rate constant based on scale thickness, and (t) is the

oxidation time. This force, which arises in the scale on both of the parallel faces of the specimen, must be balanced by one acting along the same direction on a unit cross section of the metal, therefore:

$$F^m = 2 F^o = 2 \sigma_g^o K_{xt}^{1/2} \quad (82)$$

Thus, the stress in the metal, due to the presence of grain boundary pressure, is given by:

$$\sigma^m = \frac{2 \sigma_g^o K_{xt}^{1/2}}{a} \quad (83)$$

where (a) is defined as the sheet thickness.

The elongation of the specimen may now be calculated as a function of time by making use of the fact that the stress and deformation rate are related as shown in Figure 104. If it is assumed that no deformation occurs by creep of the metal when the applied stress is zero, then the creep data for the metal may be fit to the following empirical formula:

$$\dot{\epsilon}_2 = 5.82 \times 10^{-4} (e^{1.22 \times 10^{-3} \sigma^m} - 1) \text{ in/in/hr} \quad (84)$$

where ($\dot{\epsilon}_2$) is the second stage creep rate. For small values of (σ^m), equation (84) may be simplified by neglecting higher order terms of the expanded exponential.

Upon substitution of equation (83) for (σ^m) , equation (84) becomes:

$$\epsilon_2 = 1.42 \times 10^{-6} \frac{\sigma_g^0 K_X t^{1/2}}{a} \text{ in/in/hr} \quad (85)$$

The value of the parabolic rate constant (K_X) , is approximately 4.0 microns/hr^{1/2}, as may be evaluated from the curve of Figure 32 which indicates that a scale thickness of approximately 16 microns is developed during 16 hours of oxidation. Substitution of this value of (K_X) into equation (85) and subsequent integration over the period of oxidation (16 hours) gives:

$$\epsilon = 2.42 \times 10^{-8} \frac{\sigma_g^0}{a} \text{ in/in} \quad (86)$$

Where (ϵ) is the total strain and the units of (σ_g^0) and (a) are pounds per square inch and centimeters, respectively.

The value of (σ_g^0) may be determined by solving equation (86) for it and using the observed values of (ϵ) given in Table 6. Doing this gives values of (σ_g^0) ranging from approximately 900 to 4000 psi. It is felt however, that the best estimate of the grain boundary pressure may be made using the measured values of extension found for the two specimens of intermediate thickness. This procedure avoids sources of error discussed elsewhere in the text.

The mean value of grain boundary pressure thus found is approximately 1500 psi. The graph of Figure 113 indicates that this estimate is probably correct within a factor of two.

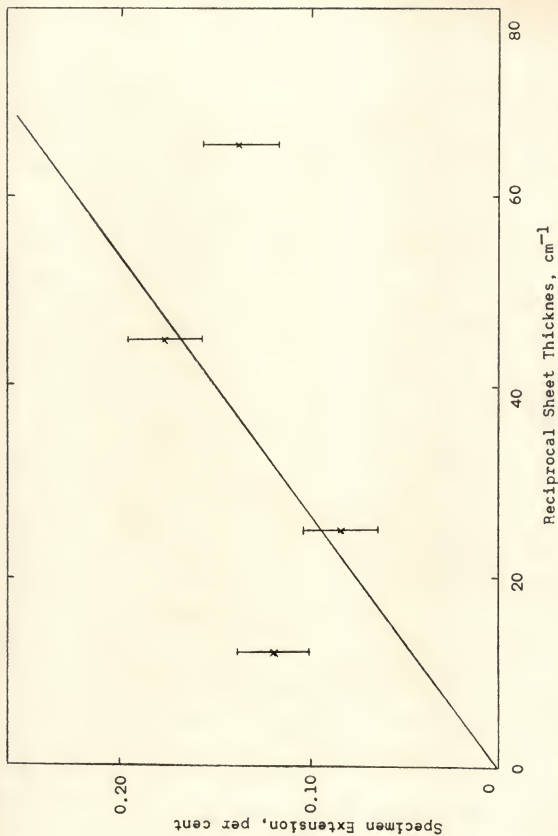


Figure 113: Comparison of observed and calculated values of the extension of flat specimens oxidized for 16 hours at 1000°C in dried oxygen. Calculated curve based upon a grain boundary pressure of 1500 psi.

LIST OF REFERENCES

1. U.R. Evans, "Mechanism of the Formation of Films on Metals," in Pittsburgh International Conference on Surface Reactions, Corrosion Publishing Co., Pittsburgh, 1948, pp 71-76.
2. O. Kubaschewski and P.E. Hopkins, Oxidation of Metals and Alloys, Butterworth and Co. Ltd., London, 1962, p 54.
3. A.U. Seybolt, "Oxidation of Metals," Adv. in Phys., 12, 1963, pp 1-43.
4. A.U. MacRae, "Low Energy Electron Diffraction," Science, 139, 1963, pp 379-388.
5. C. Wagner, "Mechanism of the Movement of Ions and Electrons in Solids and the Interpretation of Reactions Between Solids," Trans. Faraday Soc., 34, 1938, pp 851-859.
6. T.P. Hoar and L.E. Price, "The Electrochemical Interpretation of Wagner's Theory of Tarnishing Reaction," Trans. Faraday Soc., 34, 1938, pp 867-874.
7. E.A. Gulbransen, "The Transition State Theory of the Formation of Thin Oxide Films on Metals," Trans. Electrochem. Soc., 83, 1943, pp 301-309.
8. N. Cabrera and N.F. Mott, "Theory of the Oxidation of Metals," Rept. Prog. Phys., 12, 1948-1949, pp 163-184.
9. N.B. Pilling and R.E. Pedworth, "The Oxidation of Metals at High Temperatures," J. Inst. Metals, 29, 1923, pp 529-582.
10. J.V. Cathcart, L.L. Hall, and G.P. Smith, "Oxidation Characteristics of the Alkali Metals -I. The Oxidation Rate of Sodium Between -79° and 48°C," Acta Met., 5, 1957, pp 245-248.

LIST OF REFERENCES (Continued)

11. D.A. Vermilyea, "The Mechanism of the Oxidation of Metals," *Acta Met.*, 5, 1957, pp 492-495.
12. L. Young, in Discussion of Reference 20, J. Electrochem. Soc., 105, 1958, pp 761-762.
13. G.I. Finch and A.G. Quarrell, "Crystal Structure and Orientation in Zinc Oxide Films," *Proc. Phys. Soc.*, 46, 1934, pp 148-162.
14. R.F. Mehl, E.L. McCandless, and F.N. Rhines, "Orientation of Oxide Films on Metals," *Nature*, 134, p. 1009.
15. J.V. Cathcart, J.E. Epperson, and G.F. Petersen, "Epitaxially Induced Strains in Cu_2O Films on Copper Single Crystals - II. Optical Effects," *Acta Met.*, 10, 1962, pp 699-703.
16. J.W. Hickman, "Investigation of Gas-Metal Reactions by Reflection Electron Diffraction," in Pittsburgh International Conference on Surface Reactions Corrison Publishing Co., Pittsburgh, 1948, pp 142-156.
17. O. Kubaschewski and B.E. Hopkins, Oxidation of Metals and Alloys, Butterworth and Co. Ltd., London, 1962, pp 9, 33-37, and 205-265
18. L. Young, "Anomalies in the Growth of Anodic Oxide Films on Rough Surfaces," *Acta Met.*, 5, 1957, pp 711-716.
19. J.V. Cathcart, J.J. Campbell, and G.P. Smith, "Microtopography of Oxide Films on Niobium," *J. Electrochem. Soc.*, 105, 1958, pp 442-446.
20. J.P. Pemsler, "Diffusion of Oxygen in Zirconium and its Relation to Oxidation and Corrosion," *J. Electrochem. Soc.*, 105, 1958, pp 315-322.
21. R.E. Pawel, J.V. Cathcart, and J.J. Campbell, "'Break-Away' Phenomena in the Oxidation of Columbium Single Crystals," in Columbium Metallurgy, Ed. by. D.L. Douglass and F.W. Kunz, Interscience Publishers, New York, 1960, pp 667-682.

LIST OF REFERENCES (Continued)

22. R.E. Pawel, J.V. Cathcart, and J.J. Campbell, "Oxide Platelet Formation in Tantalum Single Crystals," *Acta Met.*, 10, 1962, pp 149-160.
23. R.E. Pawel, J.V. Cathcart, and J.J. Campbell, "Stress Generation in Tantalum During Oxidation," *J. Electrochem. Soc.*, 110, 1963, pp 551-557.
24. W.W. Smeltzer and M.T. Simnad, "Oxidation of Hafnium," *Acta Met.*, 5, 1957, pp 328-334.
25. U.R. Evans, "Influence of Residual Stress on Chemical Behavior," in Symposium on Internal Stresses in Metals and Alloys, Inst. of Metals, London, 1948, pp 291-310.
26. J.A. Sartell, R.J. Stokes, S.H. Bendel, T.L. Johnston, and C.H. Li, "Role of Oxide Plasticity in the Oxidation Mechanism of Pure Copper," *Trans. Am. Inst. Min. Met. Eng.*, 215, 1959, pp 420-424.
27. P.W. Dunnington, F.H. Beck, and M.G. Fontana, "The Mechanism of Scale Formation on Iron at High Temperature," *Corrosion*, 8, 1952, pp 2-13.
28. P.D. Dankov and P.V. Churaev, "Deformation Effects of Metallic Surface Layers During Oxidation," *Doklady Akad. Nauk. SSSR*, 73, 1950, pp 1221-1224.
29. W. Jaenicke, and S. Leistikow, "Mechanische Spannungen bei der Bildung von Oxydschichten," *Z. Physik. Chem.*, N.F., 15, 1958, pp 175-195.
30. W. Jaenicke, S. Leistikow, and A. Stadler, "Mechanical Stresses during the Oxidation of Copper and their Influence on Oxidation Kinetics - III," *J. Electrochem. Soc.*, 111, 1964, pp 1031-1037.
31. H. Engell and F. Wever, "Über einige Grundfragen der Bildung und der Haftung von Zunder auf Eisen," *Acta Met.*, 5, 1957, pp 695-702.
32. O. Kubaschewski and O. von Goldbeck, "Die Oxydationsgeschwindigkeit von Nickel," *Z. Metallkunde*, 39, 1948, pp 158-160.

LIST OF REFERENCES (Continued)

33. J.G. Thompson, Nickel and its Alloys, NBS Circular 592, Washington, 1958.
34. H.P. Rooksby, "Structure Changes in Some Non-Stoichiometric Oxides of the Transition Elements," Trans. Brit. Ceram. Soc., 56, 1957, pp 581-589.
35. R.F. Tylecote, "Factors Influencing the Adherence of Oxides on Metals," J. Iron and Steel Inst., 196, 1960, pp 135-141.
36. M. Hansen and K. Anderko, Constitution of Binary Alloys, McGraw-Hill Book Co., Inc., New York, 1958, pp 1024-1026.
37. International Nickel Co., Inc., Basic Data, Nickel-270, Huntington, 1963.
38. J.T. Baker Chemical Co., Phillipsbury, N.J., 1963
39. Beitrag zur Theorie des Anlaufvorganges, III C. Wagner and K. Grunewald, Z. Physik. Chem., 408, 1938, pp 455-475.
40. C. Kubaschewski and E. L.I. Evans, Metallurgical Thermochemistry, 2nd Ed., John Wiley and Sons, Inc., New York, 1956, pp 331-338.
41. O. Kubaschewski and B.E. Hopkins, Oxidation of Metals and Alloys, Butterworth and Co. Ltd., London, 1962, p 13.
42. G.I. Finch and K.P. Sinha, "A New Superstructure of Nickel Oxide," Trans. Faraday Soc., 53, 1957, p 623.
43. E.I. Allesandrina and J.F. Freedman, "The Observation by Electron Diffraction of a 'Superlattice' in Annealed Single Crystal Nickel Films," Acta Cryst., 16, 1963, pp 54-57.
44. R.L. Park and H.E. Farnsworth, "The Interaction of Oxygen with a Clean (111) Nickel Surface," Appl. Phys. Letters, 3, 1963, pp 167-168.

LIST OF REFERENCES (Continued)

45. F.J. Morin, "Electrical Properties of NiO," Phys. Rev., 93, 1954, pp 1199-1204.
46. R. Newman and R.M. Chrenke, "Optical Properties of Nickel Oxide," Phys. Rev., 114, 1959, pp 1507-1513.
47. S.P. Mitoff, "Electrical Conductivity and Thermodynamic Equilibrium in Nickel Oxide," J. Chem. Phys., 35, 1961, pp 882-889.
48. B.M. Vasyutinskiy and G.N. Kartmazov, "Mechanism of Nickel Oxidation," Phys. Met. and Metallog., 15, 1963, pp 120-122.
49. O. Kubaschewski and R.E. Hopkins, Oxidation of Metals and Alloys, Butterworth and Co., Ltd., London, 1962, pp 22, 23, 90-92.
50. E.J.W. Verwey, P.W. Haaijman, F.C. Romeijn, and G.W. van Dosterhout, "Controlled-Valency Semiconductors," Philips Resh. Repts., 5, 1950, pp 173-189.
51. W.J. Moore and J.K. Lee, "Kinetics of the Formation of Oxide Films on Nickel Foil," Trans. Faraday Soc., 48, 1952, pp 916-920.
52. E.A. Gulbransen, "Classical Theory of Diffusion and the Oxidation of Metals," Ann. New York Acad. Sci., 58, 1954, pp 830-842.
53. A. Preece and G. Lucas, "The High-Temperature Oxidation of Some Cobalt-Base and Nickel-Base Alloys," J. Inst. Metals, 81, 1952-53, pp 219-227.
54. S. Mrowec and T. Werber, Discussion on "High-Temperature Oxidation of High-purity Nickel," E.A. Gulbransen and K.F. Andrew, J. Elec. Soc., 104, 1957, pp 451-454.
55. J.A. Sartell and C. H. Li "The Mechanism of Oxidation of High-Purity Nickel in the Range 950°-1200°C.," J. Inst. Metals, 90, 1961-1962, pp 92-96.
56. A. Dravnieks and H.J. McDonald, "The Zone of Metal Phase Consumption in Gas-Metal Reactions," Trans. Electrochem. Soc., 94, 1948, pp 139-151.

LIST OF REFERENCES (Continued)

57. C.E. Birchenall, "Kinetics of the Formation of Porous or Partially Detached Scales," J. Electrochem. Soc., 103, 1956, pp 619-624.
58. J.D. MacKenzie and C.E. Birchenall, "Plastic Flow of Iron Oxides and the Oxidation of Iron," Corrosion, 13, 1957, pp 783t-785t.
59. D.W. Juenker, R.A. Meussner, and C.E. Birchenall, "Cavity Formation in Iron Oxide," Corrosion, 14, 1958, pp 39t-46t.
60. R.F. Mehl and E.L. McCandless, "Oxide Films on Iron," Trans. Am. Inst., Min. Met. Eng., 125, 1937, pp 531-553.
61. D. Caplan, A. Harvey, and M. Cohen, "Oxidation of Chromium at 890°-1200°C.," Corrosion Sci., 3, 1963, pp 161-175.
62. C.H. Desch, "The Solidification of Metals from the Liquid State," J. Inst. Metals, 11, 1914, pp 57-106.
63. H.C. Boydell, "Metasomatism and the Linear Force of Growing Crystals," Econ. Geol., 21, 1926, pp 1-55.
64. K. Kohn and S. Iida, "X-ray Diffraction Study of Twin Walls of NiO Single Crystals," J. Phys. Soc. Japan, 19, 1964, pp 344-350.
65. T.W. Bridgman, Large Plastic Flow and Failure, McGraw-Hill Book Co., Inc., New York, 1952, p 339.
66. D.H. Bangham, "The Initial Stages of the Reaction Between Copper and Oxygen," J. Sci. Inst., 22, 1945, pp 230-231.
67. R. Phelps, E.H. Gulbransen, and J. Hickman, "Electron Diffraction and Electron Microscope Study of Oxide Films Formed on Metals and Alloys at Moderate Temperatures. Stripped Oxide Films of Metals," Ind. and Eng. Chem., 18, 1946, pp 391-400.
68. U.M. Martius, "The Initial Oxidation of Nickel," Can. J. Phys., 33, 1955, pp 466-472.

LIST OF REFERENCES (Continued)

69. D. McLean, Grain Boundaries in Metals, Oxford University Press, London, 1957, pp 258-295.
70. C.S. Smith, "Grains, Phases, and Interfaces; An Interpretation of Microstructure," Trans. Am. Inst. Min. Met. Eng., 175, 1948, pp 15-50.
71. C. Herring, "Some Theorems on the Free Energies of Crystal Surfaces," Phys. Rev., Ser. 2, 82, 1951, pp 87-93.
72. C.S. Barrett, "Preferred Orientations" in A.S.M. Metals Handbook, Cleveland, 1948, p 18.
73. M. Otter, "Das Aufwachsen von Nickeloxyd auf Nickelein Kristallkugeln mit glatter, unberührter Oberfläche," Zeit. für Naturf., 14a, 1959, pp 355-361.
74. E.A. Gulbransen and K.F. Andrew, "The Kinetics of Oxidation of High Purity Nickel," J. Electrochem. Soc., 101, 1954, pp 128-140.
75. J.P. Baur, R.W. Bartlett, J. N. Ong Jr. and W.M. Fassell Jr. "High-Pressure Oxidation of Metals, Nickel in Oxygen," J. Electrochem. Soc., 110, 1963, pp 185-189.
76. R. Lindner and A.A. Kerstrom, "Diffusion of Nickel-63 in Nickel Oxide," Disc. Faraday Soc., 23, 1957, pp 133-136.
77. T. Yamashina and T. Nagamatsuya, "Effect of Vacuum Annealing of Oxide Films on the Oxidation of Copper-Nickel Alloy," J. Electrochem. Soc., 111, 1964, pp 249-252.
78. G. Pfefferkorn, "Elektronmikroskopische Untersuchungen an Metalloxyoschichten," Zeit. für Metall., 46, 1955, pp 204-207.
79. J. Paidassi, "Oxidation of Copper to Cu_2O and CuO ," J. Electrochem. Soc., 104, 1957, pp 740-750.
80. J.L. Meijerling and M.L. Verheijke, "Oxidation Kinetics in the Case of Aging Oxide Films," Acta Met., 7, 1959, pp 331-338.

LIST OF REFERENCES (Continued)

81. D.W. Aylemore, S.J. Gregg, and W.B. Jepson, "High Temperature Oxidation of Beryllium. Part I, In Dry Oxygen," J. Nuc. Metals, 2, 1960, pp 169-175.
82. T.E. Leatonis and F.N. Rhines, "Rates of High-Temperature Oxidation of Magnesium and Magnesium Alloys," Am. Inst. Min. Met. Eng., T.P. 2003, 1946, pp 1-28.
83. Y. Oishi and W.D. Kingery, "Self Diffusion of Oxygen in Single Crystal and Polycrystalline Aluminum Oxide", J. Chem. Phys., 33, 1960, pp 480-486.
84. C.W. Correns, "Growth and Dissolution of Crystals Under Linear Pressure," Disc. Faraday Soc., No. 5, 'Crystal Growth', 1949, pp 267-271.

BIOGRAPHICAL SKETCH

James Stephen Wolf was born July 26, 1933, in Cleveland, Ohio. In February, 1951, he graduated from Collinwood High School and enrolled at the Case Institute of Technology, Cleveland, Ohio. After receiving the degree of Bachelor of Science in Physics in June, 1954, he was employed by the Cold Metal Process Company of Youngstown, Ohio, as a research engineer. From January, 1955 through 1956 he served in the Antiaircraft Command of the United States Army as a radar electronics technician. After separation from the military, he joined the staff of the National Advisory Committee for Aeronautics at Cleveland, Ohio where he was trained as a research metallurgist. In December, 1957 he married Viola M. Bluhm of Cleveland, Ohio. He was enrolled as a part-time student in the Graduate School of the Case Institute of Technology in September, 1958 and received the degree of Master of Science in Engineering in June, 1960. In September, 1961 he was granted a leave of absence from Federal service in order to enter the Graduate School of the University of Florida, where he received the degree of Doctor of Philosophy April, 1965.

This dissertation was prepared under the direction of the chairman of the candidate's supervisory committee and has been approved by all members of that committee. It was submitted to the Dean of the College of Engineering and to the Graduate Council, and was approved as partial fulfillment of the requirements for the degree of Doctor of Philosophy.

April, 1965

Thomas L. Martin Jr.
Dean, College of Engineering

Dean, Graduate School

Supervisory Committee:

J. N. Rhines
Chairman
John Kramstein
J. A. Scott
C. E. Reid
R. E. Reed-Hill